CHARLES UNIVERSITY
Faculty of mathematics
and physics

DOCTORAL THESIS

Adam Frtús

Mechanotransduction of Hepatic Cancer Cells cultured in a 3D Collagen Scaffold

Institute of Physics of the Czech Academy of Sciences

Supervisor of the doctoral thesis: PharmDr. Šárka Kubinová, Ph.D.

Study program: Biophysics, Chemical and Macromolecular Physics

Prague 2023

ACKNOWLEDGEMENT

Title: Mechanotransduction of Hepatic Cancer Cells cultured in a 3D Collagen Scaffold

Author: Mgr. Adam Frtús

Department: Department of Optical and Biophysical Systems, Institute of Physics of the Czech Academy of Sciences

Supervisor: PharmDr. Šárka Kubinová, Ph.D., Department of Optical and Biophysical Systems, Institute of Physics of the Czech Academy of Sciences

Abstract: Cell culture models transformed over time from a simple monolayer culture in 2D Petri dish to advanced 3D platforms, that provide conditions and features for cellular growth in all directions, similarly to *in vivo*. Moreover, cells experience distinct microenvironmental features within the extracellular matrix in tissues, that 3D cell culture might replicate. In fact, majority of studies indicate that physical cues generated from extracellular microenvironment drive the cellular behavior and functions. In this dissertation thesis, we attempt to provide the mechanistic explanation behind the changes in cellular metabolism and molecular signaling pathways induced by physical cues of 3D cell culture. We have used the advanced biomaterial-based 3D cell culture, biochemical assays, genetic manipulation and photobiomodulation in order to reveal the molecular mechanisms of mechanotransduction in hepatic cancer cells under physical cues of 3D collagen scaffold culture. By conducting this research, we not only aim to gather fundamental knowledge about tumor cell plasticity and signaling pathways, but we also believe it may provide insights into more predictive and reliable cell culture systems that may possess practical interest, e.g., in liver organoid models for new drug validation.

Keywords: 3D cell culture; Mechanotransduction; Cancer; Mitochondria; Cytoskeleton; Extracellular Matrix; Cell Plasticity

Název práce: Vliv mechanotransdukce na nádorové jaterní buňky kultivované v 3D kolagenovém nosiči

Autor: Mgr. Adam Frtús

Katedra: Oddělení optických a biofyzikálních systémů, Fyzikální ústav AV ČR

Školitel: PharmDr. Šárka Kubinová, Ph.D., Oddělení optických a biofyzikálních systémů, Fyzikální ústav AV ČR

Abstrakt: Modely buněčných kultur se v průběhu času transformovaly z jednoduchých monovrstvých kultur v Petriho miskách do pokročilých 3D platforem, které poskytují podmínky a vlastnosti pro růst buněk ve všech směrech, podobně jako *in vivo*. Buňky tkání ovlivňuje mikroprostředí okolní extracelulární matrix, které 3D buněčná kultura může replikovat. Výsledky výzkumu naznačují, že mechanické signály generované extracelulárním mikroprostředím ovlivňují buněčné chování a funkce. V této disertační práci jsme se zaměřili na odhalení molekulárních mechanismů mechanotransdukce, změn buněčného metabolismu a molekulárních signálních drah v 3D kultuře jaterních nádorových buněk v kolagenovém nosiči. Využili jsme celou řadu biochemických testů sledujících proliferaci, expresi signálních proteinů, imunofluorescenční barvení a konfokální mikroskopii, genetickou manipulaci a fotobiomodulaci. Náš výzkum si klade za cíl nejen získat základní znalosti o plasticitě nádorových buněk a molekulárních signálních drah v 3D prostředí, ale věříme, že může poskytnout základ pro více prediktivní systémy buněčných kultur, což může být prakticky využitelné, například v modelech jaterních organoidů pro validaci nových léčiv.

Klíčová slova: 3D buněčná kultura; Mechanotransdukce; Rakovina; Mitochondrie; Cytoskeleton; Extracelulární Matrix; Buněčná Plasticita

TABLE OF CONTENTS

LIST OF ABBREVIATIONS

LIST OF ABBREVIATIONS

2D	Two Dimensional
3D	Three Dimensional
ADP	Adenosine Diphosphate
ANOVA	Analysis of Variance
ATCC	American Type Culture Collection
ATP	Adenosine Triphosphate
AU	Arbitrary Units
BSA	Bovine Serum Albumin
CAMs	Cell Adhesion Molecules
CCCP	Carbonyl Cyanide m-chlorophenylhydrazone
cDNA	Complementary Deoxyribonucleic Acid
CMOS	Complementary Metal-oxide-semiconductor
CS	Collagen Scaffold
CSC	Cancer Stem Cells
DIC	Differential Interference Contrast
DNA	Deoxyribonucleic Acid
ECM	Extracellular Matrix
ER	Electromagnetic Radiation
ETC	Electron Transport Chain
FA	Focal Adhesion
FAK	Focal Adhesion Kinase
GAPDH	Glyceraldehyde 3-phosphate Dehydrogenase
GPa	Gigapascal
HCC	Hepatocellular Carcinoma
HFLP	High-fluence Low-power
HIF-1	Hypoxia-inducible Factor
ICLAC	International Cell Line Authentication Committee

Imy	Ionomycin
KCN	Potassium Cyanide
kDa	Kilodaltons
kPa	Kilopascal
LDH	Lactate Dehydrogenase
LED	Light-emitting Diode
LLLT	Low-level Laser (Light) Therapy
LUT	Look-up Table
MC	Monolayer Culture
mitoROS	Mitochondrial Reactive Oxygen Species
MMPs	Matrix Metalloproteinases
mPTP	Mitochondrial Permeability Transition Pore
mRNA	Messenger RNA
MTCO	Mitochondrially Encoded Cytochrome C Oxidase
mtDNA	Mitochondrial DNA
mTOR	Mammalian Target of Rapamycin
MWCO	Molecular Weight Cut-Off
NADH	Nicotinamide Adenine Dinucleotide
NIR	Near Infrared
PBM	Photobiomodulation
PBS	Phosphate Buffer Saline
PCNA	Proliferating Cell Nuclear Antigen
PCR	Polymerase Chain Reaction
PFK	Phosphofructokinase
PM	Plasma Membrane
pmTOR	Phosphorylated Mammalian Target of Rapamycin
PSC	Pluripotent Stem Cells
PVDF	Polyvinylidene Difluoride

RNA	Ribonucleic Acid
ROI	Region of Interest
ROS	Reactive Oxygen Species
RT-PCR	Reverse Transcriptase Polymerase Chain Reaction
SEM	Scanning Electron Microscopy
siRNA	Small Interfering RNA
STR	Short Tandem Repeats
VCL	Vinculin
YAP	Yes-Associated Protein
$\Delta\Psi m$	Mitochondrial Membrane Potential

1 INTRODUCTION

1.1 Mechanobiology of living cells

A living cell is a basic structural and functional unit of a multicellular organism. It is the smallest independently functioning unit, that can perform the essential processes required for life. It possesses a defined structure with specialized organelles and performs a wide array of functions necessary for the survival and growth. The most essential functions of the living cell include metabolism, reproduction, homeostasis, transport, communication, differentiation and also response to changes in cellular environment. Cells are highly adaptable and play a crucial role in maintaining the complex functions in multicellular organisms. The living cell consists of nucleus, that contain genetic information and is the cell´s control center (Figure 1). Cell is surrounded by selective barrier consisting of a lipid bilayer, so-called plasma membrane. A cytoplasm is a gel-like substance within the cell, where important chemical reactions and cellular organelles occur. Organelles are highly specialized structures, that has specific functions. Cellular organelles include lysosomes, endoplasmic reticulum, Golgi apparatus and mitochondria. Finally, cytoskeleton is a network of filamentous proteins, that provide structural support and assists in cell division, adhesion and transport (Figure 1) [1].
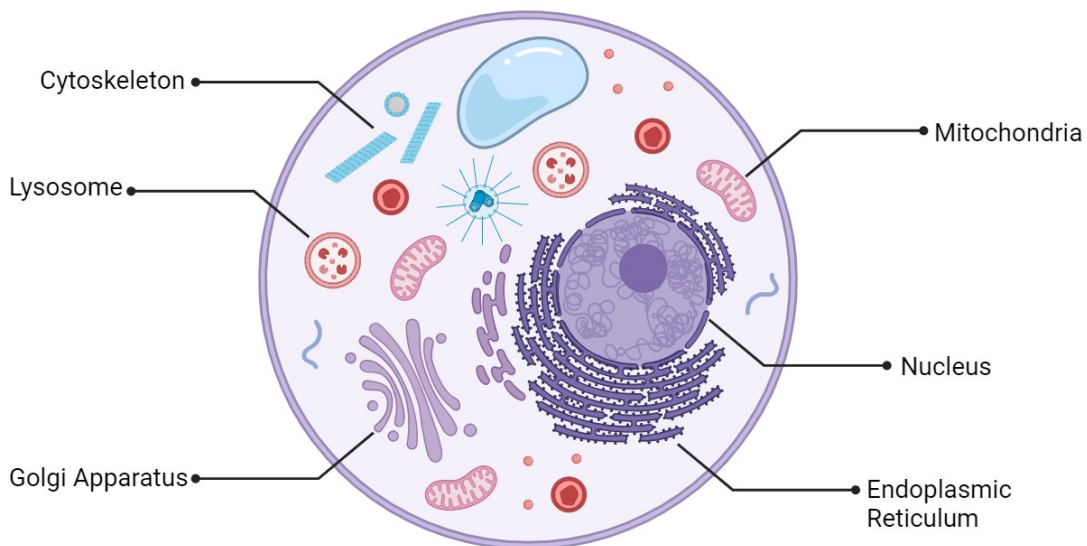
Figure 1: Generic animal cell. *Created with BioRender.com.*

Mechanobiology explores the interaction between a cell and its environment, elucidating the cell´s capability to perceive and react to the stiffness of its substrate and

the implications of these mechanisms in living organisms. A cellular environment is a 3D microarchitecture structure that surrounds cells and creates a functional milieu. *In vivo*, we recognize the extracellular matrix (ECM) that is providing a platform for cellular growth and interactions between the cells and the ECM itself, but also with other cells and extracellular fluids. ECM is a highly dynamic structure that supports cells while also playing a role in tissue differentiation and homeostasis [2]–[5]. Specifically, the ECM structure and function is tightly connected to the state of the tissue condition, such as normal, aged, wounded, fibrotic or tumorous [2]. Cells are in constant interaction with its surrounding via cell adhesion. Cell adhesion is a phenomenon describing the attachment of cell-cell or cell-ECM interaction [1]. Cell-ECM interactions includes focal adhesions (FA) (Figure 2) [6] and hemidesmosomes [7]. At those sites, cell-adhesion molecules (CAMs) act as a physical action of the connection [8]. CAMs, including integrins, vinculin, paxillin, talin, filamin and focal adhesion kinase (FAK), are complex molecular linkers, located at the interface between cells and ECM (Figure 2). CAMs play an essential role in fundamental cellular behavior and its changes can lead to multiple pathologies, such as cancer [9], [10]. Protein vinculin (VCL) is highly abundant at FA sites and provide actin anchoring to the membrane. Specifically, VCL sustain the extended conformation of other FA proteins [11].
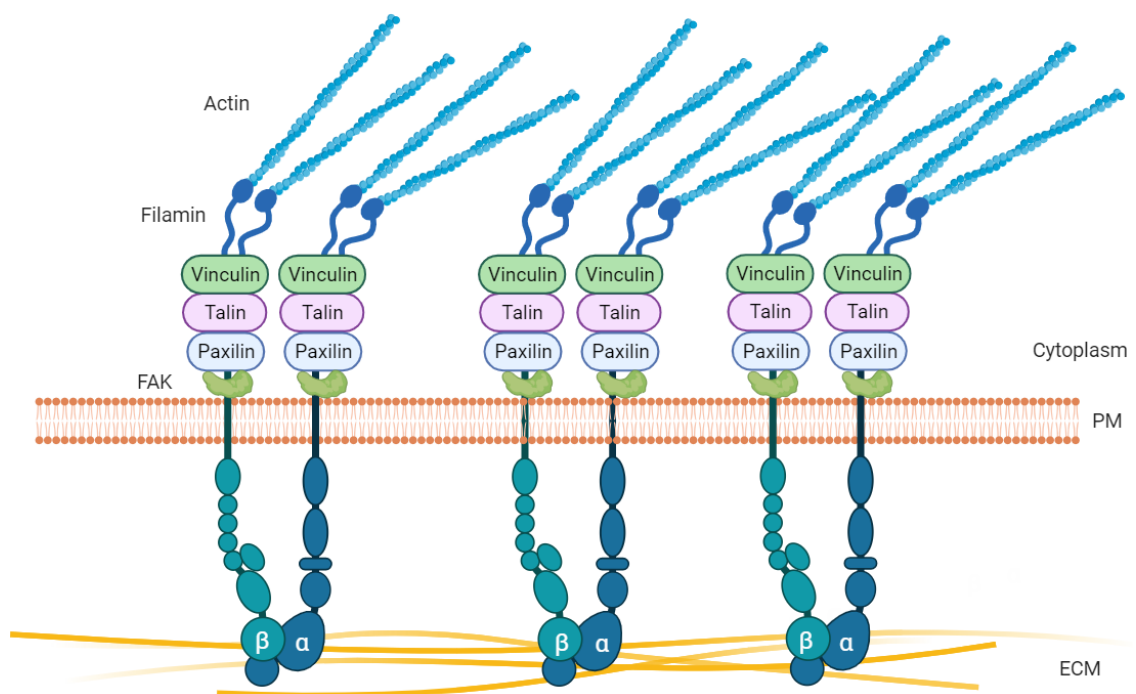
Figure 2: Schematic representation of focal adhesion (FA). *ECM – Extracellular Matrix, PM – Plasma Membrane, FAK – Focal Adhesion Kinase. Created in BioRender.com.*

Mechanotransduction defines the intricate cellular processes that convert mechanical stimuli into biochemical signals and facilitate the adoption to physical environment of cells [12]. A growing body of research demonstrates that the physical/mechanical cues such as viscoelasticity (stiffness of the material), poroelasticity and plasticity originated in the cellular physiological microenvironment have a significant impact on the functions of cells, including growth, survival, apoptosis, differentiation, and morphogenesis [13], [14]. Viscoelasticity deals with materials that exhibit both viscous and elastic behavior and poroelasticity deals with materials that have both solid and fluid components, while each mentioned involve the deformation of material. A key mechanical cue that controls cellular behavior and function is the stiffness of the material that surrounds the cell [15]. It is generally acknowledged that physical stimuli like substrate stiffness, shear stress, topography, and mechanical strain can be sensed by cells and cause them to respond [14] [16]. Biomechanical forces originating in the cellular microenvironment, including external shear stress, are thought to be one of the main regulators of fundamental cellular properties such as proliferation, motility and plasticity [14], [17]. Therefore, cellular mechanotransduction signaling is a fundamental component of maintaining cellular homeostasis ensuring proper cell function and influencing cell destiny [18]. The Focal Adhesion (FA) protein complex is crucial for mediating mechanotransduction [19], [20].

Despite recent developments in the field of mechanotransduction [21]–[23], there is still a lack of knowledge regarding the regulation of mechanosensing in hepatic cancer cell lines. To the best of our knowledge, there aren't many studies that examine how low-stiffness 3D collagen scaffold affects genetically distinct but closely related hepatic cell lines. It's important to note that different cell lines, even those that are closely related, react to stimuli in different ways. Nowadays, scientists realized that cellular environment plays a crucial role in many aspects, therefore it might be beneficial to mimic this environment *in vitro* to provide more realistic cell culture models.

Physical cues (called also mechanical cues) include topological features of 3D cellular environment as well as material stiffness, directly affects the cellular behavior [24]. The stiffness of ECM in vital and diseased tissue differs. Usually, the stiffness of animal organs is in kilopascal (kPa) range (Figure 5), while plastic used for cell culture offers the stiffness in gigapascal (GPa), that is out of the range for physiological and pathological values. Therefore, shift towards the ~kPa scale in biomaterial-based 3D cell culture might mimic the physiological as well as pathological conditions of tumor environment. Moreover, the physical cues including stiffness, could mechanically affect cellular behavior in process called mechanotransduction, that become highly discussed in literature over recent years (Figure 3).
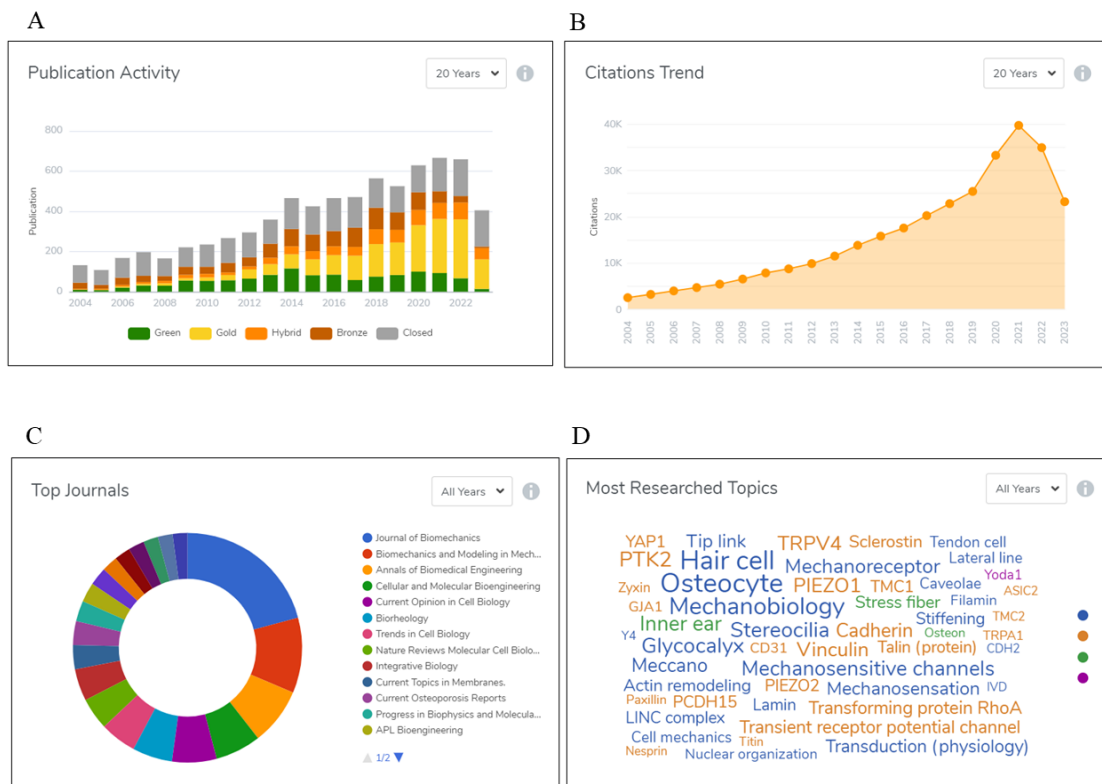
Figure 3: Statistical overview for topic "mechanotransduction". *(A) Graph of publication activity in different publication access categories during last 20 years. (B) Graph of citation trends during last 20 years. (C) Pie chart of most popular scientific journals for mechanotransduction. (D) Word cloud for the keywords that are most popular within the research for "mechanotransduction". Sourced from https://www.wizdom.ai/.*

Yes-associated protein 1 (YAP) is an oncoprotein and transcriptional regulator that functions as a corepressor and coactivator, and is an important downstream regulatory target in the Hippo signaling pathway, regulating proliferation and survival [25], [26]. Moreover, YAP is the principal regulator of the interaction between cells and the extracellular matrix (ECM) [27]. Hippo signaling pathway key objective is to inhibit the downstream transcriptional coactivators YAP/TAZ, in order to control organ size via regulating the proliferation, differentiation and apoptosis [28]. It is worth to note here, that YAP is deregulated in many cancers, including hepatocellular carcinoma (HCC) [28]. In fact, it was revealed that increased YAP/TAZ levels contribute to liver tumorigenesis [28] and that YAP participate in metabolic reprogramming of cancer cells, such as glycolysis [29], [30]. In tumors, activation of YAP results in cellular uptake of glucose and promotion of glycolysis rate [31]–[33]. Nardone et al. revealed, that cell mechanics is determined by YAP-induced focal adhesions (FA) assembly and that YAP is directly regulating the FA-related gene expression [27]. Evidence points to cell density, shape, and matrix stiffness as factors, that affect YAP activity [23], [34]. TAZ, a homolog of YAP, has also been identified as a key mechano-transducer alongside YAP and is an effector in the Hippo pathway [34]. It is worth noting here, that YAP and TAZ are part of Hippo metabolic pathway, that in organs control the size and tumorigenesis [35]. Dephosphorylated and activated YAP changes its subcellular localization, and it is translocated into the nucleus, where it controls tissue growth and differentiation as well as cell division [35].

Interestingly, YAP modulate stem cell-based tissue renewal controlling the proliferation and differentiation via activation of mTOR [36]. It is possible, that mTOR and YAP may both participate in mechanosensing during tumorigenesis as a result of YAP's mechanosensitivity. We demonstrated how the hepatic tumor cell lines in a soft tumor microenvironment (storage modulus G' ~94 Pa) alters cellular size and significantly slows cellular proliferation through YAP-mTOR signaling axis [37]. However, the molecular mechanisms by which microenvironment stiffness promotes the development of liver pathologies, particularly tumor formation, remain poorly understood. YAP/TAZ mechanosensors are proposed to fill the gap between biophysical cues and the metabolic

transformation in tumor niche [38]. It is not surprising, that YAP/TAZ represent promising target for therapeutics to use in cancer treatment [28].

1.2   Liver pathology and stiffness

Liver is a multifunctional organ, maintain the detoxification of metabolites, decomposition of blood cells, protein biosynthesis, glycogen storage and production of digestive elements [39]. Liver is a large organ located in the upper right side of the abdomen. In human, liver normally weights approx. 1,5 kg and the width is about 15 cm. Liver is divided into left (smaller) and right (bigger) lobe. Within those lobes, there are functional units called hepatic lobules, that are characteristic with hexagonal shape. Inside hepatic lobules are located hepatic cells, that include macrophages, stellate cells, endothelial cells, biliary epithelial cells and hepatocytes. Hepatocytes are the most abundant cells within the liver and maintain a wide range of functions including metabolism of sacharides, proteins and lipids, detoxification the toxins, drugs and metabolic waste products, bile production, glycogen storage and albumin synthesis. Resident macrophages, so-called Kupffer cells are specialized immune cells localized within the liver sinusoid (Figure 4) and their primary role is the phagocytosing bacteria and foreign particles. Stellate cells produce collagen and play a crucial role in liver fibrosis, when liver injured or inflamed. Endothelial cells form the blood vessel, so-called sinusoid – a one cell-thin capillary, that maintain the transport of molecules between blood and hepatocytes. Finally, biliary epithelial cells, also called cholangiocytes, building a 3D network of bile ducts, also known as biliary tree [40].
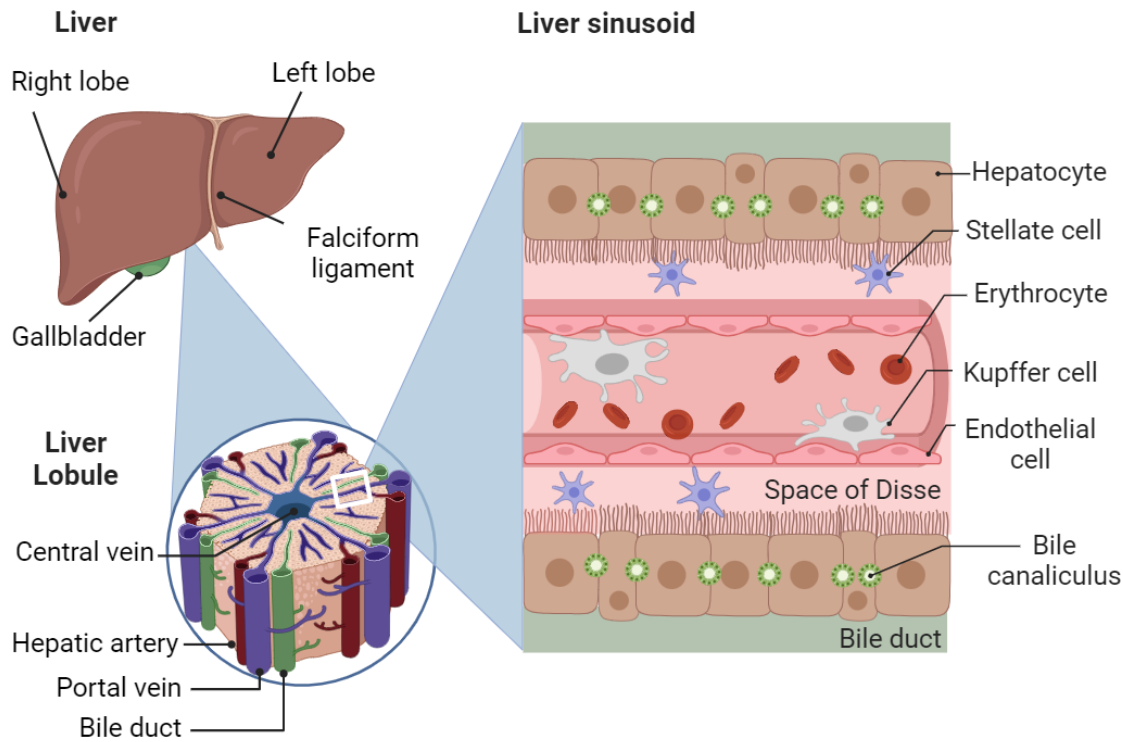
Figure 4: Schematic representation of liver, liver lobule and cross-section of liver sinusoid. *Endothelial capillary of sinusoid contains resident hepatic macrophages, so-called Kupffer cells. In Space of Disse are located stellate cells. Adapted from* [41]. *Created with Biorender.com.*

Hepatocellular carcinoma (HCC) is a highly abundant primary malignant tumor of the liver around the world [42] and one of the deadliest cancers at all [43]. Primary liver cancer is the 7th most frequently occurring cancer disease worldwide and 2nd most common cause of cancer disease mortality [44]. In global merit, HCC is the most abundant type of liver cancer, with ~75% abundance [45]. In Czech Republic, the data for malignant neoplasm of liver and intrahepatic bile ducts are following: in year 2021 the incidence was 988 people (absolute numbers) and mortality 883 people (absolute numbers) (source: ÚZIS ČR).

Cross-linked fibrous proteins and carbohydrates, such as collagen, elastin, laminin, and fibronectin, are present in the extracellular matrix (ECM) of the liver [46]. Metabolism of collagen is significantly deregulated in tumor progression, with either increased collagen expression, increased collagen deposition, altered organization or

increased matrix metalloproteinase, or matrixins (MMPs) activity [47]. MMPs are proteases capable to degrade ECM proteins and play a critical role in tumor cell invasion, carcinogenesis, angiogenesis, vasculogenesis and metastasis [47]. It is worth noting here, that high levels of MMPs correlate with poor prognosis in cancer [48]. Unfortunately, synthetic MMP inhibitors have failed as a promising treatment in clinical trial settings [47]. Inconsistently, type I collagen represents a physical barrier against tumor invasion, but elevated expression level of collagen is linked to incidence of metastasis [49]. A striking physical and mechanical characteristic of solid tumors is matrix stiffening (increase of the stiffness), which is primarily caused by excessive ECM protein deposition and cross-linking [50]. Increased stiffness is linked to an epithelial-mesenchymal transition (EMT) and enhanced proliferation in HCC.

A recent study demonstrated the morphological changes that occurred when HCC cell lines were grown on various substrate types. In contrast to the widely dispersed and flattened cells that grew on stiff supports (12 kPa), those that grew on soft supports (1 kPa) had a smaller, more rounded cell shape [51]. According to recent research, liver stiffness values between 1-5,5 kPa are considered as normal. In healthy adults, the liver stiffness is approximately 5,5±1,6 kPa [52]. Pathological occurrences, such as fibrosis, cirrhosis, and cancer progression, are associated with changes in the stiffness of the liver ECM. In fact, values between 10-75 kPa are associated with liver cancer [53]–[55]. Median value of liver stiffness from 17 patients with HCC was 55 kPa [56]. Cirrhotic livers were measured by transient elastography and revealed the values of stiffness in range from 12,5 to 75,5 kPa (Figure 5) [57]. Overall, a stiffer extracellular matrix (ECM) has been linked to chemotherapeutic resistance and the promotion of proliferation in HCC [51], [58], as well as accelerated cancer cell migration [59]. It is worth noting here, that cancerous tissue exhibits mechanical heterogeneity: the front tissue is significantly stiffer than the tumor core [60], [61]. In addition, low ECM stiffness (1-5 kPa) is associated with cancer stemness promotion or dormancy, which is a stage in cancer progression where the cells survive in a quiescent state while waiting for appropriate environmental conditions to begin proliferation again [62].
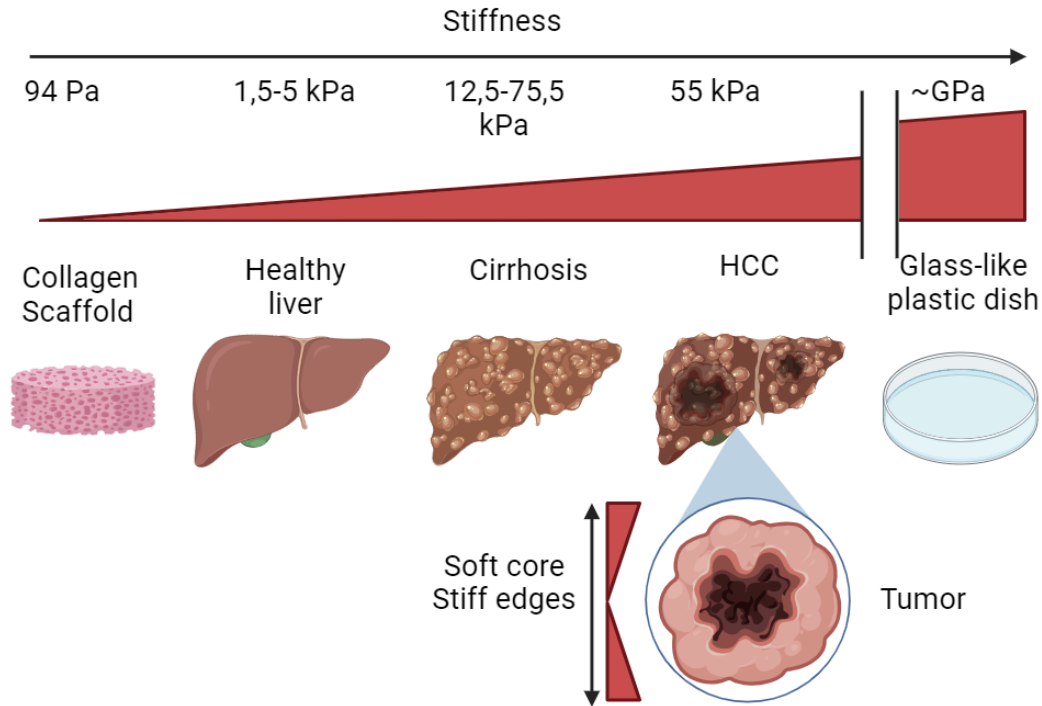
Figure 5: Schematic representation of stiffness measured in used experimental model and liver pathology. Created in BioRender.com.

In this dissertation, we used hepatocyte-derived immortalized cell lines, that are genetically different. These cells lines are derived from human patients with hepatocellular carcinoma (HCC) and/or hepatoblastoma (HB) [63], namely Alexander (also known as PLC/PRF/5) (ATCC) and HepG2 (American Type Culture Collection, ATCC). Alexander cell line (RRID: CVCL_0485) was originally isolated from a 24 years old African male donor with primary hepatocellular carcinoma (HCC), also called hepatoma and contains hepatitis B surface antigen, however they don't produce infectious virus [64]. HepG2 cell line (RRID: CVCL_0027) was isolated from a 15 years old Caucasian male donor and hepatitis B surface antigens are absent. Originally, HepG2 cells were identified as a hepatocellular carcinoma. However, there is conflicting evidence regarding the pathology of HepG2 cells and recently was proposed that HepG2 is hepatoblastoma [63]. Used cell lines are considered as a reliable cancer model and are often use for drug development and toxicity testing [65]–[67].

While it's true that not all cancer cell lines fully replicate in vivo tumor models, they still serve as a dependable preclinical model for fundamental research. [67]. HCC

cell lines such as HepG2 and Alexander have been found to retain the genomic and transcriptomic characteristics of primary HCC [65], [66]. Using HCC cell lines as preclinical models for basic research is therefore scientifically well-justified [65], [66].

1.3 Advanced 3D cell culture systems

In the liver, hepatocytes are parenchymal cells responsible for serum protein synthesis, bile production and drug metabolism [39]. The major sources of cells in hepatocyte cultivation are primary hepatocytes [68], immortalized hepatic cell lines [69] and pluripotent stem cells (PSC) [70]. Primary hepatic cells are the best qualified *in vitro* model, that represents liver landscape the most. However, the cultivation of primary hepatocytes has several drawbacks, such as limited lifespan and rapid dedifferentiation. Moreover, primary hepatocytes are difficult to maintain and require specialized culture conditions and media [71]. On the other hand, hepatic cell lines have theoretically unlimited lifespan and stable phenotype. In comparison with primary cultures, cell lines culturing conditions are simple and easy to implement. The major drawback of hepatic cell lines lies in drug metabolism capacities; cells like HepG2 express only few enzymes that are responsible for drug detoxication [71]. As we mentioned in previous chapter, liver cells, such as hepatocytes are under mechanical stimuli of extracellular matrix while developing a pathology, such as fibrosis or cancer. Therefore, the selection of immortalized cancer cell lines with genomic stability, such as Alexander and HepG2, is feasible to elucidate the mechanotransduction signaling pathways in modulation of cellular plasticity.

In general, there are different methods to cultivate hepatocytes, including 2D monolayer culture (MC), 3D cell culture, co-culture and spheroid culture [72]. 2D MC is a well-established and easy to maintain cultivation technique. Investigation carried out on 2D MC is robust and can be proceeded in high throughput screening analysis. Moreover, 2D MC might be decorated with ECM-derived biomaterial, including collagen, fibronectin or commercially-available Matrigel [72]. The aim of the 3D cell culture technique is to mimic ECM-like conditions in vivo. This was first achieved by "sandwiching" a monolayer of hepatocytes with a collagen layer on two sides, so-called sandwich culture [73]. With this approach, hepatocytes are embedded within two layers

of ECM molecule, that is imitating the Space of Disse from liver sinusoid anatomy (Figure 4). Nowadays, hydrogel-based techniques are available and represent a vital option for hepatocyte cultivating [74], [75]. 3D cell culture bridges the gap between *in vitro* and *in vivo* experimental conditions, that significantly improves the research and pharmaceutical development in drug discovery, toxicology and disease modeling [76]. The most advanced 3D cell culture is organotypic culture, so-called liver organoid [77].

3D cell cultures offer a physiologically relevant model for basic research in toxicology, disease modeling, and drug discovery [37], [78], [79]. 3D cell culture systems represent an advanced system, that is not always easy to analyze. Therefore, there is a growing interest to separate and mimic the specific microenvironmental cues, that 3D cell culture systems could yield [78], such as adhesion, mechanics and soluble factors. In comparison, traditional 2D monolayer cultures are robust, well-established, inexpensive, and easy to analyze [80]. In fact, 3D cell cultures point towards *in vivo*-like conditions and hold great promise in cell culture-based research. The extracellular matrix (ECM), which contains cross-linked proteins and carbohydrates, including collagen, is in fact a functional and specific substrate for liver cells such as hepatocytes.

3D cell culture systems have many advantages and strengths, including the fact that they could mimic *in vivo* settings [81], [82]. Moreover, substrate that contain ECM features induce cell-cell contact, communication and activation of signaling pathways [83]. 3D culture is highly versatile and could be supplemented by additional factors, such as proteins, that are found in tumor microenvironment [83]. Cells that are embedded in 3D culture are heterogenous population, that have distinct phases of cell cycle, such as hypoxic, proliferating and necrotic cells [84], [85]. Molecular patterns of protein expression level as well as cellular behavior are approaching *in vivo* conditions [86]–[89]. The key strength of 3D culture is the fact, that it provides *in vitro* model for inclusion of different cell types and create multicellular model for anti-cancer drug testing [90]. On the other hand, there are also disadvantages and limitations, that 3D cell culture possess. The variability of biomaterial-based 3D matrices could result into non-reproducible experimental results [75]. [83]. The biggest weakness of 3D cell culture systems is the

lack of vasculature, that is essential in tumor growth, survival and drug delivery as well [91], [92].

In fact, cellular attributes such as morphology [93], proliferation [51], [58], cytoskeletal remodeling [93], exposure to medium [51], adhesion [93], stage of cell cycle [51], gene/protein expression [37] and drug sensitivity [37], [94] varies greatly between 2D and 3D cell culture systems (Figure 6) [76]. Specifically, MCF-7 breast cancer cells in 2D culture system appears sheet-like flat and stretched, while cells cultured in 3D system occurred in round shape [79]. Prostate carcinoma cells LNCaP were cultivated in a 3D hyaluronic acid-based bilayer hydrogel system and display reduced ability to proliferate, in comparison with cells cultured in 2D monolayer [95]. In general, cells in 2D monolayer culture are exposed equally to cultivation media, that contains growth factors and nutrients, while in 3D cell culture this is not a case, because cells near the core of culture might not receive as many nutrients and growth factors as cells on the edge of 3D culture (Figure 6) [85], [90]. Because of that, majority of cells cultured in 2D culture are in the same cell cycle stage, while cells in 3D would experience wide array of stages, including proliferation, quiescence, hypoxia or necrosis [84], [85].
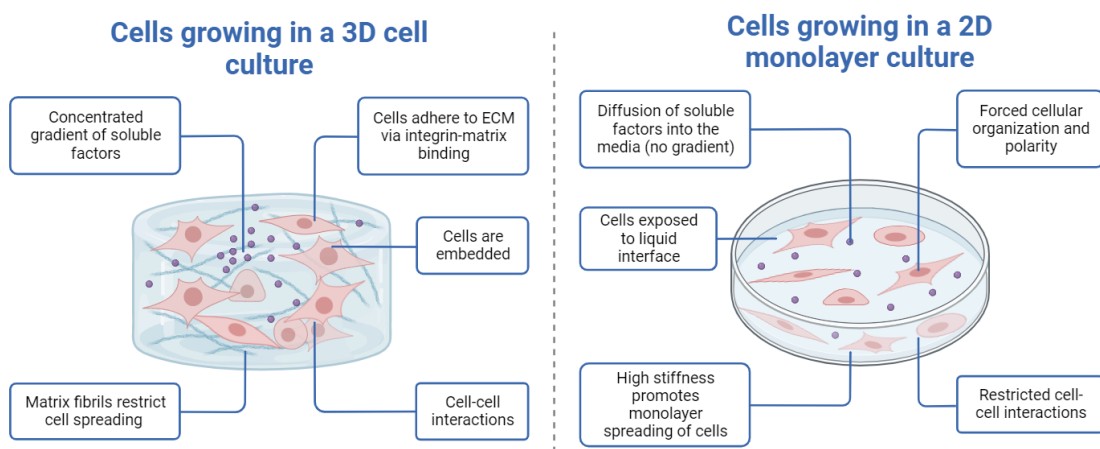
Figure 6: Comparison of 3D and 2D cell culture. Created with BioRender.com.

The methods used in tailoring the 3D cell cultures, include spontaneous aggregation, liquid overlay cultures, scaffold-based cultures, gyratory and spinner flasks, microcarrier beads, pre-engineered collagen composite scaffolds and rotary cell culture system [96]. It

is possible to produce in-house 3D cell culture systems, moreover usage of commercially available options, such as Matrigel, increasing the reproducibility of the research, because constant conditions are maintained [97].

In general, 3D cell culture represents an evolving platform that better mimic *in vivo*-like conditions of human or animal tissues. In comparison with 2D monolayer culture, 3D cultures permit cells to grow and interact with their surroundings in all directions as it is *in vivo*. Thus, adding one extra dimension offer distinct conditions that living cells can experience, in comparison with 2D cell culture. In recent years, the publication activity concerning the 3D cell culture is raising (Figure 7).
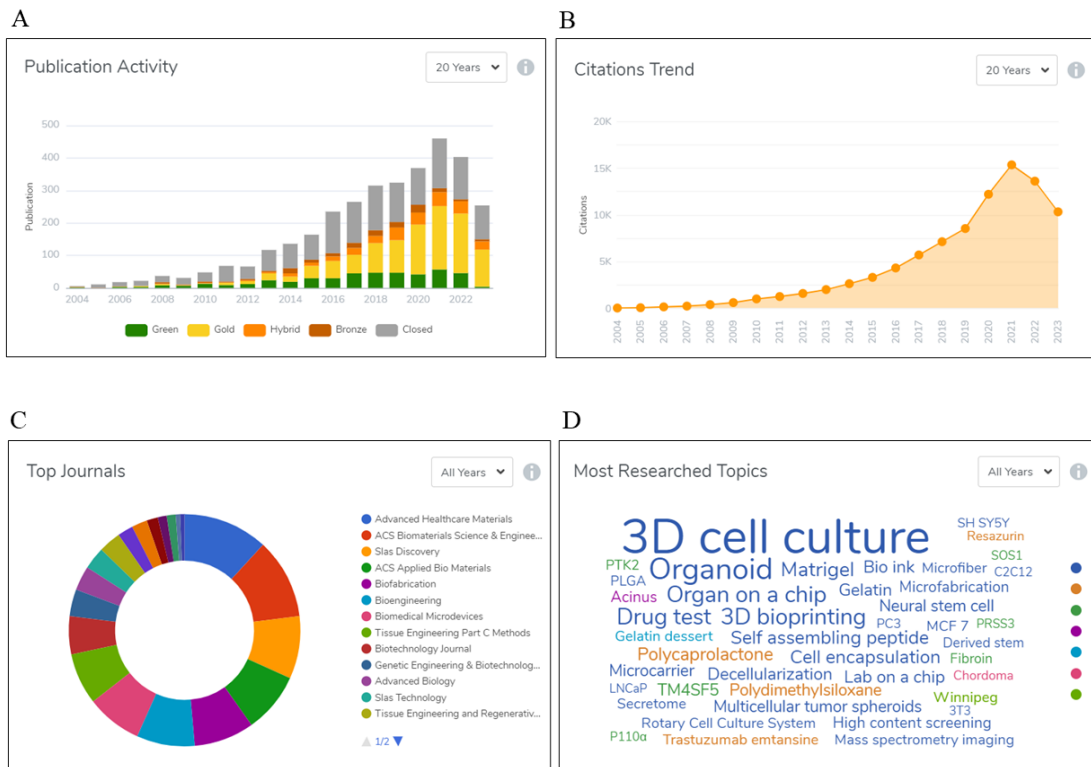
Figure 7: Statistical overview for topic "3D cell culture". *(A) Graph of publication activity in different publication access or closed categories during last 20 years. (B) Graph of citation trends during last 20 years. (C) Pie chart of most popular scientific journals for 3D cell culture, including ACS Biomaterials Science & Engineering [98]. (D) Word cloud for the keywords that are most popular within the research for "3D cell culture". Sourced from https://www.wizdom.ai/.*

1.4   Photobiomodulation as a tool modulating living cells

Light, as a natural phenomenon represents an amazing example of physical tool. With light we can modulate molecules and regulate biological processes [99], [100]. There is an exceptional association between light and biology. Microorganisms operate light-gated ion channels to perform phototaxis [101], plants convert solar energy into chemical energy in process called photosynthesis [102], and higher organisms are equipped with phototransduction-based vision system [103], [104]. Therefore, utilization of light sources, such as laser (acronym for Light Amplification Stimulated by Emission of Radiation) or light-emitting diode (LED) in biomedical applications is a logical extension of the evolutionary aspect of light in nature [104]–[109]. Moreover, light is a central modulator of circadian rhythms [110]. Certainly, light-based methods are exclusive and trusted tools in diagnosis, surgery and therapy [104]. Photobiomodulation (PBM), formerly known as Low-level Laser (Light) Therapy (LLLT) represents an advanced medical therapy approach, where laser or LED is modulating or improving the cellular target conditions [111]–[115]. "Low – level" refer to utilization of red and near infrared (NIR) light, because energy density of this light is low in comparison with laser therapy, such as ablation [111]. Historically, the development of this physics-based medical approach started in 1960s [111], when gradually solid-state and gas laser were invented. In 1967, at Semmelweis University in Budapest, scientists recorded that ruby laser could stimulate the regeneration not only of mechanically induced wounds, but also of burns in white mouse [116]. Later, the same research team applied their approach to human patients, in order to treat non-healing skin ulcers [117]. In 21st century, the current research of photobiomodulation is focusing on chronic joint disorders [118], rheumatoid arthritis [119] and osteoarthritis [120] disease treatment.

Fundamentally, light as a part of electromagnetic radiation (ER), is an important tool in diagnosis and treatment of human disease [104]. Certainly, ER spectrum waves and rays possess duality phenomenon, that the radiation is represented by particles as well as by waves [111]. In optics, light as a wave is described by Maxwell´s Equations, that supposed to have amplitude, that determines brightness of the light, wavelength that determines light color and vibration angle (polarization) [111]. According to quantum theory, ER consists of photons, a lightspeed and massless packets ("quanta") of energy

where number of photons determines brightness of the light, energy of photon determines the color and polarization is described in space and time (4D polarization) [111]. Underlying mechanistic principle of the PBM treatment is the induction of photochemical reaction in a living cell [111]. Light photon is absorbed by a chromophore (a part of the molecule, that absorbs specific wavelength) in the treated cells and become excited and jump from a low-energy orbit to a higher-energy orbit [113], [121].

Photobiomodulation operation is characteristic by biphasic dose response or so-called Arnt-Schulz curve [111]. Biphasic dose response means that lower doses of light are more beneficial than high doses [111], [121]–[124]. More specifically, if the applied light is not of sufficient irradiance or the irradiation time is too short that results into no response. On the other hand, if the irradiance is too high or treatment time is too long, then the response may be inhibited [125]–[127]. PBM/LLLT as a therapy remains controversial, because molecular mechanism of action and executive biochemical metabolism foundations of living cells interacting with light remains enigmatic [111], [114]. Secondly, in order to choose light parameters for each treatment application, one has to consider parameters including wavelength, fluence, power density, pulse structure and timeframe of the procedure [111]. It is worth to note here, that sub-optimal selection of parameter values may not only result in decreased effectivity of the treatment, but also negative therapeutic outcome or no effect may occur [111]. Red and NIR light (600-1070 nm) wavelengths fall into "optical/therapeutical window", that is defined by minimized absorption and scattering of light in key tissue chromophores within the NIR region [128].

There are some insights into molecular mechanism of PBM action. It was shown, that mitochondria might serve as a "sensor" and "effector" of non-specific interaction between laser light and living cells [104], [129]–[131]. It was found, that red laser induces MTCO activation [104], [129]–[131]. Matching spectra with laser light range used in PBM indicates that MTCO is the key chromophore in PBM response [132], [133]. Inner mitochondrial transmembrane protein complex cytochrome C oxidase (MTCO) is a bulky protein structure, that consists of two copper centers and two heme-iron centers and servers as a component of electron transport chain metabolic pathway [134]. Electron transport chain (ETC) represents a fundamental biological mechanism of ATP generation

using the oxidative phosphorylation [1]. Through ETC protein complexes, high-energy electrons from electron carriers passthrough a sequence of transmembrane proteins, including MTCO to the final electron acceptor, generating a proton gradient that trigger ATP production [1]. PBM of tissue results in an elevated cellular respiration via increase of metabolic products, including ATP, NADH, protein and RNA [135].

1.5 Challenges and perspectives

A substantial body of current research has consistently demonstrated that alterations in physical cues within the cellular environment led to corresponding shifts in cell behavior and functionality. While these studies yield valuable insights into cell plasticity, they often lack a comprehensive mechanistic explanation that examine the underlying processes driving these changes. Consequently, there is a critical knowledge gap concerning the intricate molecular mechanisms through which these factors exert their influence on cellular behavior and functionality. Therefore, the acquisition of a research in this regard holds great significance, serving both fundamental and practical interests. It not only contributes to our fundamental comprehension of molecular biology of living cells, but also holds the potential to offer practical applications in various areas, ranging from regenerative medicine to designing advanced therapeutic strategies in cancer treatment. By deciphering the intricate interplay between physical cues and cellular responses, we are looking for innovative interventions and technologies that can harness these mechanisms for improved scientific advancements and health outcomes.

2 AIMS

In this dissertation thesis we intended to elucidate the molecular mechanism of mechanotransduction and cellular plasticity under the physical cues of 3D cell culture in liver cancer cells. Therefore, we conduct comparative research analysis of hepatic liver cancer cell lines HepG2 and Alexander cultured in 3D cell culture in a soft ~94 Pa collagen scaffold (CS) under physical cues provided by CS, i.e., fibers and pores. As a comparison we used widely used traditional stiff (~GPa) 2D monolayer culture (MC) on a plastic dish (Figure 8).

The aims of this thesis are following:

- Develop and characterize the microarchitecture 3D cell culture model using the major liver ECM component collagen I

- Establish the cell culture of genetically validated Alexander and HepG2 liver cancer cell lines in 3D cell culture of collagen scaffold (CS)

- Capture the differences between hepatic cancer cell lines HepG2 and Alexander cultured either in soft 3D cell culture and in traditional 2D cell culture on stiff (~GPa) plastic dish

- Rigorously analyze the cellular behaviour, including cellular size alteration, proliferation dynamics, cytoskeletal protein element's structure reorganization and cellular adhesion of Alexander and HepG2 under the physical cues of CS

- Reveal the biochemical signaling of mechanotransduction and key molecular determinants involved in the cellular response to 3D soft ECM conditions such as YAP and mTOR

- Reveal the mitochondrial dynamics using the chemical agent's treatment and marked mitochondrial membrane potential in 3D CS

- Expose how physical cues of 3D CS affects metabolism, including glycolysis pathway, energy metabolism and autophagy

- Explain how photobiomodulation treatment with red laser light affect cells cultured in 3D CS and what are the mechanistic foundations for cellular response in 3D culture

Soft (~94 Pa) 3D Collagen Scaffold (CS)

Stiff (~GPa) 2D Monolayer Culture (MC)
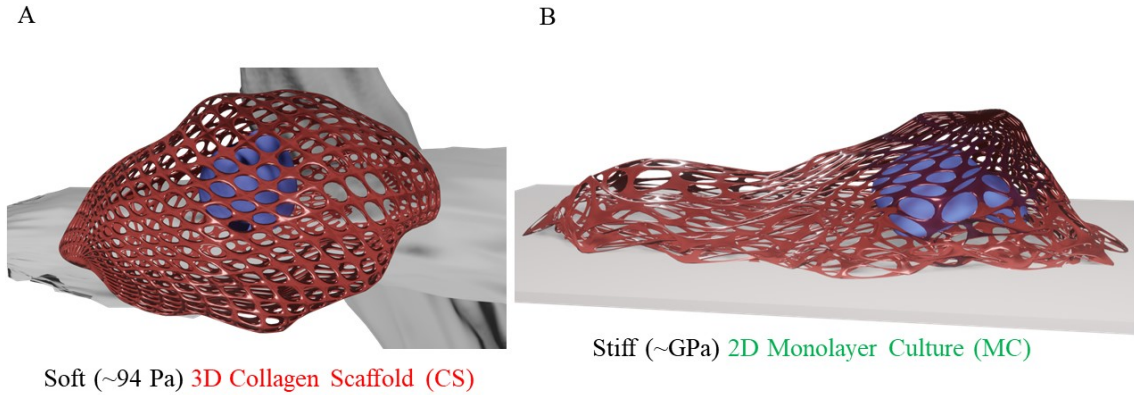
Figure 8: Schematic representation of living cell cultured either in 3D collagen scaffold or in 2D monolayer culture (plasma membrane in red, nucleus in blue). *(A) Schematic round cell attached to collagen fiber in 3D collagen scaffold (CS) that consists of fibers and pores. (B) Schematic stretched cell attached to the plastic Petri dish in 2D Monolayer Culture (MC). Rendered in Blender 3.3.*

To achieve these aims, we used advanced biomaterial-based 3D cell culture platform, i.e., collagen scaffold, biochemical assays, biophysical approach, genetic manipulation and photobiomodulation treatment. Specifically, we induce the mechanotransduction in HepG2 and Alexander hepatic cancer cell culture in 3D collagen scaffold. Our intention was to observe the alterations in the morphology and proliferation and reveal the changes in molecular signaling pathways and metabolic changes.

3 EXPERIMENTAL METHODS

This doctoral thesis represents a cross-disciplinary study and various methodology including biochemistry, biophysics and genetic engineering, that were used to achieve proposed aims. Briefly, description of methodology is listed here, while full experimental design and extended information for used methodological approaches are part of scientific papers published in Q1 journals [37], [98], and can be found in appendices (Appendix I, II).

3.1 Characterization of 3D collagen scaffold

For the preparation of disc-shaped collagen scaffold (CS) [37], [98], we used medical grade lyophilized collagen I (VUP Medical, a.s., Brno, Czech Republic) with dry basis min. 80% and used cryostructuring technique [136]. The CS preparation as well as CS stiffness determination was done by dr. Yuriy Petrenko and a team at the Department of Biomaterials and Biophysical Methods in the Institute of Experimental Medicine (ÚEM AVČR) in research group led by dr. Šárka Kubinová. In general, cryostructuring technique is widely used and consists of three stages: gelation, freezing and removal of frozen solvent [136]. We estimated the viscoelastic properties of the crafted biomaterial scaffold (CS). Rheological measurements were performed with modular compact rheometer MCR 92 (Anton Paar Ltd., St Albans, UK) with plate-plate crosshatched geometry setup using oscillatory strain sweep mode of frequency 1 Hz [37]. Using this setup and the oscillatory strain sweep mode with frequency 1 Hz we determined the storage modulus G´ and loss modulus G´´[37].

We were interested in microporous nature of collagen scaffolds (CS). Therefore, we used fluorescence contrast technique to visualize collagen fibers and pores. In order to expose the morphology of the CS in a native liquid environment, we labelled CS with low molecular weight fluorescent probe Col-F (ImmunoChemistry Technologies, LLC, Bloomington, USA), that exhibits affinity for collagen [137]. Particularly, we were interested in physical features of CS (so-called physical/mechanical cues), that are pores and fibers.

3.2   Cell culture of HepG2 and Alexander cell lines

Cell culture of HepG2 and Alexander cell lines was kept in Eagle´s Minimum Essential Medium (EMEM) culture medium (ATCC), that was enriched with 10% fetal bovine serum (FBS, ThermoFisher Scientific, Waltham, MA, USA) and 1% penicillin/streptomycin (ThermoFisher Scientific, Waltham, MA, USA) and changed once a week [37] [98]. Cell culture incubator was set to humidified 5% CO_2 atmosphere at 37 °C and represents our cultivation conditions (Figure 9B) [37] [98].

For 3D cell culture we used in-house synthesized soft collagen scaffold (CS) material described in the previous chapter. Briefly, after cells has been sub-cultured, harvested cells were seeded into CS. Approximately, 10^5 of HepG2 and Alexander viable cells in 30 µl were seeded into CS and placed in classic 6-well plate [37], [98]. After 1 hour of incubation at cultivation conditions (Figure 9B), a fresh and 37 °C-tempered medium was added to cover up the whole volume of the CS [37]. For every cell culture experiment, cells had been cultivated in CS for 7 days at cultivation conditions and EMEM medium was changed every other day (Figure 9) [37] [98]. As a 2D monolayer cell culture model, we used standard 35-mm wide standard glass bottom dishes (Cellvis, Sunnyvale, CA, USA) or 6-channel µSlide (Ibidi, Martinsried, Germany) [37], [98].

In order to improve the scientific validity, reliability, relevancy and overall quality of studied cellular model systems (HepG2 and Alexander cell lines), we verified the authenticity of human cell lines and match with standardized short tandem repetition (STR) genetic code profile reference [138], [139], using the commercially available service (ATCC, Manassas, VA, USA). According to the service provider instructions, we prepared cell culture samples of HepG2 and Alexander and shipped the sample to ATCC company for genetic analysis of STR using PowerPlex® 18D System (Promega).

In order to keep validity of the cell culture system models we monitor level of Mycoplasma contamination [140], [141] using selective biochemical test MycoAlert™.
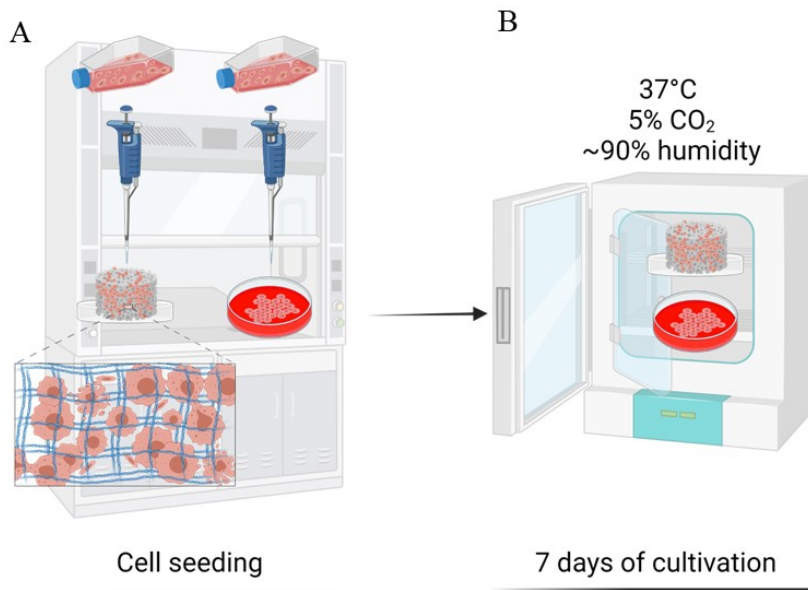
Figure 9: Schematic representation of procedure for cell seeding and culturing. *(A)*
Cells were seeded into collagen scaffold (CS) and monolayer culture (MC). (B) Cell
culture conditions of incubator. Created with Biorender.com.

3.2.1 siRNA transient transfection

siRNA transient transfection represents a genetic engineering method and
advanced molecular biology technique. We have used commercially-available product
Lipofectamine 3000 that is increasing the transfection efficiency of RNA, including small
interfering RNA (siRNA), in cell cultures using the lipofection. In this thesis, we used this
genetic manipulation technique in 2D monolayer cell culture in order to transiently
decrease the expression of YAP protein. Briefly, cells were seeded onto 12-well plates at
a density of 400,000 cells per well [37]. After 24 hours, cells were transfected with 1.5 μg
of YAP1 Silencer Select per well using Lipofectamine 3000 transfection reagent (Thermo
Fisher Scientific, Waltham, USA) and followed the manufacturer instructions [37]. After
24 and 48 hours from siRNA transfection procedure, cell lysates were collected for protein
analysis. For utilization of transfected cells in immunofluorescence, we seeded viable cells
onto 6-channel μSlide (Ibidi, Martinsried, Germany) at a density of 1,5 x 10^4 /channel
[37]. After 24 hours of incubation at cultivation conditions (Figure 9B), cells were
transfected with 150 ng of YAP1 Silencer Select siRNA [37]. After 48 hours of siRNA
transfection, cells were stained for immunofluorescence microscopy.

3.2.2 Cell extracts and immunoblot analysis

To compare different protein expression profiles between 2D monolayer and 3D cell culture, we used immunoblot analysis (also known as Western blot). In order to execute that, we collected cell extracts using the lysis radioimmunoprecipitation assay (RIPA) 1x solution (Millipore, Burlington, VT, USA) supplemented with protease and phosphatase inhibitors [37], [98]. We performed the assay according to the manufacturer directions and our verified protocol [140]. Briefly, aliquots of whole-cell lysates containing equal amounts of protein concentration were prepared using Micro BCA™ Protein Assay kit (Thermo Fisher Scientific) [37]. Individual proteins were separated at denatured conditions, using sodium dodecyl sulfate–polyacrylamide gel electrophoresis (SDS-PAGE) [37], [98]. Later, separated proteins on polyacrylamide gel were transferred to Invitrolon™ polyvinylidene difluoride (PVDF) membrane (Invitrogen, USA), that has 0.45 µm pore size [37], [98]. Invitrolon™ PVDF membranes are suitable for high sensitivity and low background immunoblotting and represents the optimal solution for Western transfers of proteins > 10 kDa (Invitrogen, USA). To prevent antibodies from binding to the membrane non-specifically, we blocked the PVDF membrane using either 5% (w/v) fat-free dried milk or, alternatively, 5% (w/v) bovine serum albumin (BSA) for 1h [37], [98]. Subsequently, PVDF membranes were incubated with various specific primary antibodies (see Appendices I and II for details) at 4°C in circular motion overnight [37], [98]. Finally, chemiluminescence signals were detected using the imaging system GBOX CHEMI XRQ (Syngene, Synoptics group, Cambridge, UK) as was described [141]. The chemiluminescence signals were recorded using acquisition software GeneTools (Syngene, Synoptics Group, Cambridge, UK) and densitometric quantification of blot protein bands were execute using GeneTools quantification software (Syngene, Synoptics group, Cambridge, UK) [37], [98]. To determine the protein band size, we used a marker Precision Plus Protein™ Dual Color Standards, that contain recombinant proteins designed to provide a consistent size ladder (10-250 kDa) (Bio-Rad, USA).

3.3 RNA isolation and quantitative measurement of gene expression from human patients

In order to measure the gene expression in human liver samples, we used real-time polymerase chain reaction (PCR). Human samples of neoplastic liver tissues were

procured from patients during surgical resection at the Transplant Surgery Department of the Institute for Clinical and Experimental Medicine (IKEM). All patients signed the informed consent. Clinical samples collection was performed according the standards and approved by the IKEM and Thomayer University Hospital Research Ethics Committee [142]. Briefly, total RNA samples from 12 human patients' cohort were isolated and purified using silica-membrane spin columns RNeasy Mini Kit (Qiagen, Hilden, Germany), followed by DNA removal procedure using RNase-Free DNase Set (Qiagen, Hilden, Germany) [98]. In order to determine the integrity, purity and quantity of isolated RNA samples, we used NanoDrop One Microvolume UV-Vis Spectrophotometer (Thermo Fisher Scientific) [98]. To generate cDNA we used Maxima H Minus First Strand cDNA Synthesis Kit (Thermo Fisher Scientific, USA). According to the previously published protocol [143] we used 2 µg of RNA to synthesize the cDNA. Real-time PCR was performed on an Applied Biosystems Viia7 Real Time PCR system (Applied Biosystems, Waltham, MA, USA) using the Fast Advanced TaqMan Gene expression Master mix (Thermo Fisher Scientific, Waltham, MA, USA) and pre-designed commercially available specific TaqMan Gene Expression Assays (Appendix II) [98]. Data were analysed using Microsoft Excel and MaxStat Pro 3.6 software (MaxStat, Cleverns, Germany) [98]. According to previously published study [144] we used $2-\Delta\Delta CT$ methodology to determine the expression of target gene by normalizing to GAPDH gene expression [98].

3.4 Spectro-fluorometrical analysis

3.4.1 Pyruvate content analysis

In order to glimpse into basic cellular regulation pathways, we analysed metabolism of pyruvate, an output of the glycolysis, where one molecule of glucose breaks down to two molecules of pyruvate. Subsequently, pyruvate enter mitochondria and it is further metabolized via tricarboxylic acid cycle. Therefore, we performed colorimetric assay, using the Pyruvate Assay Kit (Sigma Aldrich, St. Louis, MO, USA) [98] and followed manufacturer directions. Briefly, we have collected cell extracts and determined protein concentration as we described in section 3.1.2. *Cell Extracts and Immunoblot analysis*. Endogenous lactate dehydrogenase (LDH) might degrade lactate, therefore we performed deproteinization of samples using a 10 kDa molecular weight cut-off (MWCO)

spin filter VIVASPIN (Sartorius, Goettingen, Germany) [98]. Deproteinized samples were mixed with Pyruvate Assay Kit chemistry according to the manufacturer direction, incubated and colorimetric assay was performed [98]. The intensity of signal was recorded using a Tecan microplate reader SpectraFluor Plus (Tecan, Männedorf, Switzerland) [98]. The amount of pyruvate was calculated using the calibration curve obtained from pyruvate standards, that run simultaneously in assay with the samples of interest. Pyruvate molecule content is expressed in nmol/mg of total protein content units [98].

3.4.2 Lactate content analysis

Another important molecule in cellular metabolism is lactate, that can be oxidized to pyruvate or converted to glucose via gluconeogenesis metabolic pathway. We have used Lactate Assay Kit (Sigma Aldrich, St. Louis, MO, USA) and performed colorimetric assay in accordance with the manufacturer directions [98]. Briefly, we have gathered cell extracts and determined out protein concentration as we described in section 3.1.2. *Cell Extracts and Immunoblot analysis*. Samples were deproteinized and processed as we describe in 3.3.1. *Pyruvate content analysis*. The intensity of colorimetric signal was detected using the Tecan microplate reader SpectraFluor Plus (Tecan, Männedorf, Switzerland) [98]. The amount of lactate was calculated using the calibration curve obtained from lactate standards, that run simultaneously in assay with the samples of interest. Lactate molecule content is expressed in µmol/mg of total protein content units [98].

3.5 Ultra-fast high-resolution confocal microscopy

We used the brand-new high-resolution spinning disk confocal system IXplore SpinSR Olympus IX3 (Olympus, Tokyo, Japan) to produce high-quality confocal images [145], [146]. A spinning disc confocal unit (CSUW1-T2S SD; Yokogawa, Musashino, Japan) and an inverted microscope (IX83; Olympus, Tokyo, Japan) that were included in the system. Spinning disk confocal microscopy represents novel and innovative approach to live-cell imaging that is used for observation and visualization of cellular components and organelles, including microtubules, mitochondria and lysosomes [147]. Fluorescence images were captured using either a 20x objective (LUCPLFLN20XPH NA 0.45 air lens, Olympus, Tokyo, Japan) or a 100x silicone immersion objective (UPLSAPO100XS NA

1.35 WD 0.2 silicone lens, Olympus, Tokyo, Japan). Fluorophores were excited at the proper wavelengths using laser diodes with output powers of 50 mW at 405 nm, 100 mW at 488 nm, and 100 mW at 561 nm. At a definition of 2048x2048 pixels, confocal images were captured. Two digital CMOS cameras ORCA-Flash4.0 V3 (Hamamatsu, Hamamatsu City, Japan) simultaneously captured the images after passing them through the necessary emission filters (BA420-460, BA575IF, BA510-550; Olympus, Tokyo, Japan). The acquisition program cellSens (Olympus, Tokyo, Japan) was used to capture and store fluorescence confocal images. HepG2 and Alexander cells were cultured in monolayer culture (MC) or collagen scaffolds (CS) under standard conditions (Figure 9B). Following that, cells were either imaged live or fixed and immunostained using the fluorescent probes and antibodies (see Appendices I and II for details). Cells were fixed with 4% paraformaldehyde for 10 minutes at room temperature in PBS with a pH of 7.4. Before staining, samples were permeabilized with 0.5% Triton X-100. Primary antibodies against various proteins, as listed in Appendix I and II, and an Alexa Fluor 568-conjugated secondary antibody (Thermo Fisher Scientific, Waltham, USA) were used for immunofluorescence staining on fixed cells (Figure 10A). The spinning disk confocal microscope IXplore SpinSR (Olympus, Tokyo, Japan) was used to capture images of stained cells (Figure 10B). For image processing and quantification, ImageJ software (NIH, Bethesda, MD, USA) was used [37] [98].
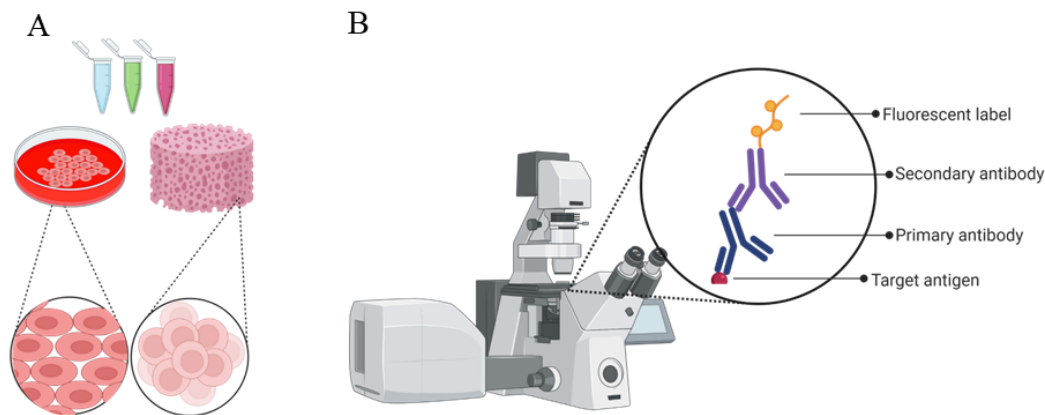

Figure 10: Schematic representation of procedure for cell labeling and capturing of immunofluorescence using ultra-fast high-resolution confocal microscopy. (A) Cells were labeled with florescent probes or primary antibodies with affinity to specific protein

and subsequently labeled with secondary antibody that was attached to a fluorophore. (B) Detail on immunofluorescent procedure and its components. Created with Biorender.com.

3.6 Photobiomodulation: High-Fluence Low-Power (HFLP) laser treatment for cell culture

In this thesis, we used a previously described laser system to expose cells to 649 nm wavelength in order to cause severe mitochondrial dysfunction [129], [148]. Experimental setup of the HFLP laser system contained a fiber taper with a waist diameter of 15±5 μm, that was used to deliver 649 nm laser light from the system to a cell culture. An optical power meter PM100D (Thorlabs, Newton, NJ, USA) was used to measure the output laser power, which was maintained at 63±1 μW [148], [129]. Before being exposed to laser radiation, cells were seeded into a collagen scaffold (CS), cultured for seven days, and labeled. We used a two-color fluorescence assay LIVE/DEAD® Viability/Cytotoxicity Kit (Thermo Fisher Scientific, Waltham, MA, USA), to determine the viability of cultured cells [98]. The optical taper was cleaned with 70% ethanol before being placed on the cells. Using an Olympus IX83 microscope (Olympus, Tokyo, Japan) connected to a Micromanipulator 5171 (Eppendorf, Wesseling-Berzdorf, Germany), the optical taper's position to the close proximity of the cellular population was established [98].

3.7 Quantitative analysis of confocal microscopy digital images and its automatization

Authentic microscopy images were captured using software cellSens (Olympus, Tokyo, Japan). ImageJ software (NIH, Bethesda, MD, USA) was used for image processing and quantitative analysis [37] [98]. The following parameters were quantified using ImageJ software (NIH, Bethesda, USA): cell and nuclei sizes, collagen pore size, collagen fiber width, cell number, and fluorescence line scans. By selecting 5 to 10 visual fields at random from each sample and using the same setting parameters (such as spinning disk speed, laser power, and offset gain), quantitative image analysis was carried out.

3.7.1 Automatization of quantitative analysis of mitochondrial membrane potential using ImageJ macros

We have created macros using the "Recorder" function in ImageJ software (NIH, Bethesda, MD, USA) in order to perform efficient and semi-automated quantification of

the JC-1 green-to-red fluorescence ratio. Using Macro 1 (Supplement Material [98] from Appendix II), contrast and brightness enhancement were carried out. Following, individual cells were manually chosen using the Region of Interest (ROI) Manager function. Additionally, integrated densities for specified ROIs of the red and green channels were measured, and Macro 2 (Supplement Material [98] from Appendix II) then calculated the ratio of the integrated densities for the red channel and green channel. Using Macro 3 (Supplement Material [98] from Appendix II), digital images were displayed as a multi-stack montage. After manually choosing the ROI for the presentation, the montage for the green, red, and combined channels was then completed using Macro 4 (Supplement Material [98] from Appendix II) [98].

3.8   Statistical analysis

Quantitative results are given as $\pm$SEM (standard error of the mean). Sample size was determined using a statistical method, stated in [149], considering the 95% confidence level and 0.9 statistical power [37]. All statistical analyses were carried out using SigmaPlot 13 (Systat Software, Palo Alto, CA, USA) and MaxStat Pro 3.6 software (MaxStat Software, Cleverns, Germany) [98]. At (*) $p < 0.05$, differences were deemed statistically significant. We used the published instructions for quantitative confocal microscopy to quantitatively analyze the images [150], [151]. A quantitative analysis was performed on images from three separate experiments. We used a statistical technique that was previously described to determine sample size [149].

4 EXPERIMENTAL RESULTS

4.1 Characterization of 3D scaffold morphological structure

In-house sponge-like collagen disc-shaped scaffolds were produced [37], [98] using the cryostructuring technique [136]. Synthesized 3D collagen scaffold has open-cell facetted architecture, that is effective for culturing high density cell suspensions [96]. Accumulating evidence suggest, that extracellular matrix (ECM) stiffness modulate the hepatic cancer cells proliferation rate. High substrate stiffness, e.g., glass, increases the proliferation rate [51], [58], while low stiffness, e.g., collagen scaffold decreases the proliferation [37], [152]. Correspondingly, ECM stiffness in range between 1-5 kPa is associated with decreased proliferation and cancer stemness promotion [62]. Specifically, phenotypic cancer stem cells (CSC) surface markers were observed in hepatocellular carcinoma (HCC) cells under soft cell culture conditions (5,9 kPa) [153]. Therefore, in order to reveal the stiffness of CS we characterize rheological/viscoelastic properties and determine storage modulus G' and loss modulus G" [37]. We found that in-house made 3D CS have values ~94 Pa for storage modulus and ~0 Pa for loss modulus [37]. In comparison, a plastic dish used for conventional 2D monolayer cell (MC) culture has stiffness in range of ~GPa [80]. Unlike on 2D MC, 3D culture provides distinct competing mechanical cues, including adhesion and pressure [37]. Basically, there are two distinct mechanical cues that cells experience in collagen scaffold, i.e., fibers and pores (Figure 11).

In order to observe porous architecture of collagen scaffold (CS) at a micrometer [μm] scale, we decided to use low molecular weight fluorescent probe ColF, that display high affinity for collagen [137]. To maintain the size and shape of disc-like morphology of CS, we intentionally avoid experimental methods, where glutaraldehyde or formaldehyde treatment and ethanol or acetone dehydration will be used. Mentioned chemical agents are fixatives, that could cause chemical changes on the morphological micro-structure [154]. Instead of that, we used a method, where sample is prepared in native liquid medium, such as phosphate-buffered saline (PBS) and ultra-fast high-resolution confocal microscopy fluorescence imaging using confocal system Olympus IXplore SpinSR.
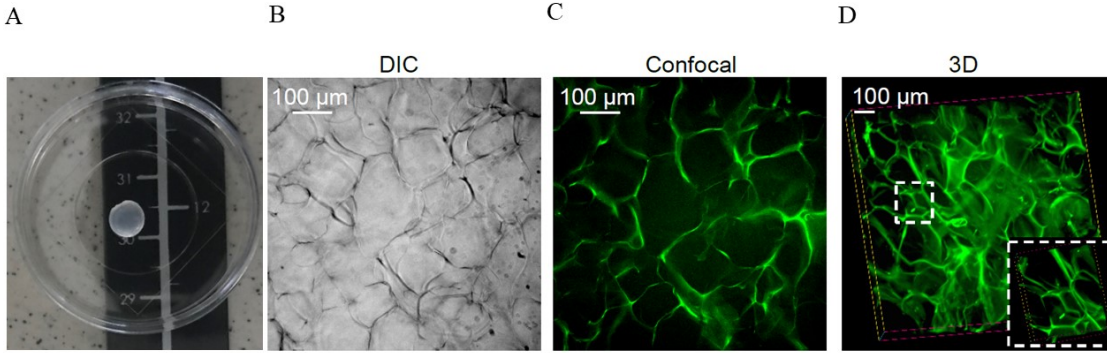
Figure 11: Collagen scaffold (CS) micro-architecture confocal microscopy analysis. *(A) Representative image of in-house cryo-structured disc-shaped collagen scaffold (CS) in plastic Petri dish, scale included [cm]. (B) Differential Interference Contrast (DIC) microscopy image of CS. (C) Confocal plane image using ColF fluorescent probe. (D) 3D reconstruction of Z-stack confocal images using the ColF fluorescent probe. Reprinted from open-access article* [37] *under the terms of the Creative Commons Attribution License.*

Using fluorescent method, we were able to observe how collagen fibers morphological organization define the alignment of fibrous network and space of pores within the CS (Figure 11,12) To describe the sizes, we measured the size of the pores (n=183) as well as the thickness of the collagen fibers (n=57) [37]. We revealed, that the thickness of the collagen fibers is in the range from ~0,8 to ~3,2 µm and the size of pores is in range from ~30 to ~200 µm (Figure 12) [37].
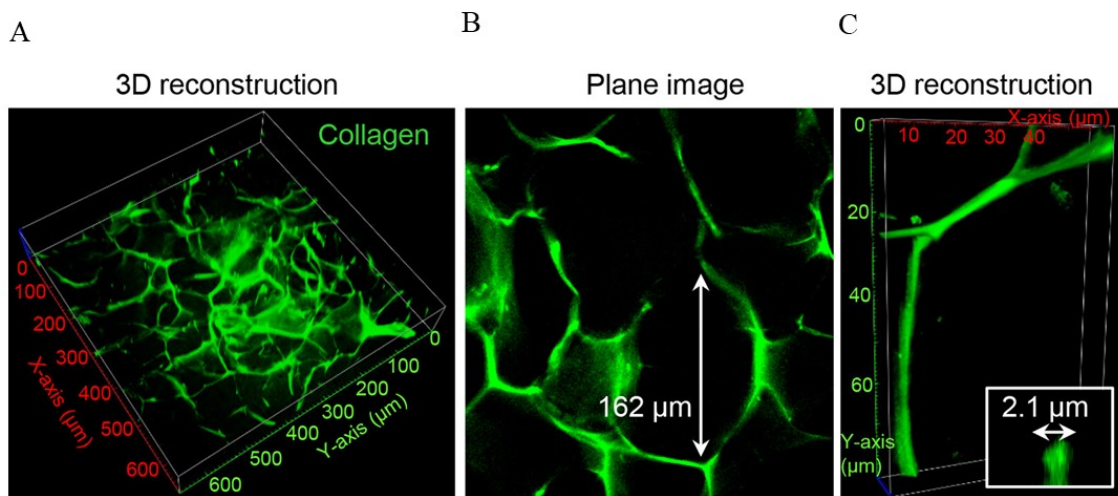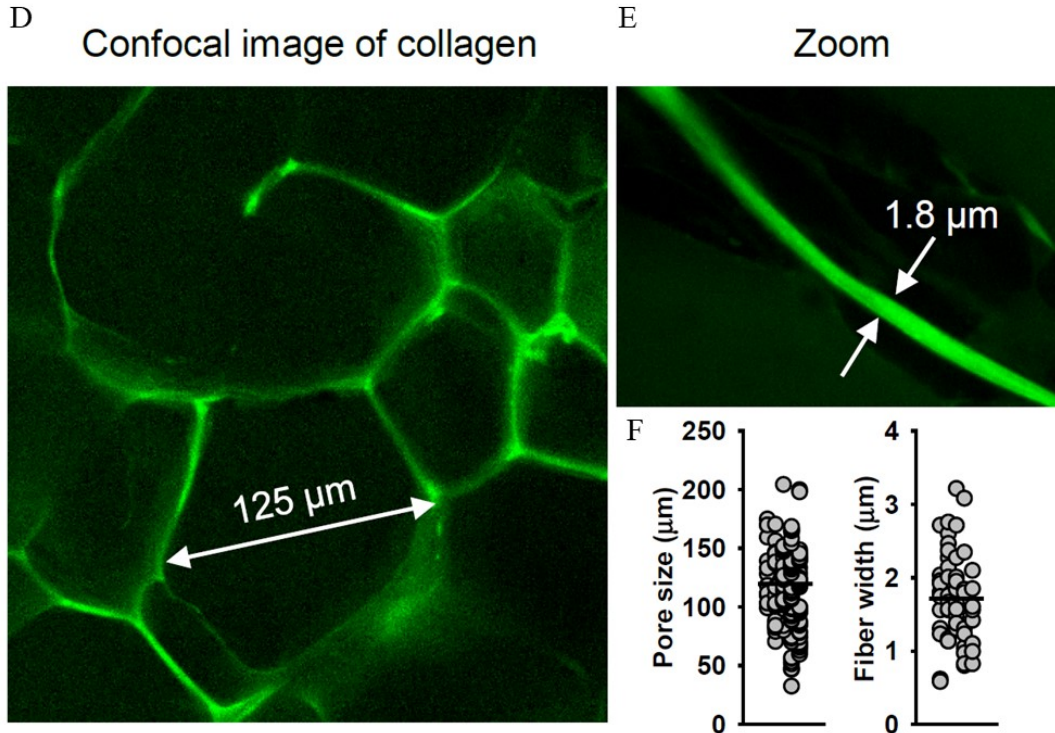
Figure 12: High-resolution confocal images of collagen scaffold (CS) labeled with ColF fluorescent probe. *(A) 3D reconstruction of Z-stack images. (B) Representative plane image of CS. (C) 3D reconstruction of Z-stack images highlighting the single collagen fiber. Insert represents the cross-section of the collagen fiber. (D) Confocal plane image of CS, highlighting the collagen pore. (E) High resolution detail of collagen fiber. (F) The physical cues of CS are pores and fibers. Quantification of pore sizes (n=183) and fiber thickness (n=57) was determined. Reprinted from open-access articles* [37], [98] *under the terms of the Creative Commons Attribution License.*

4.2 Genetic validity of Alexander and HepG2 cell lines

There are many reasons why to question and validate authenticity of cell lines, including growing concerns about reproducibility issues in cell culture models and improve the scientific data credibility [155], [156]. Recently, Liu et al. [157] used multi-omics approach to reveal the biological variations across 14 HeLa cell samples [157]. Investigation of more than 10,000 scientific papers revealed, that discussion for laryngeal cancer or normal intestine were based on studies using cell lines contaminated with HeLa cell line [158]. According to the International Cell Line Authentication Committee (ICLAC) there is a 582 misidentified cell lines and 535 cell lines has unknown authentic

stock source [159]. Therefore, it is an essential to check the authenticity of used cell lines in cancer research [159]. To address this question, we prepared the samples of HepG2 and Alexander cell lines and purchased genetic analysis for Human Cell STR Profiling, commercial service from company American Type Culture Collection (ATCC). STR markers are specific DNA repetitive motifs, that are unique to each organism, therefore human have different set of STR in comparison with other species, such as mouse [160], [161]. It was confirmed that, STR markers are overlapping with ATCC reference database with Alexander (also known as PLC/PRF/5), Hepatoma; Human (Homo Sapiens) for Alexander cells sample on 100% (Table 1) For Alexander cell line, 8 core STR markers plus amelogenin were examined (Table 1). Some STRs contain one value for number of repeats, which means the homozygosity, while others display two values, which means heterozygosity. Briefly, chromosomes are present in the human genome in pairs (2x23 chromosomes), while one chromosome from pair is from one parent, the other one chromosome from pair is from another parent. Amelogenin locus reveals the gender of the donor.

Table 1: Genetic analysis of 8 core STR loci plus amelogenin for Alexander cells. The number of shared alleles between sample and database profile is an exact match and 100% overlap.

STR Genetic locus	Alexander Cells line Test sample		Alexander ATCC Reference Database	
TH01	8		*8*	
D5S818	12		*12*	
D13S317	11	12	*11*	*12*
D7S820	9	11	*9*	*11*
D16S539	13		*13*	
CSF1PO	10		*10*	
Amelogenin	X		*X*	
vWA	15	16	*15*	*16*
TPOX	8		*8*	

Further, STR markers are overlapping with ATCC reference database with HepG2; Hepatocellular; Carcinoma; Human (Homo Sapiens) for HepG2 cells sample on 100% (Table 2). For HepG2 cell line, 8 core STR markers plus amelogenin were examined

(Table 2). We provide the full profile and scoring values for analysis of each cell line (Table 1,2). According to the genetic analysis of STR (provided by ATCC), both cell lines Alexander and HepG2 were well-maintained and 100% authentic (Table 1,2).

Table 2: Genetic analysis of 8 core STR loci plus amelogenin for HepG2 cells. The number of shared alleles between sample and database profile is an exact match and 100% overlap.

STR Genetic locus	HepG2 cells sample Test sample		*HepG2 ATCC Reference Database*	
TH01	9		*9*	
D5S818	11	12	*11*	*12*
D13S317	9	13	*9*	*13*
D7S820	10		*10*	
D16S539	12	13	*12*	*13*
CSF1PO	10	11	*10*	*11*
Amelogenin	X	Y	*X*	*Y*
vWA	17		*17*	
TPOX	8	9	*8*	*9*

4.3 Cellular and nuclear size alteration under the physical cues of 3D collagen scaffold cell culture

After 7 days of cultivating the cells in CS we were interested how size and shape of cells Alexander and HepG2 was affected by physical cues of 3D CS. Therefore, we used spinning disk confocal microscopy Olympus IX83 and fluorescent probes to detect the size of nucleus and cellular plasma membrane [37], [98].

In order to visualize how cells interact with collagen fibers, we used ColF fluorescent probe (green) to label collagen I and CellMask™ Orange (red) and Hoechst 33342 (blue) to counterstain the nucleus (Figure 13) [37]. We found that cells experience distinct conditions inside the collagen scaffold depending on whether they are attached close to the fiber or are located within the collagen pore (Figure 13CD) [37]. We observed that cells in the collagen pores display round shape, while cells attached to collagen fiber were stretched and flat [37].
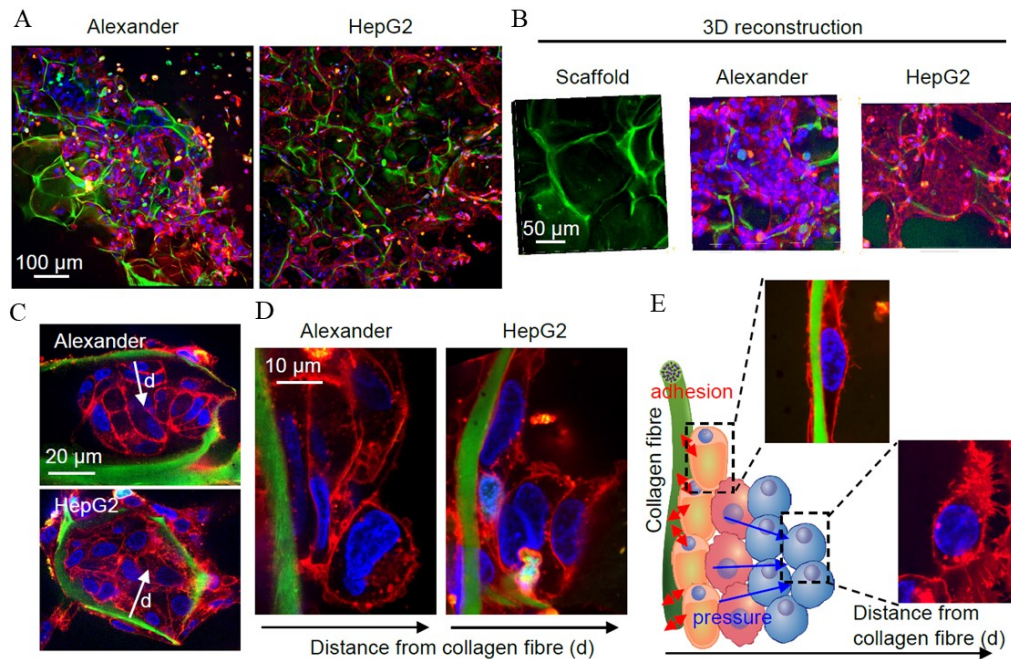
Figure 13: Alexander and HepG2 cancer cells were cultured in 3D collagen scaffold (CS) for 7 days and captured by confocal microscopy. Used fluorescent probes: CellMask™ Orange (red) for plasma membrane, ColF (green) for collagen, and Hoechst 33342 (blue) for cellular nucleus. (A) Representative images of cells, at magnification 20x. (B) 3D reconstruction of captured Z-stack images for CS without cells, and with Alexander and HepG2 in CS. (C) Detail on single collagen pore populated with Alexander or HepG2 cells. (D) Detail on a collagen fiber and cells. (E) Schematic representation of proposed concept of distinct physical cues that arouse from CS and affect cell plasticity and features. Reprinted from open-access articles [37] under the terms of the Creative Commons Attribution License.

High-resolution confocal analysis of HepG2 and Alexander cells (Figure 14AC) displayed that cultivation in CS resulted in a decrease of cellular size in both, Alexander and HepG2 cells, while nucleus size was decreased only in Alexander cells and was not affected in HepG2 cells (Figure 14B).
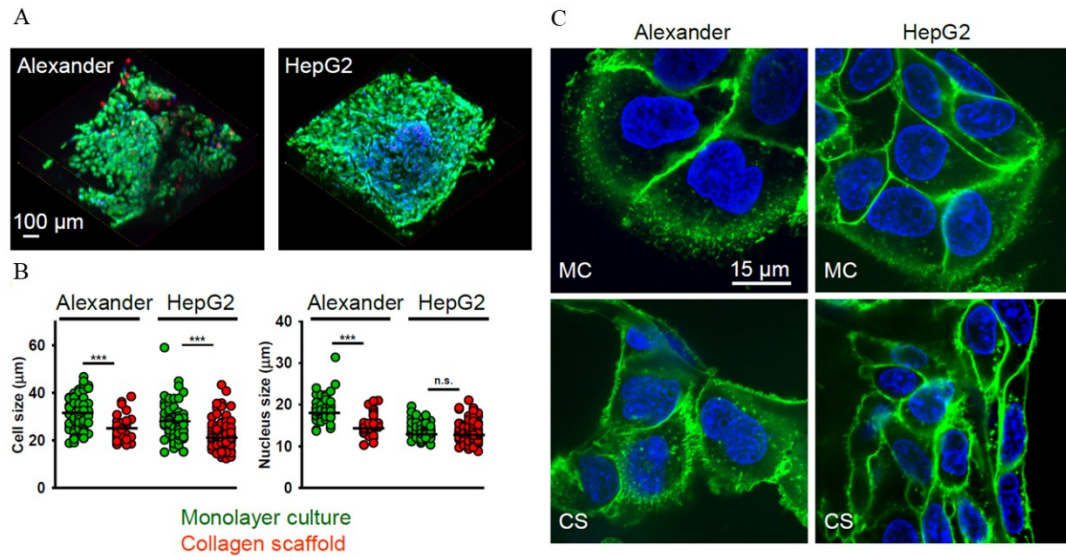
Figure 14: Viability and size alternation under physical cues of 3D collagen scaffold (CS) in comparison with 2D monolayer culture (MC). (A) Cells were labeled with calcein-AM (green), ethidium homodimer (red) and counterstained with Hoechst 33342, 3D reconstruction was done from captured Z-stack confocal images. (B) Quantitative assessment of cellular size and nuclear size of Alexander and HepG2. (C) Representative confocal images of Alexander and HepG2 cells cultured either in CS or MC and labeled with CellMask™ (green) and Hoechst 33342 (blue). Reprinted from open-access article [37] *under the terms of the Creative Commons Attribution License.*

4.4 Proliferation kinetics

The level of proliferation in living cells is an essential feature of cancer disease development and progression [162]. Alexander and HepG2 cell lines have malignant origin of either HCC or hepatoblastoma, therefore, marked proliferation might be expected. However, tumors have different stiffness, with soft core and stiff edges, which might affect proliferation significantly [60].

In order to estimate the rate of the proliferation of Alexander and HepG2 hepatic cancer cells, we initially used Hoechst 33342 nuclear staining to observe the alterations in proliferation dynamics during the four days of cultivation (Figure 15A). In order to determine the proliferation changes exactly, we used specific markers, including Ki-67 and proliferating cell nuclear antigen (PCNA). Ki-67 is a nuclear antigen and represents indicator of active cell proliferation within the cellular population. Ki-67 function has

peak in expression during G2 phase and mitosis [163]. Ki-67 is a functional protein entity, that serve as a keeper of distance for mitotic chromosomes and also contribute to the formation of peri-chromosomal protein assembly [163]. As a prominent cancer marker, its evaluation is used in many types of cancers [164]. Ki-67 protein correlate with metastasis, therefore it represents promising target in diagnosis and treatment of cancer disease [165]. We used immunofluorescent detection on confocal microscope and measured the Ki-67 proliferation index [152]. We repeatedly captured confocal images of Alexander and HepG2 cells cultured either in MC or CS and stained them at the 7th days of cultivation with Hoechst 33342 and anti-Ki-67 (Figure 15C) [37], [98]. Ki-67 proliferation index is expressed in percentage and it´s defined as follows: Ki-67 proliferation index (%) = number of Ki-67 positive cells/number of all cells. We repeatedly measured that the Ki-67 labeling index (%) and revealed significant decrease in HepG2 and Alexander cells cultured in CS in comparison with cells cultured in MC (Figure 15D) [152]. In fact, increased nuclear presence of Ki-67 protein compartmentalization in cells (HepG2 and Alexander) is shown on Figure 15C [152]. PCNA is another marker of proliferation that was examined [37]. Specifically, PCNA is a part of DNA sliding clamps protein family and represents a ring-shaped protein, that encompass the DNA molecule [166]. Together with replication factor C (RFC), PCNA is responsible for DNA replication fork assessment and function during DNA synthesis phase in cell cycle [166], [167]. Moreover, PCNA has also crucial function in processes such as tumor stemness and invasion [168]. PCNA marker showed significant decrease in protein expression in HepG2 and Alexander cells cultured in CS in comparison with cells cultured in monolayer culture (MC) (Figure 15B) [37]. Based on immune-detected proliferation markers Ki-67 and PCNA we revealed the significant decrease of proliferation of HepG2 and Alexander cells that were cultured in soft (~94 Pa) 3D CS (Figure 15) [37], [152], that is in line with research conducted by other research groups [51], [58].
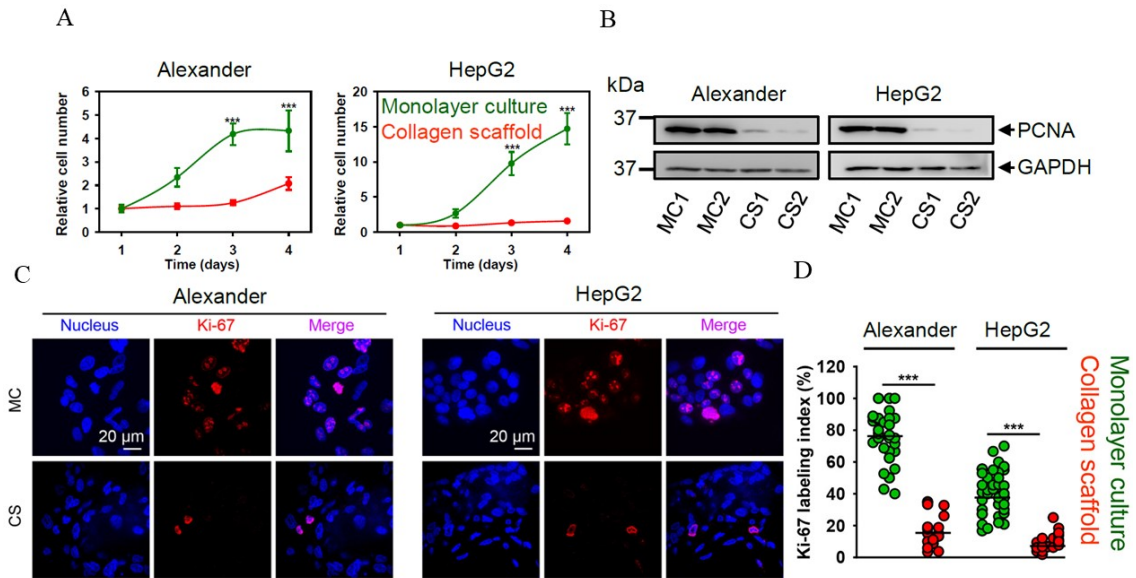
Figure 15: Proliferation dynamics analysis of Alexander and HepG2 cell cultures either in CS or MC. (A) Growth curves of 4 days long cultivation. Relative cell number is based on DNA-binding staining (Hoechst 33342) and ImageJ plugin CellCounter, ***p<0.001 stand for significant differences. (B) Immunodetection of proliferative cell nuclear antigen (PCNA) proliferation marker using the Western blot in Alexander and HepG2 cells. GAPDH was used as a loading control. (C) Immunofluorescent analysis of Ki-67 proliferation marker using confocal microscopy. (D) Ki-67 labeling index (%) determination. Reprinted from open-access articles [37], [98] *under the terms of the Creative Commons Attribution License.*

4.5   Modulation of YAP signaling and cytoskeleton remodeling

In general, cytoskeleton is a highly dynamic network that has three main functions: spatial organization of the cellular content; interconnecting the cell with the external micro-environment; and force generation that enable cellular movement [169]. Cytoskeletal organization is distributed in all regions of a living cell and consists of filamentous molecular structures, including microtubules, intermediate filaments and microfilaments. Microfilaments cytoskeleton fibers contain actin subunits, while microtubules contain tubulin subunits. Tension and reorganization of cytoskeleton is driven by the cellular environment, either ECM or artificial [170]. Actin filaments might transmit stress from one spot to the long distance over the cell [171]. Moreover, ubiquitously expressed β-actin controls cell growth and migration [172].

46

We have analyzed how physical cues of 3D CS cell culture affect the cytoskeleton components in HepG2 and Alexander cells (Figure 16AB) using confocal microscopy. We found that the average length of F-actin and β-tubulin filaments is lower in 3D CS than in 2D MC in both cell lines (Figure 16 CD) [37], [98].
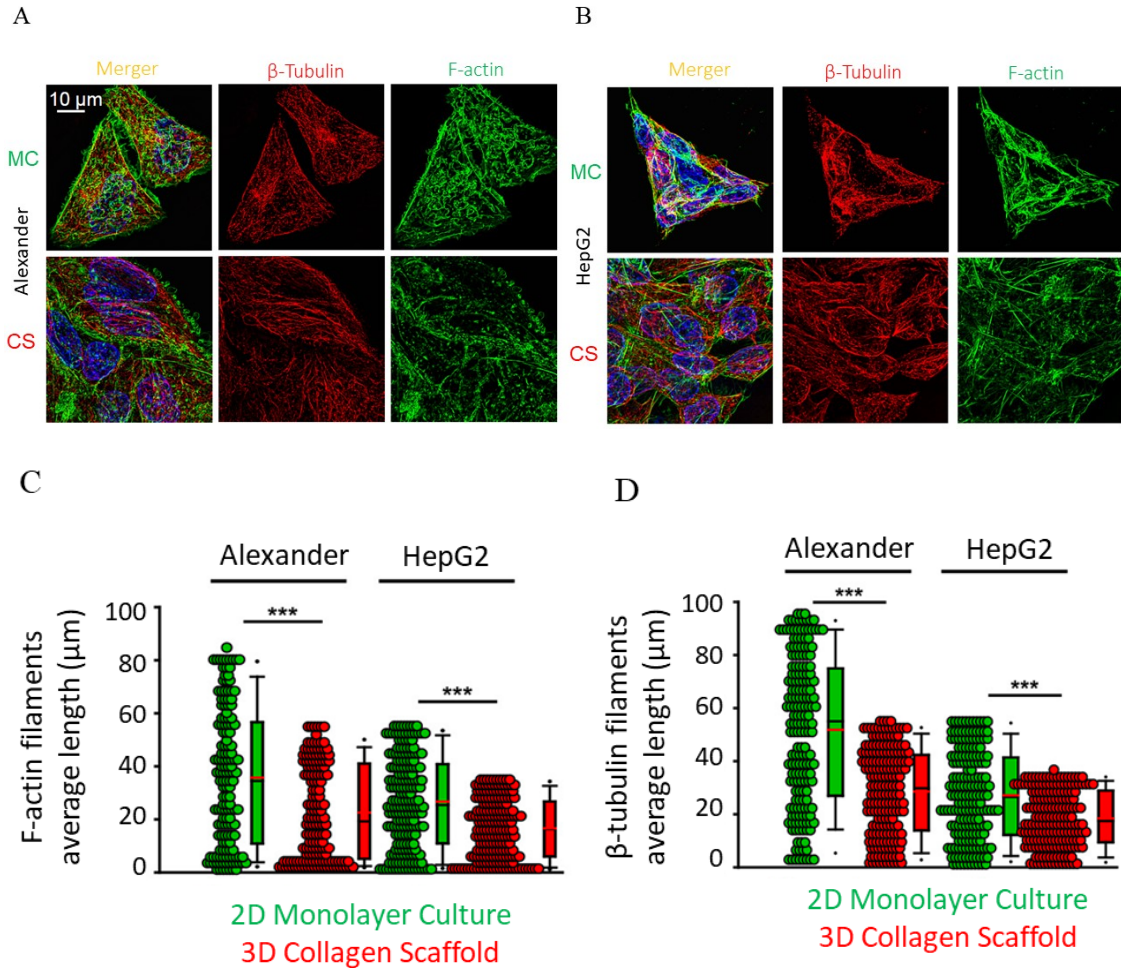

Figure 16: Cytoskeleton remodeling of Alexander and HepG2 cells cultured in 3D CS, in comparison with cells cultured in 2D MC. *(A) Maximum intensity projections of Z-stack images for Alexander cells after seven days of culturing and stained with F-actin (green), β-tubulin (red) and counterstained nucleus with Hoechst 33342 (blue) and captured by confocal microscopy. (B) Maximum intensity projections of Z-stack images for HepG2 cells after seven days of culturing and stained with F-actin (green), β-tubulin (red) and counterstained nucleus with Hoechst 33342 (blue) and captured with confocal microscopy. (C) F-actin filaments average length (μm) was determined. (D) β-tubulin*

filaments average length (µm) was determined. Reprinted from open-access articles [37], [98] *under the terms of the Creative Commons Attribution License.*

In order to visualize the ultrastructure of cytoskeletal organization (actin and tubulin) we used 3D reconstruction from Z-stack digital images captured by confocal microscopy and found the changes of cytoskeletal components organization using 3D reconstruction, specifically decrease in the length of each filament type (Figure 17A) [98].

We have also performed analysis of the adhesion proteins, such as vinculin using the immunofluorescence confocal microscopy. We observed, that in stiff 2D MC vinculin was allocated with F-actin at the edge of the cell, while in 3D CS vinculin was less dense and spot-like distributed (Figure 17B) [98].
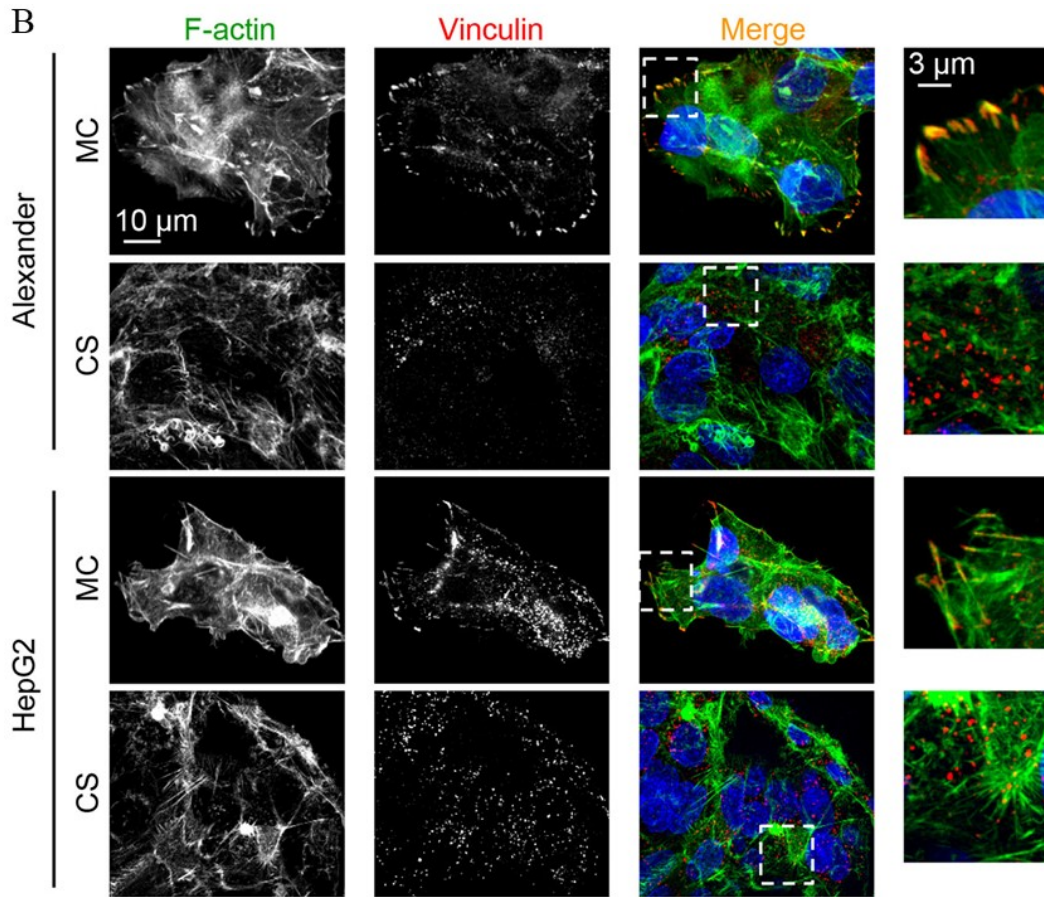
Figure 17: Cytoskeleton and focal adhesion immunofluorescence of vinculin in Alexander and HepG2 cells cultured for 7 days either in CS or MC. Images were captured using confocal microscopy. *(A) 3D reconstruction of Z-stack images. F-actin was labeled using the ActinGreen™ 488 ReadyProbes™ chemistry, β-tubulin was labeled using the anti- β-tubulin antibody and nucleus was counterstained with Hoechst 33342. (B) Focal adhesion (FA) analysis was achieved using anti-vinculin antibody staining (red), F-actin (green) using ActinGreen™ 488 ReadyProbes™ chemistry and nuclear counterstain Hoechst 33342 (blue). Reprinted from open-access article* [98] *under the terms of the Creative Commons Attribution License.*

Then, we performed immunodetection of β-actin and β-tubulin and observe decrease in protein expression in HepG2 and Alexander cells cultured in 3D CS in comparison with 2D MC (Figure 18AB) [98]. In addition, Yes-associated protein (YAP) signaling pathway has a key role in transducing the effects of physical cues [23], [34]. Specifically, YAP regulate mechanotransduction by FA assembly control [27].

49

Interestingly, actin regulates YAP [173] and YAP regulates actin driving force underlying cellular motility [174]. The integral membrane protein Caveolin-1 (CAV1) was identified as an upstream regulator of YAP [175]. CAV1 control YAP activity via the control of actin cytoskeleton dynamics [175]. Recently, it was shown, that decreasing stiffness of artificial cellular environment negatively affects protein expression of cytoskeletal elements, such as F-actin and α-tubulin in human hepatocytes cell line L-02 [176].

Therefore, we were interested about the expression level of YAP, β-actin and β-tubulin protein. We revealed, that in 3D CS-induced mechanotransduction, there was a downregulation of YAP, β-actin and β-tubulin proteins in comparison with cells cultivated in 2D MC (Figure 18A-C) [37].
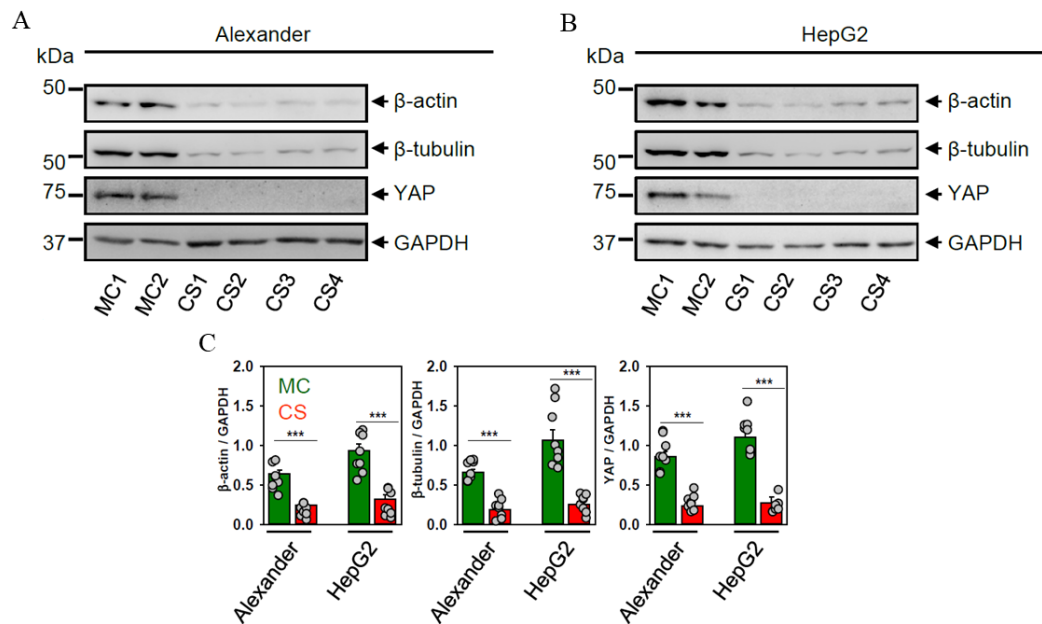

Figure 18: Immunodetection of β-actin, β-tubulin and Yes-associated protein 1 (YAP) using Western blot. MC1-2 and CS1-4 represent replicates. *(A) Expression levels of proteins in Alexander cells cultured either in CS or MC, GAPDH served as a loading control. (B) Expression level of proteins in HepG2 cells cultured either in CS or MC, GAPDH served as a loading control. (C) Densitometric quantification expressed in graphs, data are expressed as mean ± SEM and *** p<0.001 stands for significant differences. Reprinted from open-access article [37] under the terms of the Creative Commons Attribution License.*

Regarding the YAP nucleocytoplasmic shuttling, it is known that stiff environments induce activation of YAP and display nuclear localization, while soft substrates display cytoplasmic localization of YAP [175].

In line with the previous findings, we immunodetected the decrease of YAP protein in HepG2 and Alexander cells cultured in 3D CS, in comparison with 2D MC culture [37]. Moreover, we used confocal microscope Olympus IX83 to reveal the distinct pattern of nucleocytoplasmic YAP ratio (Figure 19AB) [37]. Using immunofluorescence analysis, we observed difference between the cells localized on the edge of fiber and the center of pore within the CS: there is a significant drop in the nuclear to cytosolic ratio for YAP in cells located in the center of CS pore (Figure 19D) [37].
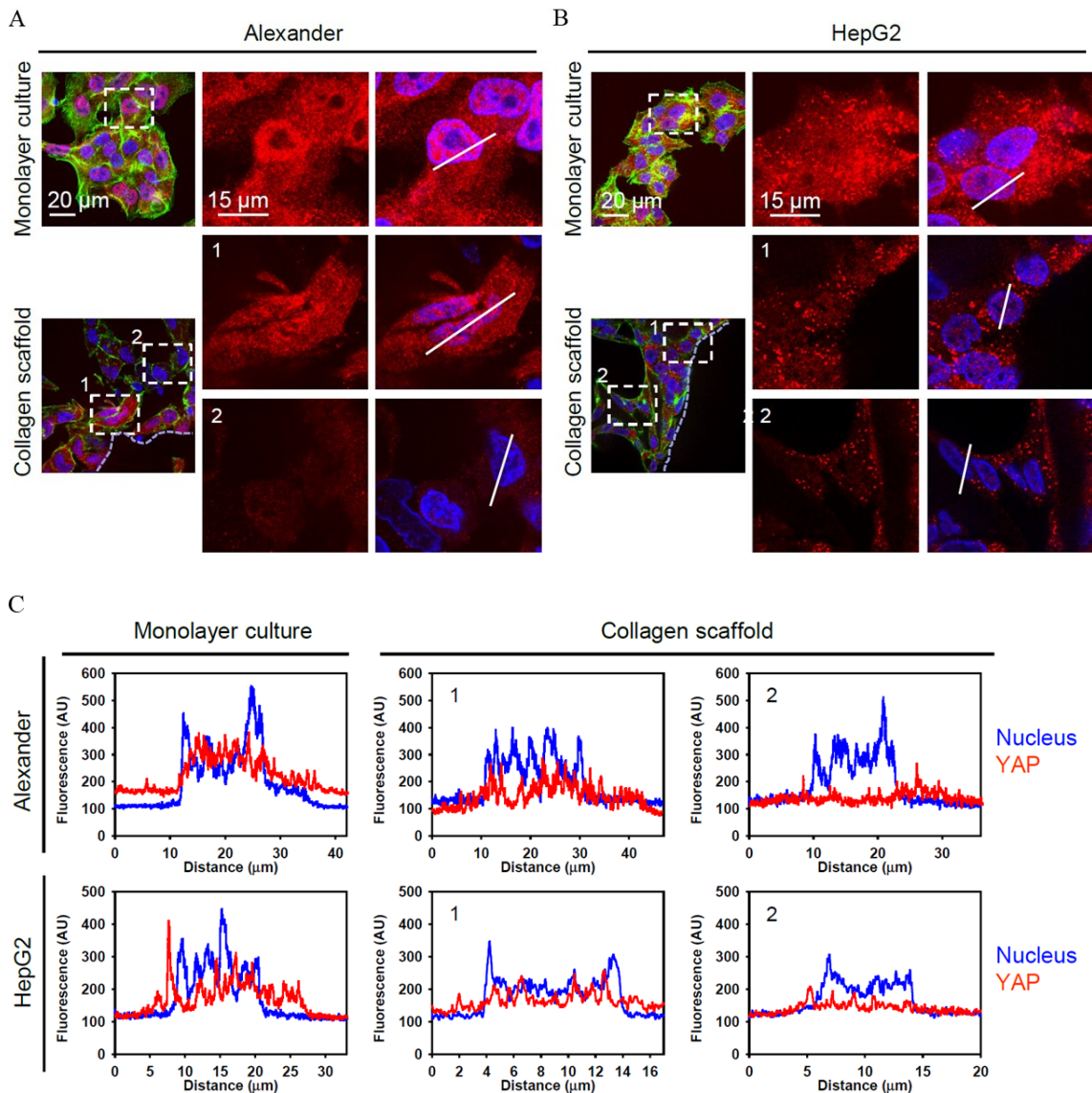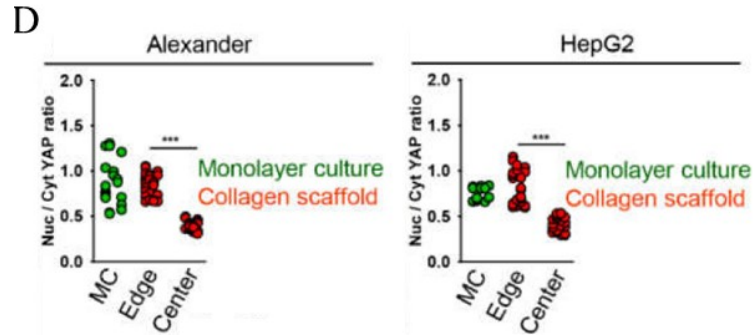
Figure 19: YAP cytosolic translocation in cells cultured in 3D CS. (A) Immunofluorescence of YAP protein in Alexander cells using anti-YAP antibody in order to assess the YAP sub-cellular localization. F-actin was labeled using ActinGreen™ 488 ReadyProbes™ (green) chemistry and nucleus was counterstained with Hoechst 33342. Dashed line indicates the interface between fiber and cells. (B) Immunofluorescence of YAP protein in HepG2 cells using anti-YAP antibody in order to assess the YAP sub-cellular localization. F-actin was labeled using ActinGreen™ 488 ReadyProbes™ (green) chemistry and nucleus was counterstained with Hoechst 33342. Dashed line indicates the interface between fiber and cells. (C) Sub-cellular localization of YAP. Representative line scans of confocal images shown in (A) and (B). Reprinted from open-access article. (D) Analysis of nuclear/cytosolic YAP ratio in cells HepG2 and Alexander cultured either in soft 3D CS or stiff 2D MC. In 3D CS we distinguish between cells that are located at the collagen fiber (the edge) or are located in the pore of collagen scaffold (the center). Reprinted from open-access article [37] under the terms of the Creative Commons Attribution License.

4.6 Autophagy and mTOR-driven metabolism regulation

The master regulator of metabolism is the mammalian/mechanistic target of rapamycin (mTOR) kinase protein. Moreover, mechanical stimuli generated by physical cues might modulate mTOR signaling [177], [178]. In addition, mTOR signaling is linked to YAP sub-cellular compartmentalization mechanical cues [179]–[181]. Therefore, we were interested, how physical cues of 3D CS affected mTOR activity and sub-cellular localization. Western blot detection of phosphorylated mTOR revealed significantly lower level of pmTOR protein expression in 3D CS in comparison with 2D MC (Figure 20C) in both cell lines Alexander and HepG2 (Figure 20AB) [37].
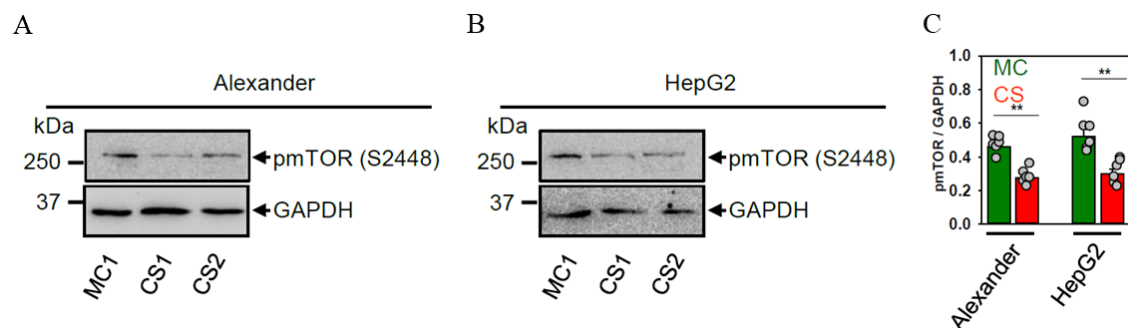
Figure 20: Immunodetection of phosphorylated mammalian Target of Rapamycin (pmTOR) in cells cultured either in CS or MC using Western blot. (A) In Alexander cells. (B) In HepG2 cells. (C) Plotted graphs for densitometric quantification for both cell lines, ** $p<0.01$ stands for significant differences. Reprinted from open-access article [37] under the terms of the Creative Commons Attribution License.

Further, beside of total level expression of pmTOR protein, we were also interested in sub-cellular localization. Therefore, we used confocal microscopy and revealed that pmTOR in 3D CS has increased cytosolic localization in the cells at the center and increased nuclear localization in the cells on the fibers (the edge of pore) (Figure 21A-C) [37]. Similarly, to YAP subcellular localization, pmTOR has followed this pattern (Figure 21A-C) [37].
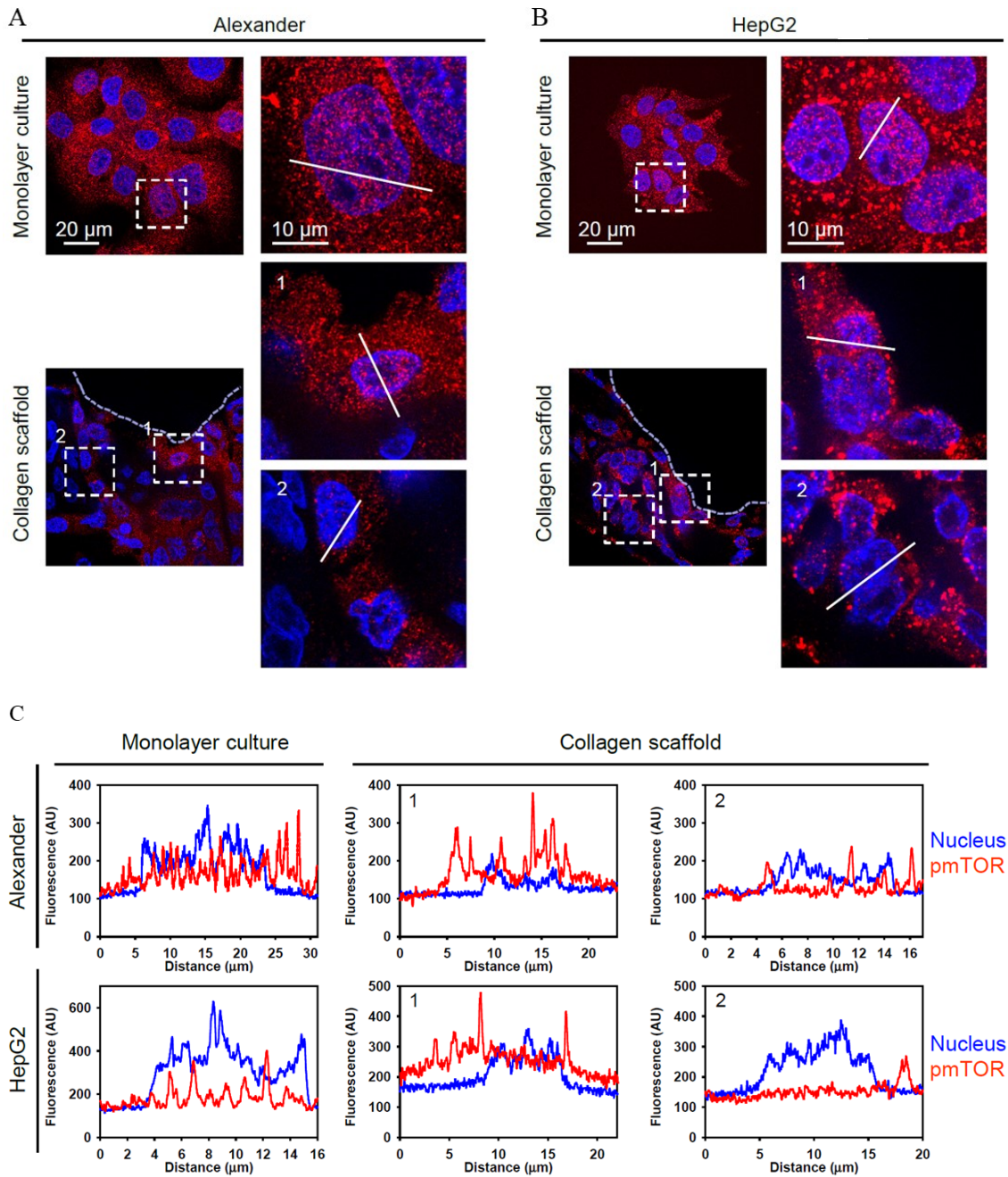
Figure 21: pmTOR sub-cellular localization using the immunoflurescence and confocal microscopy. Cells were cultured either in CS or MC for 7 days and then were labeled with specific antibody anti-pmTOR (red) and counterstained with Hoechst 33342 to label nucleus (blue). *(A) Alexander cells. (B) HepG2 cells. (C) Representative line scans demonstrating the sub-cellular localization of pmTOR from (A) and (B). Reprinted from open-access article* [37] *under the terms of the Creative Commons Attribution License.*

Previously, it was shown that mechanical stimulus in form of shock wave treatment leads to pmTOR association with actin stress fibers and ultimately supports cellular proliferation [182]. In order to characterize the involvement of pmTOR and cytoskeleton structure remodeling in cellular proliferation in soft 3D CS, we used super-resolution confocal microscopy to analyze the pmTOR localization within the F-actin fibers (Figure 22A) [98]. Our super-resolution confocal microscopy analyses uncovered that pmTOR distribution was punctuated in cytoplasm in cells cultured in 3D CS, while cells cultured in 2D MC have pmTOR distributed in vesicle-like inclusions within the actin stress fibers (Figure 22A) [37].

It is known, that mTOR inhibition leads to autophagy promotion [183]. Autophagy is a process, where redundant and dysfunctional proteins or cellular structures (commonly termed as a cargo) are engulfed to the membrane-based system and discarded [184]. At early stage of autophagy, LC3-phosphatidylethanolamine conjugate (LC3-II) is recruited to autophagosomal membranes to engulf the cargo [185]. We use antibody staining and confocal microscopy to label LC3 puncta, that are markers of autophagy [185]. We found in Alexander and HepG2 cells that were cultured in 3D CS have an increase in abundance of LC3-positive puncta (Figure 22B) [37].
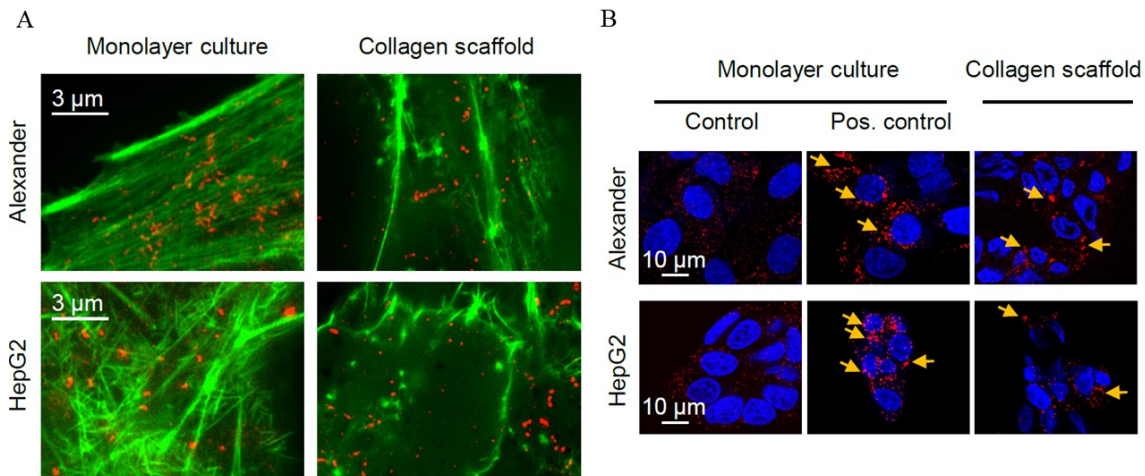

Figure 22: pmTOR immunofluorescence and autophagosome detection. *(A) Confocal microscopy images of pmTOR (red) and F-actin (green). (B) Autophagic flux detection via the immunodetection autophagosome using anti-LC3 antibody. Arrows indicate LC3-puncta. As a positive control we used 14 hours serum starvation (in Alexander cells) or*

10 mM H₂O₂ treatment for 30 minutes (in HepG2 cells). Reprinted from open-access article [37] *under the terms of the Creative Commons Attribution License.*

4.7 YAP and mTOR interplay under physical constraints of CS

YAP and mTOR interplay in mechanotransduction were proposed in a couple of studies [179], [186]. Moreover, it was found that the stiff ECM together with integrin receptors might activate mTOR signaling axis [187]. We decide to downregulate the YAP protein in cells cultured in 2D MC in order to reveal possible impact on cellular shape and mTOR autophagy-related signaling [37]. Therefore, we used the small interfering RNA (siRNA) transfection to transiently silence the gene expression of YAP protein [37]. First of all, we cross-checked the efficiency of performed siRNA transient transfection by immunoblotting [37]. We found that the siRNA transfection for YAP protein downregulation was successful and most efficient after 48 hours post-transfection (Figure 23A) [37]. Moreover, conducted immunoblot also display no effect on β-actin protein expression (Figure 23A) [37]. Further, we were interested, how YAP downregulation affects the autophagic flux and perform the immunodetection of autophagy marker LC3 [37]. We revealed that YAP downregulation increases the autophagic flux, as is shown on immunoblot with increased level of LC3 in cells Alexander and HepG2 treated with YAP siRNA (Figure 23B) [37]. Notably, YAP downregulation affects the cytoskeleton protein structure organization or cellular morphology (Figure 23C) [37].
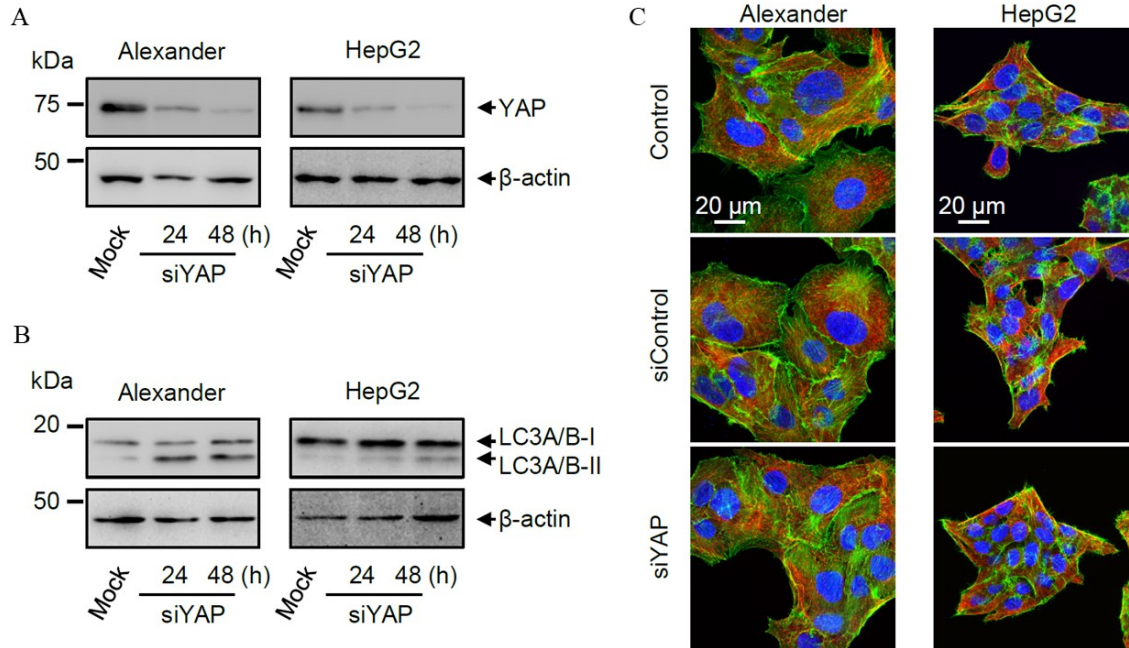
Figure 23: YAP protein downregulation in cells cultured in Monolayer Culture (MC) using small interfering RNA (siRNA). *(A) Efficiency of YAP downregulation after 24 and 48 hours using Western blot. (B) YAP downregulation increases the levels of LC3-II. (C) YAP downregulation has no effect on morphology of cells or cytoskeleton organization, immunofluorescence was done with labels anti-β-tubulin antibody (red), ActinGreen™ 488 ReadyProbes™ (green) and nucleus was counterstained with Hoechst 33342 (blue). Reprinted from open-access article* [37] *under the terms of the Creative Commons Attribution License.*

Strikingly, YAP siRNA downregulation has no effect on pmTOR compartmentalization (Figure 24AB) or protein expression in Alexander and HepG2 cells (Figure 24C) [37]. This suggests that YAP downregulation by siRNA in 2D MC is distinct from the YAP downregulation by mechanical cues in 3D CS [37].
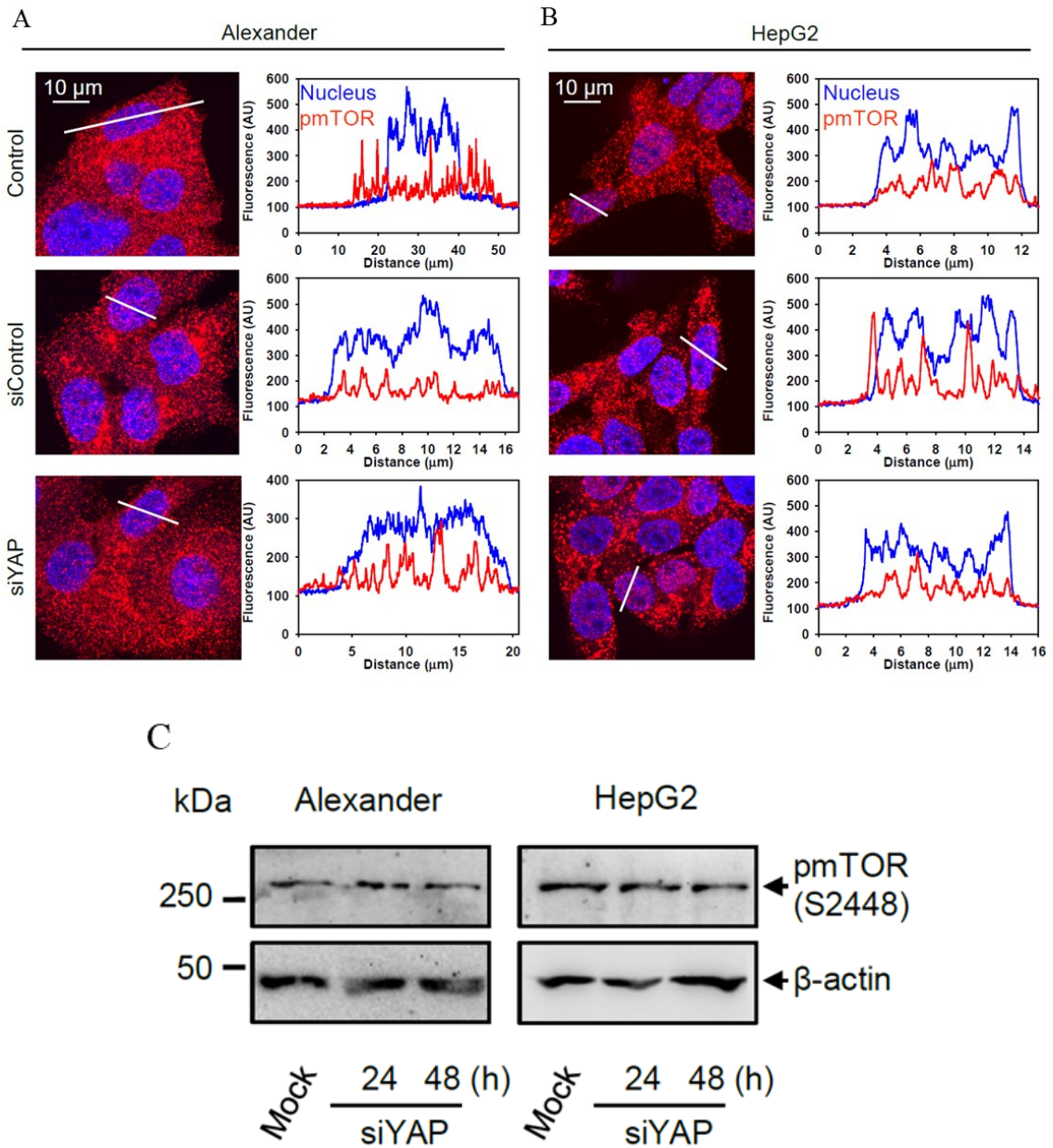
Figure 24: YAP downregulation has no effect on pmTOR signaling pathway in cells cultured in MC. *(A) Analysis of pmTOR (red) after 48 hours of siRNA YAP transfection in Alexander cells. (B) Analysis of pmTOR (red) after 48 hours of siRNA YAP transfection in HepG2 cells. (C) Western blot analysis of pmTOR after 48 hours of siRNA YAP transfection in both cell lines. Reprinted from open-access article* [37] *under the terms of the Creative Commons Attribution License.*

4.8 Mitochondrial dynamics and metabolic signaling

Mitochondrion, as a cellular organelle, is an important hub for molecular signaling and metabolism in a living cell [1] providing the energy via electron transport chain in form of ATP [1]. Mitochondria is a dynamic structure, that undergo through cycles of fission (one mitochondrion is divided into two mitochondria) and fusion (where two mitochondria fuse into one mitochondrion) [188]. It is known, that actin filaments are essential for controlling the fission and fusion dynamics of mitochondria [189]–[191]. In addition, it becomes evident, that mechanical forces could affects mitochondrial fission and metabolism [192], [193]. In view of this, we decide to assess the mitochondrial morphology dynamics of Alexander and HepG2 cells in the 3D CS (Figure 25A-D) [98]. We used the confocal microscopy to reveal the mitochondrial morphology shape during live cell imaging (Figure 25AB) [98]. We found that cells cultured on stiff 2D MC displayed network organization of tubular mitochondria (Figure 25AB) [98]. On the other hand, cells cultured in soft 3D CS showed fragmented and granular mitochondria (Figure 25AB) [98]. To quantify these observations, we counted the mitochondria and divide them into three categories: tubulated, intermediate and fragmented (Figure 25 CD) [98]. We found that both cell lines cultured in 3D CS have decreased number of tubulated mitochondria and increased number of fragmented mitochondria (Figure 25CD) [98]. To conclude, we found that soft 3D CS induce mitochondrial fission [98].
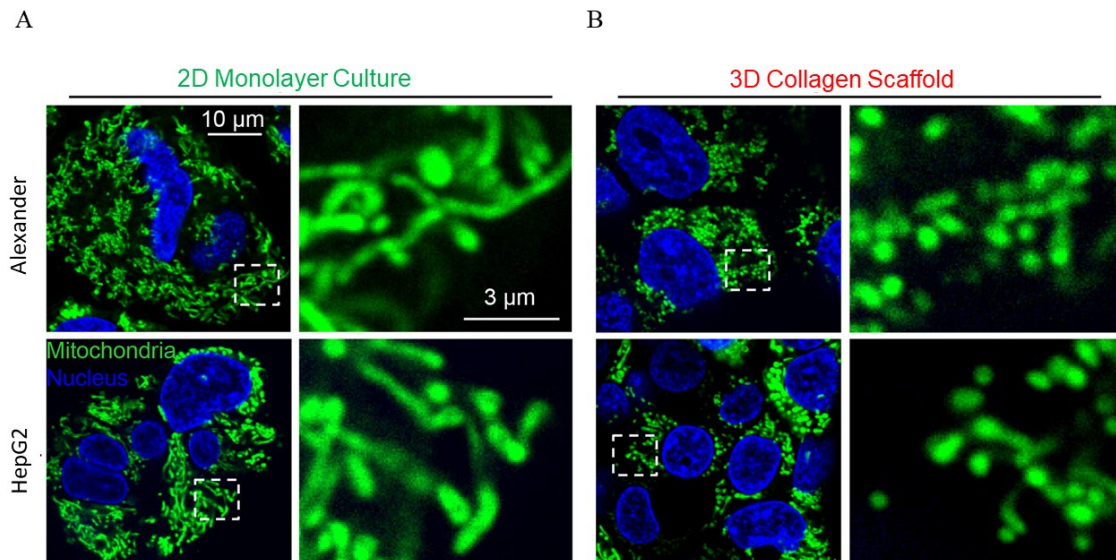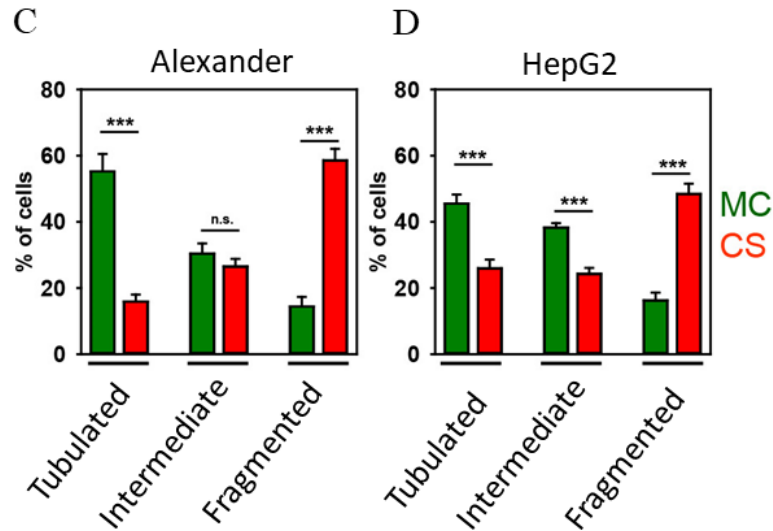
Figure 25: Mitochondrial morphology dynamics. *(A) Mitochondria in 2D Monolayer culture and (B) 3D Collagen Scaffold. Ratio of tubulated, intermediate and fragmented mitochondria in (C) Alexander. and (D) HepG2. Reprinted from open-access article* [98] *under the terms of the Creative Commons Attribution License.*

Mitochondrial reactive oxygen species (mitoROS) are generated during the oxidative phosphorylation process, that is occurring at the inner membrane of mitochondria [194]. Mitochondrial oxidative stress might induce wide variety of cellular responses, including mitochondrial fission and autophagy [194]. Therefore, using a fluorescent probe, we monitored mitoROS using confocal microscopy [98]. We found that there was a significant drop in the mitoROS abundance in cells cultured in 3D CS in comparison with cells cultured in 2D MC (Figure 26A) [98]. It becomes evident, that fragmentation of mitochondria leads to decrease in $\Delta\Psi$m (mitochondrial membrane potential) [195], [196]. Moreover, it was found that promoted mitochondrial fission leads to decrease in proliferation and cellular respiration [195]. Accordingly, we analyzed how physical cues of 3D CS affects the $\Delta\Psi$m (Figure 26BC) [98]. We have used fluorescent probe JC-1 and confocal microscopy in order to reveal the $\Delta\Psi$m (Figure 26 C) [98]. In order to determine the value for $\Delta\Psi$m, we calculated ratio between JC-1 aggregate and monomer using semi-automatized approach in ImageJ (NIH) via multiple macro codes (see methods) [98]. We found that $\Delta\Psi$m was significantly lower in cells cultured in 3D CS in comparison with cells cultured in 2D MC (Figure 26B) [98].
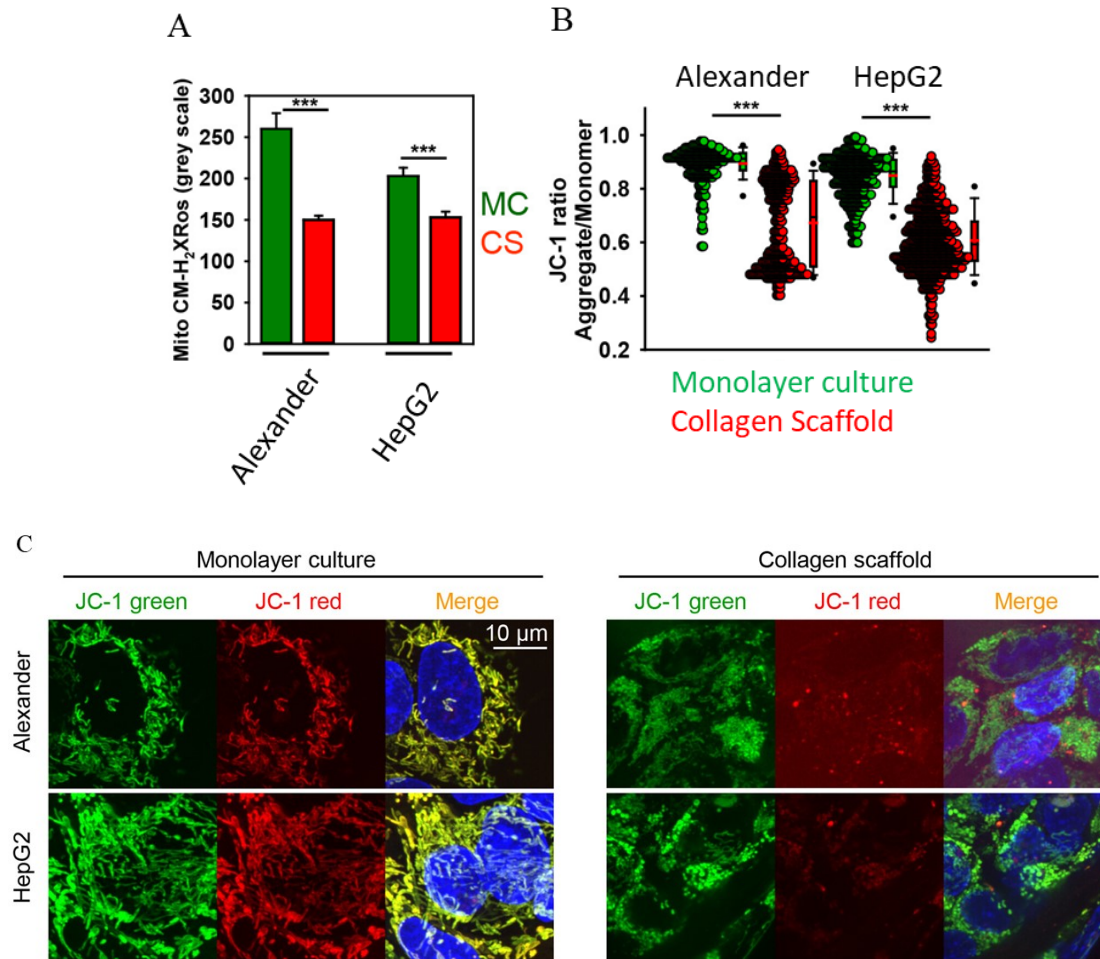
Figure 26: Mitochondrial dynamics, reactive oxygen species (ROS) and mitochondrial membrane potential (ΔΨm) in Alexander and HepG2 cells cultured either in CS or MC. *(A) Quantification of mitoROS. (B) Quantification of ΔΨm in both cell lines cultured in CS or MC. (C) Representative confocal images of JC-1 labeled cells. Reprinted from open-access article [98] under the terms of the Creative Commons Attribution License.*

To examine the ΔΨm of cells cultured in 3D CS rigorously, we used different chemical entities that serve as a ΔΨm depolarizing agents, including ionomycin (Imy), carbonyl cyanide m-chlorophenylhydrazone (CCCP) and potassium cyanide (KCN) (Figure 27A-C) [98]. Imy is an ionophore, which binds calcium (Ca^{2+}) preferably, but also magnesium (Mg^{2+}) and cadmium (Cd^{2+}) [194]. Imy also acts as an antibiotic, but more importantly as an ionophore it affects opening or inhibition of the mitochondrial permeability transition pore (mPTP) [197]. Ultimately, Imy via corrupting the calcium homeostasis induce mitochondrial membrane depolarization [198]. CCCP is also a proton

ionophore acts as an uncoupling agent of oxidative phosphorylation in mitochondria [199]. In general, uncoupling agents of oxidative phosphorylation block the coupling between the electron transport and phosphorylation reactions that leads to ATP synthesis inhibition, increasing mitoROS concentration and mitochondrial membrane depolarization [200]. KCN is a cytotoxic agent that inhibits the cytochrome c oxidase (MTCO) or complex IV [201]. However, recent study suggests, that cyanide might have biphasic effect on MTCO, where high (micromolar) concentrations of cyanide inhibit MTCO, while low (nanomolar) concentrations of cyanide stimulate MTCO activity [202]. We used high concentration of KCN, in order to observe inhibitory effect of MTCO [98]. According to our treatment with mentioned depolarizing agents, we found that cells cultured in 3D CS were more sensitive towards those treatments in comparison with 2D MC (Figure 27A-C) [98].
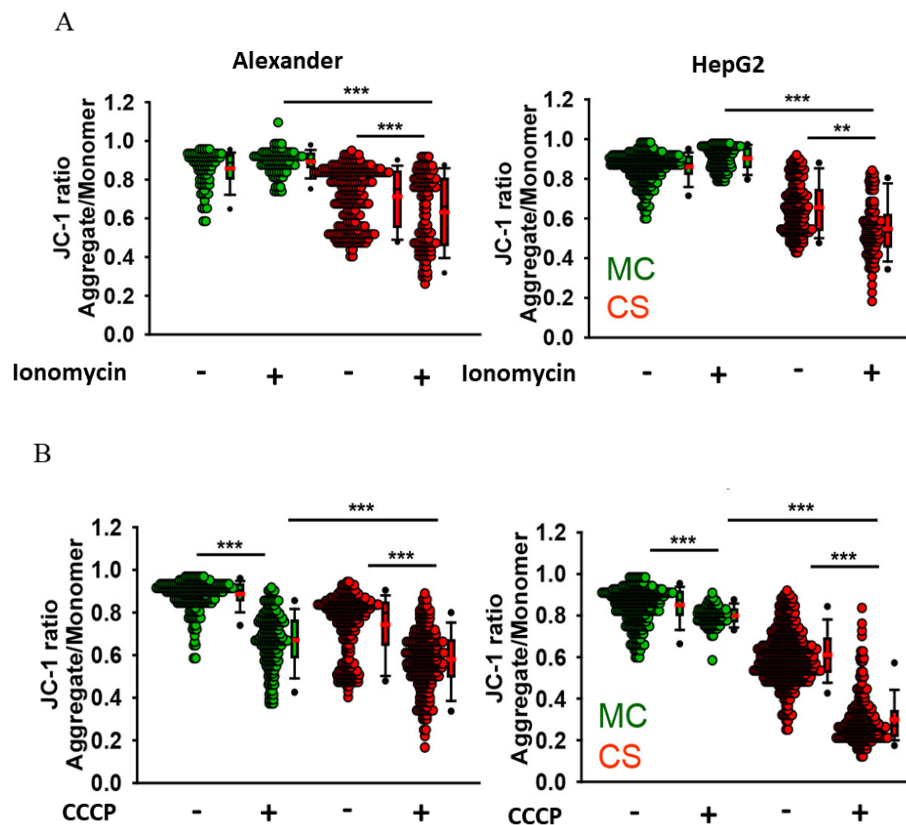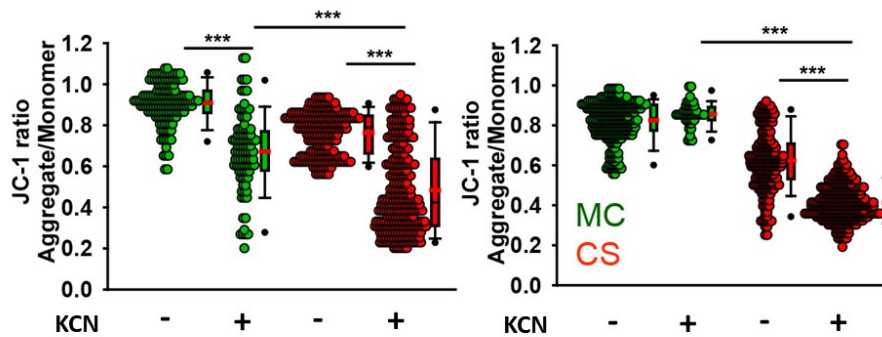
C

*Figure 27: Mitochondrial membrane potential sensitivity treated with different depolarizing agents using 1 μM JC-1 labeling in Alexander and HepG2 cells cultured in CS or MC. (A) 1 μM Ionomycin treatment for 10 minutes. (B) 10 μM carbonyl cyanide m-chlorophenylhydrazone (CCCP) treatment for 30 minutes. (C) 5 mM potassium cyanide (KCN) for 30 minutes. Quantification was performed out of three independent experiments; n ≥ 100 cells per experiment. ** p<0.01; *** p<0.001 stand for significant differences. Reprinted from open-access article [98] under the terms of the Creative Commons Attribution License.*

Hepatocellular carcinoma (HCC) progression of cancer cells is associated with oxidative phosphorylation enzymes downregulation, that lead to decreased oxygen consumption and adaptation to hypoxia [203], [204]. Therefore, we decided to analyze the expression of (MTCO) (Figure 28) [98]. MTCO, also known as complex IV of electron transport chain (ETC), contains 14 subunits, while 3 subunits are encoded by mitochondrial genome (mtDNA), other 11 subunits are encoded by nuclear genome (in mammals) [1]. We analyzed subunit 1 (MTCO1) using the Western blot technique and revealed the drop of protein expression in Alexander and HepG2 cells cultured in 3D CS, in comparison with 2D MC (Figure 28 AB) [98]. Moreover, to have also patients' perspective, we had the opportunity to examine a small cohort of 12 patients with HCC [98]. Using the reverse transcriptase polymerase chain reaction (RT-PCR), we analyzed the HCC tumor resections as well as tissue around the tumor [98]. We found that mRNA expression of MTCO1 was lower in tumor tissue in comparison with tissue surrounding the tumor (Figure 28C) [98].
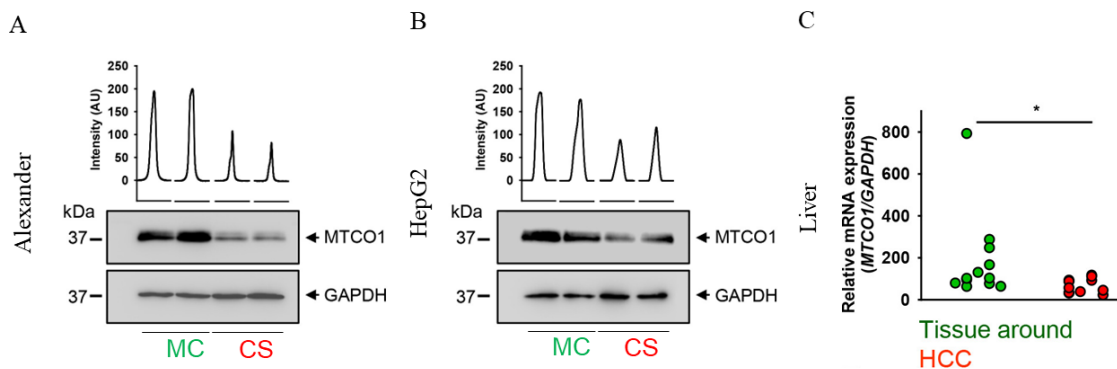
Figure 28: Mitochondrially encoded Cytochrome C oxidase subunit 1 (MTCO1) expression analysis. *(A) Immunoblot analysis in Alexander cells. (B) Immunoblot analysis in HepG2 cells. (C) RT-PCR analysis of hepatocellular carcinoma (HCC) and tissue around the tumor from human patient's livers. Reprinted from open-access article* [98] *under the terms of the Creative Commons Attribution License.*

4.9 Glycolysis modulation under physical cues of 3D cell culture in collagen scaffold (CS)

Glucose, the six-carbon saccharide, is of the key biomolecules in the living cell metabolic pathways [1]. In the catabolic pathway of cellular metabolism, glycolysis is a pathway to breakdown the glucose [1]. Through a sequence of intermediate metabolites, the process of glycolysis converts one molecule of glucose into two molecules of pyruvate [1]. In HCC, glucose uptake is facilitated by GLUT1 hexose transporter [205]. Specifically, GLUT1 is a key rate-limiting factor in the transport of glucose metabolism [1]. Suppression of GLUT1 expression negatively affect growth and migration in HCC [205]. GLUT1 inhibition results in decreased glucose uptake as well as lactate secretion [205].

We challenged Alexander and HepG2 cells that were cultured in 3D cell culture of CS with analysis of metabolic markers pyruvate and lactate. We revealed, that both markers, pyruvate and lactate were significantly increased in cells cultured in 3D in comparison with cells cultured in 2D monolayer culture (Figure 29AB) [98]. The cumulation of pyruvate and lactate propose increase in glycolytic flux in cells cultured in 3D CS [98].
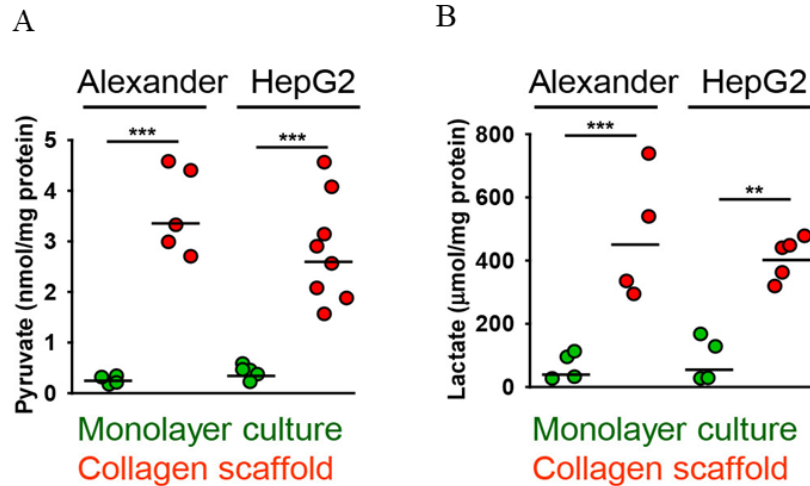
Figure 29: Absorbance analysis of metabolic markers involved in glycolysis of Alexander and HepG2 cells cultured either in CS or MC. *(A) Pyruvate (B) Lactate. ** p< 0.01, *** p<0.001 stands for significant differences. Reprinted from open-access article* [98] *under the terms of the Creative Commons Attribution License.*

Generation of F-actin stress fibers might be induced by physical or mechanical cues of cellular environment [206]. F-actin stress fibers protects from the proteasomal degradation of the rate-limiting glycolysis enzyme phosphofructokinase (PFK) [206]. This protection from degradation results in a higher rate of glycolysis [206]. We used fluorescent probe to label F-actin fibers and used the look-up table (LUT) Physics in ImageJ (NIH) in order to generate pseudo-color scale (Figure 30AB) [98]. We found that, in both Alexander and HepG2 cell lines, there was increased density in F-actin stress fibers in 3D CS in comparison with 2D MC (Figure 30AB) [98].
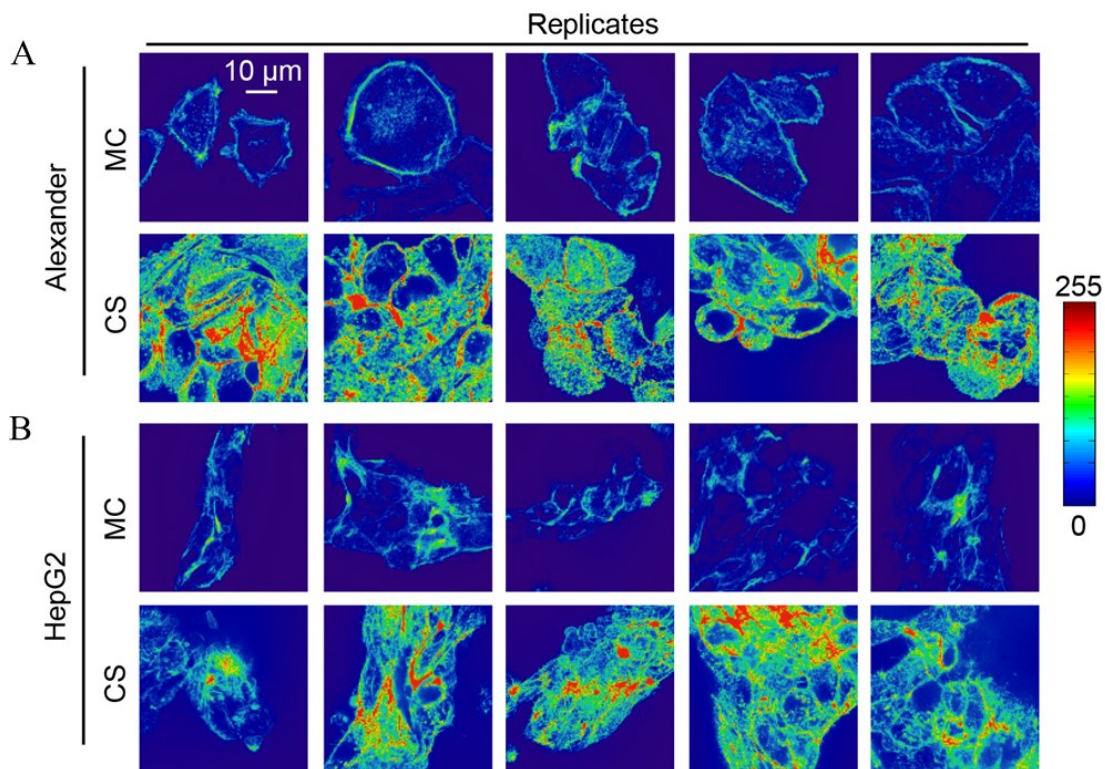
Figure 30: Confocal analysis of the cytoskeleton structure in cells under physical cues of CS in comparison with MC. F-actin was labeled with ActinGreen™ 488 ReadyProbes™. Fluorescence intensity and distribution of F-actin fibers is expressed as pseudo-color on scale 0-255. The tension of F-actin fibers was visualized using the look-up table (LUT) Physics using the ImageJ (NIH) software tool. (A) Alexander cells (B) HepG2 cells. Reprinted from open-access article [98] under the terms of the Creative Commons Attribution License.

4.10 High-Fluence Low-Power (HFLP) Laser treatment

We conducted the cell survival analysis using red 649 nm laser light treatment, in a so-called high-fluence low-power (HFLP) laser treatment also known as photobiomodulation [98]. It was shown previously, that HFLP treatment with laser light in wavelength range 620-760 nm consequences to cell death changes in $\Delta\Psi m$ [129], [148], [207]. We found, that 649 nm HFLP treatment of Alexander and HepG2 cells in 3D CS decreased the viability in comparison with 2D MC (Figure 31AC) [98]. Decrease in green fluorescence of calcein-AM indicate decrease in esterase activity, that is unique characteristic of live cells. Increase in red fluorescence of ethidium homodimer indicate

loss of plasma membrane integrity (Figure 31A-D). We also performed the time-resolved dynamics of fluorescence accumulation and release in Alexander and HepG2 cells during the HFLP treatment (Figure 31BD) [98].
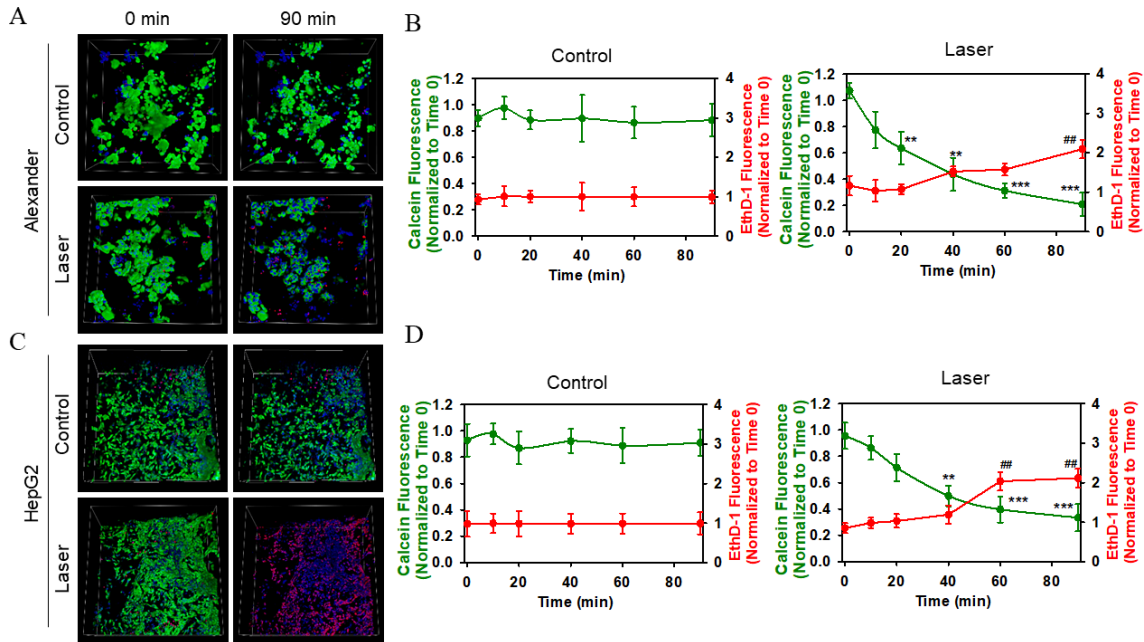

Figure 31: Time-resolved dynamics of high-fluence low-power (HFLP) treatment of Alexander and HepG2 cells in 3D collagen scaffold (CS) cell culture with 649 nm red laser light for 90 minutes. Cells were cultured for 7 days, then were labelled with calcein-AM (green) and ethidium homodimer (red), while Hoechst 3334 was used as a nuclear counterstain. *(A) Confocal microscopy images of Alexander cells of control group (untreated cells) and laser treatment group at timepoints 0 and 90 minutes. (B) Time-resolved dynamics plotted graphs of Alexander cells in control group as well as laser treatment group. (C) Confocal microscopy images of HepG2 cells of control group (untreated cells) and laser treatment group at timepoints 0 and 90 minutes. (D) Time-resolved dynamics plotted graphs of HepG2 cells in control group as well as laser treatment group.* ## *$p<0.01$,* ** *$p<0.01$ and* ***$p<0.001$ stand for significant differences.* *Reprinted from open-access article* [98] *under the terms of the Creative Commons Attribution License.*

Previously, it was found that HepG2 cells cultured in 2D MC were not sensitive to 649 nm HFLP and the treatment did not result in cell death [129]. It is known, that

HepG2 cells display high levels of anti-apoptotic Bcl-2 protein expression, in comparison with other hepatic cancer cell lines [129]. Therefore, we also performed the 649 nm HFLP treatment against the Alexander and HepG2 cells cultured either in MC or CS (Figure 32 AB) [98]. Both cell lines cultured in 3D CS were more sensitive toward the cell death in comparison with cells cultured in 2D MC (Figure 32 AB) [98]. We have hypothesized, that 3D cell culture of CS might affect the Bcl-2 protein expression in HepG2 cells [98]. Therefore, we used the Western blot technique and determine the Bcl-2 protein expression and revealed, that HepG2 cells cultured in 3D CS have lower level of pro-survival protein Bcl-2 (Figure 32C) [98].
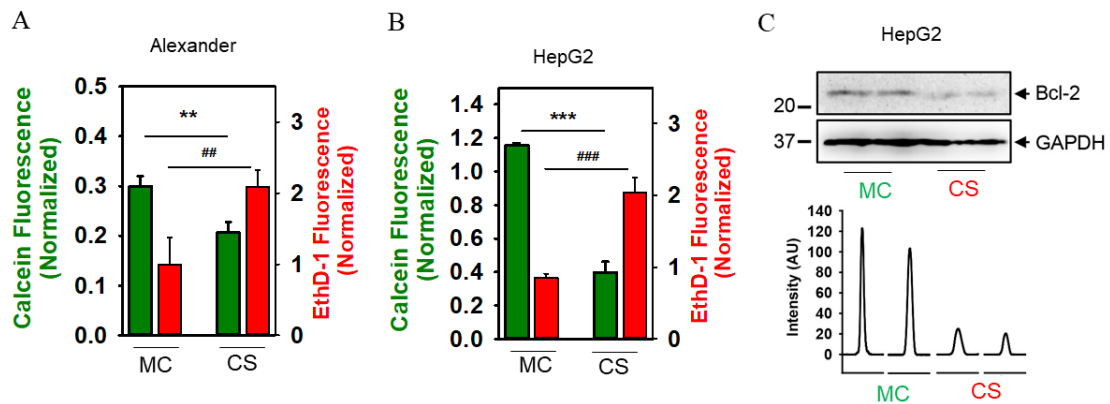

Figure 32: High-fluence low-power (HFLP) treatment of Alexander and HepG2 cells cultured in CS and MC. Cells were cultured for 7 days, then were labelled with calcein-AM (green) and ethidium homodimer (red), while Hoechst 3334 was used for nucleus counterstaining. Finally, photobiomodulation with 649 nm red laser light was performed. (A) Alexander MC and CS (B) HepG2 MC and CS (C) Bcl-2 anti-body immunodetection and quantification. ##p<0.01, ###p<0.001, **p<0.01, ***p<0.001 stands for significant differences. Reprinted from open-access article [98] under the terms of the Creative Commons Attribution License.

5   DISCUSSION

3D cell culture represents an innovative and advanced platform for testing the cellular metabolism and signaling pathways *in vitro* [78], [208], [209]. It is known that 3D cell culture directly affects the cellular behavior of hepatocytes [209], [210]. However, 2D MC is still prevalent in drug testing, that might result in misleading conclusions. In this dissertation thesis, we aimed to reveal the molecular bases of cellular plasticity in soft 3D cell culture. Specifically, we conducted the comparative analysis, where HepG2 and Alexander liver cancer cells were cultivated either in soft (~94 Pa) 3D CS or stiff (~GPa) 2D monolayer culture (MC) [37], [98]. We intended to investigate the fate of cells cultured in a substrate imitating the pathological *in vivo* conditions and compare it to the widely used 2D cell culture on a stiff plastic dish. In particular, we focused on how pores and fibers of soft 3D CS affect cellular size and morphology, proliferation dynamics, metabolic activities and signaling pathways. We provided also insights not only into dimensionality of cell culture, but also about the stiffness. Stiffness of the ECM is key feature of pathologies, including tumors [4], [52], [54], [211].

We used immunodetection and immunofluorescence to evaluate the changes in signaling pathways as well as cellular plasticity. Using the ultra-fast high-resolution spinning disk confocal microscopy, we found that under the physical cues of soft 3D CS hepatic cancer cells undergoing morphological changes, such as decrease in cellular size and nuclear size. In addition, cells changed their morphology depending on their localization within the 3D CS. We observed that cells in the collagen pores display round shape, while cells attached to collagen fiber were stretched and flat. This suggests, that soft ECM environment together with 3D dimensionality affect cellular size and shape dramatically. In fact, cells are sensitive to the mechanical stiffness of the environment, which affects the morphology and functions of hepatic cancer cells. Moreover, further evidence underlines these morphological changes and reveals the key signaling pathways, that are affected by 3D CS, such as YAP and mTOR.

We proved, that the distinct physical cues in the pores and fibers in CS modulate the activity of YAP pathway, which is known for controlling the cellular density and shape [23], [34]. We detected the nuclear compartmentalization of YAP protein in cells located near the collagen fibers, while cells localized within the collagen pore displayed cytosolic

69

compartmentalization of YAP. Therefore, we suggest that neighboring pressure modulate YAP protein nuclear localization and reorganization of the cytoskeleton. [37] In comparison with 2D MC, YAP expression in 3D CS was profoundly lower [37]. We therefore proved, that YAP is an important mediator of physical cues, that might be generated by ECM [23], [34].

Similarly, master metabolism regulator mTOR followed the compartmentalization pattern of YAP. Not only we detected decrease of phosphorylated mTOR expression in cells cultured under 3D CS, but also distinct expression profiles within the 3D structure. Similarly, as for YAP, we observed nuclear localization of pmTOR protein in cells located near the collagen fibers, while cells localized within the collagen pore displayed cytosolic localization of pmTOR [37]. Previously, it was noted that mechanical stress might modulate mTOR signaling pathway [178], [212]. Here we propose that both, YAP and mTOR signaling pathways, are linked in 3D CS and their interplay is in positive relation to proliferation of HepG2 and Alexander cell lines [37]. Moreover, we found a convergence of mTOR and YAP signaling axis in 3D CS, because of similar patterns in immunodetection [37]. It is known, that YAP might regulate mTOR and vice versa [179], [186].

We used the genetic manipulation, specifically siRNA transient transfection to reveal the cross-talk between mechanotransduction marker YAP and metabolic master regulator mTOR. We found that interplay of YAP and mTOR is profound only in 3D CS, because siRNA YAP downregulation in 2D MC did not affect phosphorylated mTOR protein expression level or subcellular localization in both cell lines Alexander and HepG2 [37]. However, we found that siRNA YAP downregulation in cells cultured on 2D MC induce the promotion of autophagy [37]. Similarly, in colorectal cancer cell lines, YAP inhibits autophagy and promotes cancer progression via Bcl-2 upregulation [213]. Our findings support a paradigm that propose participation of YAP pathway in autophagy regulation [214], which was more pronounced in soft CS scaffold than in 2D MC [37].

We also found that soft 3D CS induce mitochondrial fission and decrease the mitochondrial membrane potential (ΔΨm) [98]. It is known that mechanical forces generated from physical cues might affect mitochondrial dynamics and metabolism [192],

[193]. Using chemical inhibition of oxidative phosphorylation, we described the trends in mitochondrial membrane potential changes in cells cultured in 3D CS. We found that cells cultured in 3D CS display $\Delta\Psi$m to be more sensitive towards the depolarizing agents in comparison with 2D MC. Moreover, HCC progression is associated with oxidative phosphorylation enzymes downregulation, such as cytochrome c oxidase [215]. Our soft 3D CS model provide a condition where MTCO is downregulated and therefore mimic a pathological condition of the tumor. Indeed, we found that cells cultured in 3D CS have protein expression level of MTCO1 significantly lower in comparison with 2D MC [98]. Moreover, we also demonstrated that gene expression of MTCO1 was lower in tumor tissue than in non-tumorous parenchyma tissue of patients with HCC [98].

It is worth noting here, that metabolic activity could be regulated by mechanical cues [206]. Therefore, we hypothesized, how physical cues of soft 3D CS will affect the glycolysis pathway. We used spectral analysis to reveal metabolic changes of glycolytic pathway and found increase of pyruvate and lactate intermediate metabolites in cells cultured in 3D CS [98], which suggests that cells experience low oxygen conditions, so-called hypoxia. Accumulation of lactate means, that cells rely more on anaerobic glycolysis. In terms of 3D cell culture, this is logical, because physical constraints of 3D CS, such as collagen fibers might create an oxygen gradient with low values of oxygen inside the 3D CS. In comparison, in 2D cell culture, cells are exposed to oxygen uniformly, without any gradient. Moreover, stiffness of cellular environment influence cell behaviour and metabolic activities as well. In 3D CS cells experience the interaction with the collagen environment as well as other cells from every direction. These interactions might affect signaling pathways that regulate metabolic activities.

Finally, we used biophysical approach in order to treat cells with red laser light and found an increased sensitivity to cell death in 3D CS culture. Previously it was shown that red laser light in high-fluence low-power (HFLP) treatment leads to $\Delta\Psi$m depolarization and cellular death [216]. Here we found that cells cultured under the 3D CS environment were sensitive towards the red laser light HFLP treatment. However, previously it was found that HepG2 cultured in 2D MC were insensitive towards the red laser light HFLP treatment, because of elevated level of Bcl-2 protein [129]. We characterized the

molecular foundations why are HepG2 cultured in 3D CS more susceptible towards the red laser light then HepG2 cultured in 2D stiff MC culture. Using immunodetection, we revealed, that HepG2 cells cultured in 3D CS possess lower expression level for anti-apoptotic and pro-survival protein Bcl-2, that leads to cell death upon treatment with 649 nm laser light. This data suggests that lower level of Bcl-2 protein in HepG2 cells cultured in soft 3D CS leads to destabilization of mitochondrial membrane and Bcl-2 protein low expression favor the pro-apoptotic proteins, such as BAX and BID, that's lead to mitochondrial perturbation and cellular death [98].

Moreover, using the Ki-67 and PCNA markers we found that proliferation kinetics is decreased in soft 3D CS, that suggest the switch to the cellular dormancy or stemness [37]. This is in line with previous research that has shown that cell proliferation increases on a rigid substrate while it decreases on a soft substrate [51], [58]. The found differences may indicate a tendency of tumor cells towards a stiffer substrate *in vivo* on which they can better adhere, i.e., migrate and proliferate, while in the soft tumor core the tumor cells remain in dormant or stemness state. In general, cancer tissue can have heterogenous stiffness. It was found that cancer tissue is composed of different regions in terms of stiffness: a dominant soft part with the stiffness 0,31-0,75 kPa, a part with the stiffness 1,54-1,99 kPa and ultimately a stiff part with the stiffness approx. 20 kPa [60]. Specifically, in HCC, the tumor part with lowest stiffness might function as a mechanical marker for HCC malignancy assessment [217]. In summary, tumors usually have a soft core along with a rigid ECM structure that can serve as a navigation and adhesion pathway during migration [61].

In conclusion, we proposed a model of the HCC resembling a tumor core with a low cell proliferation, down regulation YAP and mTOR, mitochondrial depolarization and fission, downregulation of MTCO1, and upregulated lactated and pyruvate. We proved, that 3D cell culture might be a useful platform to study basic molecular mechanisms of mechanotransduction of the various cells, while recapitulating the *in vivo* pathophysiological conditions of the liver cancer cells.

Additional discussion can be found in the published original research papers [37], [98] or in Appendices I and II respectively.

6 CONCLUSIONS

In this doctoral thesis, we investigated how physical cues of soft (~94 Pa) 3D collagen scaffold affects the cancer liver cells Alexander and HepG2. We have used the biochemical analysis, biophysical approach and genetic manipulation in order to explore the molecular mechanisms behind the mechanotransduction of hepatic cancer cells in 3D cell culture.

Specifically, we have characterized the microarchitecture of in-house made 3D collagen scaffold (CS) cell culture and distinguish between collagen pores and fibers and found the average values for collagen fibers thickness as well as collagen pores diameter.

We have established the cell culture of genetically validated Alexander and HepG2 hepatic cell lines in 3D CS using genetic analysis of short tandem repeats (STR).

We have captured the morphological differences and found that cellular and nuclear sizes in cells cultured in 2D monolayer culture (MC) were higher than in cells cultured in 3D CS. Using proliferation markers PCNA and Ki-67, we found that both cell lines cultured in 3D CS have decreased proliferation dynamics in comparison with 2D MC.

We characterized the cytoskeletal structure remodeling as well as decrease of cellular adhesion in 3D CS. Using immunodetection and immunofluorescence we found that YAP was downregulated in cells cultured in 3D CS. Moreover, we found that there is a cross-talk between YAP and mTOR in 3D CS. Decrease in mTOR in 3D CS was accompanied with the promotion of autophagy, as we found using LC-3 autophagy marker.

In 3D CS, mitochondrial dynamics was shifted towards the mitochondrial fission and cells were more sensitive towards the chemical treatment with ionomycin, CCCP and KCN. Using colorimetric assays, we found the decrease for metabolic markers of glycolysis in 3D CS, namely pyruvate and lactate.

Ultimately, we used the photobiomodulation treatment with red laser light in order to monitor viability of cells in 3D CS. We found, that both cell lines were sensitive towards the photobiomodulation treatment in 3D CS and found a decrease in viability. On the other hand, cells cultured on 2D MC were not sensitive towards photobiomodulation treatment as shown by sustained levels of viability marker Calcein. Therefore, in case of HepG2

cells, we hypothesized that this result might be mediated via Bcl-2 axis, that is protecting cells against the apoptosis. Using immunodetection, we found a decrease level of Bcl-2 in HepG2 cells cultured in 3D CS, that supports our hypothesis.

To conclude, proposed doctoral thesis provides insights into the fundamentals of molecular signaling pathways in cells as well as metabolic changes upon the culturing the cells in soft 3D cell culture. We believe that soft 3D cell culture of collagen scaffold might serve as a versatile model for further research in area of mechanical regulation in living cells.

BIBIOLOGRAPHY

[1]   Bruce Alberts, *Molecular biology of the cell*, 6th ed. Second edition. New York : Garland Pub., [1989] ©1989, 1989. [Online]. Available: https://search.library.wisc.edu/catalog/999598982402121

[2]   C. Frantz, K. M. Stewart, and V. M. Weaver, "The extracellular matrix at a glance," *Journal of Cell Science*, vol. 123, no. 24. pp. 4195–4200, Dec. 15, 2010. doi: 10.1242/jcs.023820.

[3]   C. Bonnans, J. Chou, and Z. Werb, "Remodelling the extracellular matrix in development and disease," *Nature Reviews Molecular Cell Biology*, vol. 15, no. 12. Nature Publishing Group, pp. 786–801, Dec. 11, 2014. doi: 10.1038/nrm3904.

[4]   P. Bedossa and V. Paradis, "Liver extracellular matrix in health and disease," *Journal of Pathology*, vol. 200, no. 4. pp. 504–515, Jul. 01, 2003. doi: 10.1002/path.1397.

[5]   G. E. Arteel and A. Naba, "The liver matrisome – looking beyond collagens," *JHEP Reports*, vol. 2, no. 4. Elsevier B.V., Aug. 01, 2020. doi: 10.1016/j.jhepr.2020.100115.

[6]   D. R. Critchley, "Focal adhesions – the cytoskeletal connection," *Curr Opin Cell Biol*, vol. 12, no. 1, pp. 133–139, 2000, doi: https://doi.org/10.1016/S0955-0674(99)00067-8.

[7]   L. Borradori and A. Sonnenberg, "Structure and function of hemidesmosomes: More than simple adhesion complexes," *Journal of Investigative Dermatology*, vol. 112, no. 4, pp. 411–418, 1999, doi: 10.1046/j.1523-1747.1999.00546.x.

[8]   P. Kanchanawong *et al.*, "Nanoscale architecture of integrin-based cell adhesions," *Nature*, vol. 468, no. 7323, pp. 580–584, Nov. 2010, doi: 10.1038/nature09621.

[9]   S. Hirohashi and Y. Kanai, "Cell adhesion system and human cancer morphogenesis," *Cancer Science*, vol. 94, no. 7. pp. 575–581, Jul. 01, 2003. doi: 10.1111/j.1349-7006.2003.tb01485.x.

[10]   T. Okegawa, R.-C. Pong, Y. Li, and J.-T. Hsieh, "The role of cell adhesion molecule in cancer progression and its application in cancer therapy *."

[11]   G. Giannone, "Super-resolution links vinculin localization to function in focal adhesions," *Nature Cell Biology*, vol. 17, no. 7. Nature Publishing Group, pp. 845–847, Jul. 02, 2015. doi: 10.1038/ncb3196.

[12]   D. E. Jaalouk and J. Lammerding, "Mechanotransduction gone awry," *Nature Reviews Molecular Cell Biology*, vol. 10, no. 1. pp. 63–73, Jan. 2009. doi: 10.1038/nrm2597.

[13]   O. Chaudhuri, J. Cooper-White, P. A. Janmey, D. J. Mooney, and V. B. Shenoy, "Effects of extracellular matrix viscoelasticity on cellular behaviour," *Nature*, vol. 584, no. 7822. Nature Research, pp. 535–546, Aug. 27, 2020. doi: 10.1038/s41586-020-2612-2.

[14]   Y. Sun, C. S. Chen, and J. Fu, "Forcing stem cells to behave: A biophysical perspective of the cellular microenvironment," *Annual Review of Biophysics*, vol. 41, no. 1. pp. 519–542, Jun. 09, 2012. doi: 10.1146/annurev-biophys-042910-155306.

[15]   D. E. Discher, P. Janmey, and Y.-L. Wang, "Tissue Cells Feel and Respond to the Stiffness of Their Substrate." [Online]. Available: http://science.sciencemag.org/

[16]   M. P. Lutolf, P. M. Gilbert, and H. M. Blau, "Designing materials to direct stem-cell fate," *Nature*, vol. 462, no. 7272. pp. 433–441, Nov. 26, 2009. doi: 10.1038/nature08602.

[17]   H. J. Lee *et al.*, "Fluid shear stress activates YAP1 to promote cancer cell motility," *Nat Commun*, vol. 8, Jan. 2017, doi: 10.1038/ncomms14122.

[18]   S. Park, W. H. Jung, M. Pittman, J. Chen, and Y. Chen, "The Effects of Stiffness, Fluid Viscosity, and Geometry of Microenvironment in Homeostasis, Aging, and Diseases: A Brief Review," *Journal of Biomechanical Engineering*, vol. 142, no. 10. American Society of Mechanical Engineers (ASME), Oct. 01, 2020. doi: 10.1115/1.4048110.

[19]   T. D. Ross *et al.*, "Integrins in mechanotransduction," *Current Opinion in Cell Biology*, vol. 25, no. 5. pp. 613–618, Oct. 2013. doi: 10.1016/j.ceb.2013.05.006.

[20]   J. Seong, N. Wang, and Y. Wang, "Mechanotransduction at focal adhesions: From physiology to cancer development," *J Cell Mol Med*, vol. 17, no. 5, pp. 597–604, May 2013, doi: 10.1111/jcmm.12045.

[21]   S. Pagliari *et al.*, "YAP–TEAD1 control of cytoskeleton dynamics and intracellular tension guides human pluripotent stem cell mesoderm specification," *Cell Death Differ*, vol. 28, no. 4, pp. 1193–1207, Apr. 2021, doi: 10.1038/s41418-020-00643-5.

[22]   X. Cai, K. C. Wang, and Z. Meng, "Mechanoregulation of YAP and TAZ in Cellular Homeostasis and Disease Progression," *Frontiers in Cell and Developmental Biology*, vol. 9. Frontiers Media S.A., May 24, 2021. doi: 10.3389/fcell.2021.673599.

[23]   S. Dupont *et al.*, "Role of YAP/TAZ in mechanotransduction," *Nature*, vol. 474, no. 7350, pp. 179–184, Jun. 2011, doi: 10.1038/nature10137.

[24]   A. Higuchi *et al.*, "Physical cues of cell culture materials lead the direction of differentiation lineages of pluripotent stem cells," *Journal of Materials Chemistry*

B, vol. 3, no. 41. Royal Society of Chemistry, pp. 8032–8058, 2015. doi: 10.1039/c5tb01276g.

[25]   J. Mo, H. W. Park, and K. Guan, "The Hippo signaling pathway in stem cell biology and cancer," *EMBO Rep*, vol. 15, no. 6, pp. 642–656, Jun. 2014, doi: 10.15252/embr.201438638.

[26]   D. Pan, "The hippo signaling pathway in development and cancer," *Developmental Cell*, vol. 19, no. 4. pp. 491–505, Oct. 19, 2010. doi: 10.1016/j.devcel.2010.09.011.

[27]   G. Nardone *et al.*, "YAP regulates cell mechanics by controlling focal adhesion assembly," *Nat Commun*, vol. 8, May 2017, doi: 10.1038/ncomms15321.

[28]   S. Zhang and D. Zhou, "Role of the transcriptional coactivators YAP/TAZ in liver cancer," *Current Opinion in Cell Biology*, vol. 61. Elsevier Ltd, pp. 64–71, Dec. 01, 2019. doi: 10.1016/j.ceb.2019.07.006.

[29]   T. Bertero *et al.*, "Vascular stiffness mechanoactivates YAP/TAZ-dependent glutaminolysis to drive pulmonary hypertension," *Journal of Clinical Investigation*, vol. 126, no. 9, pp. 3313–3335, Sep. 2016, doi: 10.1172/JCI86387.

[30]   K. Du *et al.*, "Hedgehog-YAP Signaling Pathway Regulates Glutaminolysis to Control Activation of Hepatic Stellate Cells," *Gastroenterology*, vol. 154, no. 5, pp. 1465-1479.e13, Apr. 2018, doi: 10.1053/j.gastro.2017.12.022.

[31]   S. W. Plouffe *et al.*, "Characterization of Hippo Pathway Components by Gene Inactivation," *Mol Cell*, vol. 64, no. 5, pp. 993–1008, Dec. 2016, doi: 10.1016/j.molcel.2016.10.034.

[32]   É. Cosset *et al.*, "Glut3 Addiction Is a Druggable Vulnerability for a Molecularly Defined Subpopulation of Glioblastoma," *Cancer Cell*, vol. 32, no. 6, pp. 856-868.e5, Dec. 2017, doi: 10.1016/j.ccell.2017.10.016.

[33]   X. Zhang *et al.*, "The role of YAP/TAZ activity in cancer metabolic reprogramming," *Molecular Cancer*, vol. 17, no. 1. BioMed Central Ltd., Sep. 03, 2018. doi: 10.1186/s12943-018-0882-1.

[34]   M. Aragona *et al.*, "A mechanical checkpoint controls multicellular growth through YAP/TAZ regulation by actin-processing factors," *Cell*, vol. 154, no. 5, pp. 1047–1059, Aug. 2013, doi: 10.1016/j.cell.2013.07.042.

[35]   B. Zhao, L. Li, Q. Lei, and K. L. Guan, "The Hippo-YAP pathway in organ size control and tumorigenesis: An updated version," *Genes and Development*, vol. 24, no. 9. pp. 862–874, May 01, 2010. doi: 10.1101/gad.1909210.

[36]   J. K. H. Hu, W. Du, S. J. Shelton, M. C. Oldham, C. M. DiPersio, and O. D. Klein, "An FAK-YAP-mTOR Signaling Axis Regulates Stem Cell-Based Tissue

Renewal in Mice," *Cell Stem Cell*, vol. 21, no. 1, pp. 91-106.e6, Jul. 2017, doi: 10.1016/j.stem.2017.03.023.

[37] A. Frtús *et al.*, "Hepatic tumor cell morphology plasticity under physical constraints in 3D cultures driven by YAP–mTOR axis," *Pharmaceuticals*, vol. 13, no. 12, pp. 1–25, Dec. 2020, doi: 10.3390/ph13120430.

[38] T. Bertero and C. Gaggioli, "Mechanical forces rewire metabolism in the tumor niche," *Mol Cell Oncol*, vol. 6, no. 3, May 2019, doi: 10.1080/23723556.2019.1592945.

[39] E. Trefts, M. Gannon, and D. H. Wasserman, "The liver," *Current Biology*, vol. 27, no. 21. Cell Press, pp. R1147–R1151, Nov. 06, 2017. doi: 10.1016/j.cub.2017.09.019.

[40] J. H. Tabibian, A. I. Masyuk, T. V. Masyuk, S. P. O'Hara, and N. F. LaRusso, "Physiology of cholangiocytes," *Compr Physiol*, vol. 3, no. 1, pp. 541–565, 2013, doi: 10.1002/cphy.c120019.

[41] M. Uzhytchak *et al.*, "Lysosomal nanotoxicity: Impact of nanomedicines on lysosomal function," *Adv Drug Deliv Rev*, vol. 197, 2023, doi: 10.1016/j.addr.2023.114828.

[42] H. B. El-Serag, "Hepatocellular carcinoma: Recent trends in the United States," in *Gastroenterology*, W.B. Saunders, 2004. doi: 10.1053/j.gastro.2004.09.013.

[43] J.-G. Chen *et al.*, "Liver Cancer Survival: A Real World Observation of 45 Years with 32,556 Cases," *J Hepatocell Carcinoma*, vol. Volume 8, pp. 1023–1034, Aug. 2021, doi: 10.2147/jhc.s321346.

[44] F. Bray, J. Ferlay, I. Soerjomataram, R. L. Siegel, L. A. Torre, and A. Jemal, "Global cancer statistics 2018: GLOBOCAN estimates of incidence and mortality worldwide for 36 cancers in 185 countries," *CA Cancer J Clin*, vol. 68, no. 6, pp. 394–424, Nov. 2018, doi: 10.3322/caac.21492.

[45] J. L. Petrick *et al.*, "International trends in hepatocellular carcinoma incidence, 1978–2012," *Int J Cancer*, vol. 147, no. 2, pp. 317–330, Jul. 2020, doi: 10.1002/ijc.32723.

[46] J. Eyckmans, T. Boudou, X. Yu, and C. S. Chen, "A Hitchhiker's Guide to Mechanobiology," *Developmental Cell*, vol. 21, no. 1. pp. 35–47, Jul. 19, 2011. doi: 10.1016/j.devcel.2011.06.015.

[47] S. Jodele, L. Blavier, J. M. Yoon, and Y. A. DeClerck, "Modifying the soil to affect the seed: Role of stromal-derived matrix metalloproteinases in cancer progression," *Cancer and Metastasis Reviews*, vol. 25, no. 1. pp. 35–43, Mar. 2006. doi: 10.1007/s10555-006-7887-8.

[48] B. Têtu *et al.*, "The influence of MMP-14, TIMP-2 and MMP-2 expression on breast cancer prognosis," *Breast Cancer Research*, vol. 8, no. 3, Jun. 2006, doi: 10.1186/bcr1503.

[49] S. Ramaswamy, K. N. Ross, E. S. Lander, and T. R. Golub, "A molecular signature of metastasis in primary solid tumors," *Nat Genet*, vol. 33, no. 1, pp. 49–54, Jan. 2003, doi: 10.1038/ng1060.

[50] K. R. Levental *et al.*, "Matrix Crosslinking Forces Tumor Progression by Enhancing Integrin Signaling," *Cell*, vol. 139, no. 5, pp. 891–906, Nov. 2009, doi: 10.1016/j.cell.2009.10.027.

[51] J. Schrader *et al.*, "Matrix stiffness modulates proliferation, chemotherapeutic response, and dormancy in hepatocellular carcinoma cells," *Hepatology*, vol. 53, no. 4, pp. 1192–1205, Apr. 2011, doi: 10.1002/hep.24108.

[52] D. Roulot, S. Czernichow, H. Le Clésiau, J. L. Costes, A. C. Vergnaud, and M. Beaugrand, "Liver stiffness values in apparently healthy subjects: Influence of gender and metabolic syndrome," *J Hepatol*, vol. 48, no. 4, pp. 606–613, Apr. 2008, doi: 10.1016/j.jhep.2007.11.020.

[53] R. Masuzaki *et al.*, "Prospective risk assessment for hepatocellular carcinoma development in patients with chronic hepatitis C by transient elastography," *Hepatology*, vol. 49, no. 6, pp. 1954–1961, Jun. 2009, doi: 10.1002/hep.22870.

[54] K. L. Choong *et al.*, "Elasticity Characterization of Liver Cancers Using Shear Wave Ultrasound Elastography: Comparison Between Hepatocellular Carcinoma and Liver Metastasis," *Journal of Diagnostic Medical Sonography*, vol. 33, no. 6, pp. 481–488, Nov. 2017, doi: 10.1177/8756479317733713.

[55] B. J. McMahon, "The natural history of chronic hepatitis B virus infection," *Hepatology*, vol. 49, no. SUPPL. 5, May 2009, doi: 10.1002/hep.22898.

[56] R. Masuzaki *et al.*, "Assessing liver tumor stiffness by transient elastography," *Hepatol Int*, vol. 1, no. 3, pp. 394–397, Oct. 2007, doi: 10.1007/s12072-007-9012-7.

[57] J. Foucher *et al.*, "Diagnosis of cirrhosis by transient elastography (FibroScan): A prospective study," *Gut*, vol. 55, no. 3, pp. 403–408, Mar. 2006, doi: 10.1136/gut.2005.069153.

[58] B. Yao, Y. Niu, Y. Li, T. Chen, X. Wei, and Q. Liu, "High-matrix-stiffness induces promotion of hepatocellular carcinoma proliferation and suppression of apoptosis via miR-3682-3p-PHLDA1-FAS pathway," *J Cancer*, vol. 11, no. 21, pp. 6188–6203, Aug. 2020, doi: 10.7150/jca.45998.

[59] Q. P. Liu, Q. Luo, B. Deng, Y. Ju, and G. Bin Song, "Stiffer matrix accelerates migration of hepatocellular carcinoma cells through enhanced aerobic glycolysis

via the MAPK-YAP signaling," *Cancers (Basel)*, vol. 12, no. 2, Feb. 2020, doi: 10.3390/cancers12020490.

[60] M. Plodinec *et al.*, "The nanomechanical signature of breast cancer," *Nat Nanotechnol*, vol. 7, no. 11, pp. 757–765, 2012, doi: 10.1038/nnano.2012.167.

[61] L. K. Chin, Y. Xia, D. E. Discher, and P. A. Janmey, "Mechanotransduction in cancer," *Current Opinion in Chemical Engineering*, vol. 11. Elsevier Ltd, pp. 77–84, Feb. 01, 2016. doi: 10.1016/j.coche.2016.01.011.

[62] S. Nallanthighal, J. P. Heiserman, and D. J. Cheon, "The Role of the Extracellular Matrix in Cancer Stemness," *Frontiers in Cell and Developmental Biology*, vol. 7. Frontiers Media S.A., Jul. 05, 2019. doi: 10.3389/fcell.2019.00086.

[63] D. López-Terrada, S. W. Cheung, M. J. Finegold, and B. B. Knowles, "Hep G2 is a hepatoblastoma-derived cell line," *Hum Pathol*, vol. 40, no. 10, pp. 1512–1515, 2009, doi: https://doi.org/10.1016/j.humpath.2009.07.003.

[64] R. J. Daemer *et al.*, "NOTES PLC/PRF/5 (Alexander) Hepatoma Cell Line: Further Characterization and Studies of Infectivity," 1980.

[65] Z. Qiu *et al.*, "Hepatocellular carcinoma cell lines retain the genomic and transcriptomic landscapes of primary human cancers," *Sci Rep*, vol. 6, Jun. 2016, doi: 10.1038/srep27411.

[66] K. Fukuyama *et al.*, "Gene expression profiles of liver cancer cell lines reveal two hepatocyte-like and fibroblast-like clusters," *PLoS One*, vol. 16, no. 2 February, Feb. 2021, doi: 10.1371/journal.pone.0245939.

[67] J. P. Gillet, S. Varma, and M. M. Gottesman, "The clinical relevance of cancer cell lines," *Journal of the National Cancer Institute*, vol. 105, no. 7. pp. 452–458, Apr. 03, 2013. doi: 10.1093/jnci/djt007.

[68] P. Godoy *et al.*, "Recent advances in 2D and 3D in vitro systems using primary hepatocytes, alternative hepatocyte sources and non-parenchymal liver cells and their use in investigating mechanisms of hepatotoxicity, cell signaling and ADME," *Archives of Toxicology*, vol. 87, no. 8. pp. 1315–1530, Aug. 2013. doi: 10.1007/s00204-013-1078-5.

[69] S. F. Lan, B. Safiejko-Mroczka, and B. Starly, "Long-term cultivation of HepG2 liver cells encapsulated in alginate hydrogels: A study of cell viability, morphology and drug metabolism," *Toxicology in Vitro*, vol. 24, no. 4, pp. 1314–1323, Jun. 2010, doi: 10.1016/j.tiv.2010.02.015.

[70] Y. Saito, T. Ikemoto, Y. Morine, and M. Shimada, "Current status of hepatocyte-like cell therapy from stem cells," *Surgery Today*, vol. 51, no. 3. Springer, pp. 340–349, Mar. 01, 2021. doi: 10.1007/s00595-020-02092-6.

[71]   J. V. Castell, R. Jover, C. P. Martínez-Jiménez, and M. J. Gómez-Lechón, "Hepatocyte cell lines: Their use, scope and limitations in drug metabolism studies," *Expert Opinion on Drug Metabolism and Toxicology*, vol. 2, no. 2. pp. 183–212, Apr. 2006. doi: 10.1517/17425255.2.2.183.

[72]   J. V. Castell and M. J. Gómez-Lechón, "Liver cell culture techniques," *Methods in Molecular Biology*, vol. 481, pp. 35–46, 2009, doi: 10.1007/978-1-59745-201-4_4.

[73]   J. C. Y. Dunn, M. L. Yarmush, H. G. Koebe, and R. G. Tompkins, "Hepatocyte function and extracellular matrix geometry: long-term culture in a sandwich configuration."

[74]   S. R. Caliari and J. A. Burdick, "A practical guide to hydrogels for cell culture," *Nature Methods*, vol. 13, no. 5. Nature Publishing Group, pp. 405–414, May 01, 2016. doi: 10.1038/nmeth.3839.

[75]   M. W. Tibbitt and K. S. Anseth, "Hydrogels as extracellular matrix mimics for 3D cell culture," *Biotechnology and Bioengineering*, vol. 103, no. 4. pp. 655–663, Jul. 01, 2009. doi: 10.1002/bit.22361.

[76]   R. Edmondson, J. J. Broglie, A. F. Adcock, and L. Yang, "Three-dimensional cell culture systems and their applications in drug discovery and cell-based biosensors," *Assay and Drug Development Technologies*, vol. 12, no. 4. Mary Ann Liebert Inc., pp. 207–218, May 01, 2014. doi: 10.1089/adt.2014.573.

[77]   Q. Liu, A. Zeng, Z. Liu, C. Wu, and L. Song, "Liver organoids: From fabrication to application in liver diseases," *Frontiers in Physiology*, vol. 13. Frontiers Media S.A., Jul. 18, 2022. doi: 10.3389/fphys.2022.956244.

[78]   B. M. Baker and C. S. Chen, "Deconstructing the third dimension-how 3D culture microenvironments alter cellular cues," *Journal of Cell Science*, vol. 125, no. 13. pp. 3015–3024, Jul. 01, 2012. doi: 10.1242/jcs.079509.

[79]   H. Huang, Y. Ding, X. S. Sun, and T. A. Nguyen, "Peptide Hydrogelation and Cell Encapsulation for 3D Culture of MCF-7 Breast Cancer Cells," *PLoS One*, vol. 8, no. 3, Mar. 2013, doi: 10.1371/journal.pone.0059482.

[80]   M. J. Lerman, J. Lembong, S. Muramoto, G. Gillen, and J. P. Fisher, "The Evolution of Polystyrene as a Cell Culture Material," *Tissue Eng Part B Rev*, vol. 24, no. 5, pp. 359–372, Oct. 2018, doi: 10.1089/ten.teb.2018.0056.

[81]   S. Abdelrahman *et al.*, "The Impact of Mechanical Cues on the Metabolomic and Transcriptomic Profiles of Human Dermal Fibroblasts Cultured in Ultrashort Self-Assembling Peptide 3D Scaffolds," *ACS Nano*, vol. 17, no. 15, pp. 14508–14531, Aug. 2023, doi: 10.1021/acsnano.3c01176.

[82] P. A. Kenny *et al.*, "The morphologies of breast cancer cell lines in three-dimensional assays correlate with their profiles of gene expression," *Mol Oncol*, vol. 1, no. 1, pp. 84–96, Jun. 2007, doi: 10.1016/j.molonc.2007.02.004.

[83] L. A. Gurski, N. J. Petrelli, X. Jia, and M. C. Farach-Carson, "3D Matrices for Anti-Cancer Drug Testing and Development," *Oncol Issues*, vol. 25, no. 1, pp. 20–25, Jan. 2010, doi: 10.1080/10463356.2010.11883480.

[84] O. Trédan, C. M. Galmarini, K. Patel, and I. F. Tannock, "Drug resistance and the solid tumor microenvironment," *Journal of the National Cancer Institute*, vol. 99, no. 19. pp. 1441–1454, Oct. 2007. doi: 10.1093/jnci/djm135.

[85] B. K. Jong, "Three-dimensional tissue culture models in cancer biology," *Seminars in Cancer Biology*, vol. 15, no. 5 SPEC. ISS. Academic Press, pp. 365–377, 2005. doi: 10.1016/j.semcancer.2005.05.002.

[86] K. Chitcholtan, P. H. Sykes, and J. J. Evans, "The resistance of intracellular mediators to doxorubicin and cisplatin are distinct in 3D and 2D endometrial cancer," *J Transl Med*, vol. 10, no. 1, Mar. 2012, doi: 10.1186/1479-5876-10-38.

[87] A. C. Luca *et al.*, "Impact of the 3D Microenvironment on Phenotype, Gene Expression, and EGFR Inhibition of Colorectal Cancer Cell Lines," *PLoS One*, vol. 8, no. 3, Mar. 2013, doi: 10.1371/journal.pone.0059689.

[88] B. Fallica, J. S. Maffei, S. Villa, G. Makin, and M. Zaman, "Alteration of Cellular Behavior and Response to PI3K Pathway Inhibition by Culture in 3D Collagen Gels," *PLoS One*, vol. 7, no. 10, Oct. 2012, doi: 10.1371/journal.pone.0048024.

[89] K. J. Price *et al.*, "Matrigel Basement Membrane Matrix influences expression of microRNAs in cancer cell lines," *Biochem Biophys Res Commun*, vol. 427, no. 2, pp. 343–348, Oct. 2012, doi: 10.1016/j.bbrc.2012.09.059.

[90] D. Yip and C. H. Cho, "A multicellular 3D heterospheroid model of liver tumor and stromal cells in collagen gel for anti-cancer drug testing," *Biochem Biophys Res Commun*, vol. 433, no. 3, pp. 327–332, Apr. 2013, doi: 10.1016/j.bbrc.2013.03.008.

[91] K. M. Yamada and E. Cukierman, "Modeling Tissue Morphogenesis and Cancer in 3D," *Cell*, vol. 130, no. 4. Elsevier B.V., pp. 601–610, Aug. 24, 2007. doi: 10.1016/j.cell.2007.08.006.

[92] D. K. Mishra *et al.*, "Human Lung Cancer Cells Grown in an Ex Vivo 3D Lung Model Produce Matrix Metalloproteinases Not Produced in 2D Culture," *PLoS One*, vol. 7, no. 9, Sep. 2012, doi: 10.1371/journal.pone.0045308.

[93] T. Yeung *et al.*, "Effects of substrate stiffness on cell morphology, cytoskeletal structure, and adhesion," *Cell Motil Cytoskeleton*, vol. 60, no. 1, pp. 24–34, Jan. 2005, doi: 10.1002/cm.20041.

[94] H. Karlsson, M. Fryknäs, R. Larsson, and P. Nygren, "Loss of cancer drug activity in colon cancer HCT-116 cells during spheroid formation in a new 3-D spheroid cell culture system," *Exp Cell Res*, vol. 318, no. 13, pp. 1577–1585, Aug. 2012, doi: 10.1016/j.yexcr.2012.03.026.

[95] X. Xu, L. A. Gurski, C. Zhang, D. A. Harrington, M. C. Farach-Carson, and X. Jia, "Recreating the tumor microenvironment in a bilayer, hyaluronic acid hydrogel construct for the growth of prostate cancer spheroids," *Biomaterials*, vol. 33, no. 35, pp. 9049–9060, Dec. 2012, doi: 10.1016/j.biomaterials.2012.08.061.

[96] B. K. Jong, "Three-dimensional tissue culture models in cancer biology," *Seminars in Cancer Biology*, vol. 15, no. 5 SPEC. ISS. Academic Press, pp. 365–377, 2005. doi: 10.1016/j.semcancer.2005.05.002.

[97] A. Passaniti, H. K. Kleinman, and G. R. Martin, "Matrigel: history/background, uses, and future applications," *Journal of Cell Communication and Signaling*, vol. 16, no. 4. Springer Science and Business Media B.V., pp. 621–626, Dec. 01, 2022. doi: 10.1007/s12079-021-00643-1.

[98] A. Frtús *et al.*, "Mechanical Regulation of Mitochondrial Dynamics and Function in a 3D-Engineered Liver Tumor Microenvironment," *ACS Biomater Sci Eng*, Mar. 2023, doi: 10.1021/acsbiomaterials.2c01518.

[99] Q. Shao and B. Xing, "Photoactive molecules for applications in molecular imaging and cell biology," *Chem Soc Rev*, vol. 39, no. 8, pp. 2835–2846, Jul. 2010, doi: 10.1039/b915574k.

[100] J. Schimer *et al.*, "Triggering HIV polyprotein processing by light using rapid photodegradation of a tight-binding protease inhibitor," *Nat Commun*, vol. 6, Mar. 2015, doi: 10.1038/ncomms7461.

[101] S. A. Josselyn, "The past, present and future of light-gated ion channels and optogenetics," *Elife*, vol. 7, 2018, doi: 10.7554/ELIFE.42367.

[102] A. Stirbet, D. Lazár, Y. Guo, and G. Govindjee, "Photosynthesis: Basics, history and modelling," *Annals of Botany*, vol. 126, no. 4. Oxford University Press, pp. 511–537, Sep. 14, 2020. doi: 10.1093/aob/mcz171.

[103] T. D. Lamb and E. N. Pugh, "Phototransduction, dark adaption, and rhodopsin regeneration: The proctor lecture," in *Investigative Ophthalmology and Visual Science*, Dec. 2006, pp. 5138–5152. doi: 10.1167/iovs.06-0849.

[104] S. H. Yun and S. J. J. Kwok, "Light in diagnosis, therapy and surgery," *Nature Biomedical Engineering*, vol. 1, no. 1. Nature Publishing Group, Jan. 10, 2017. doi: 10.1038/s41551-016-0008.

[105] E. L. Tanzi, J. R. Lupton, and T. S. Alster, "Lasers in dermatology: Four decades of progress," *J Am Acad Dermatol*, vol. 49, no. 1, pp. 1–34, Jul. 2003, doi: 10.1067/mjd.2003.582.

[106] H. A. Wigdor, J. T. Walsh, J. D. B. Featherstone, S. R. Visuri, D. Fried, and J. L. Waldvogel, "Lasers in Dentistry," 1995.

[107] "Phototherapy for Neonatal Jaundice," 2008. [Online]. Available: www.nejm.org

[108] T. Schwarz and S. Beissert, "Milestones in Photoimmunology," *Journal of Investigative Dermatology*, vol. 133, pp. E7–E10, Jul. 2013, doi: 10.1038/skinbio.2013.177.

[109] H. W. Lim, N. Silpa-Archa, U. Amadi, A. Menter, A. S. Van Voorhees, and M. Lebwohl, "Phototherapy in dermatology: A call for action," *Journal of the American Academy of Dermatology*, vol. 72, no. 6. Mosby Inc., pp. 1078–1080, Jun. 01, 2015. doi: 10.1016/j.jaad.2015.03.017.

[110] T. A. Legates, D. C. Fernandez, and S. Hattar, "Light as a central modulator of circadian rhythms, sleep and affect," *Nature Reviews Neuroscience*, vol. 15, no. 7. Nature Publishing Group, pp. 443–454, 2014. doi: 10.1038/nrn3743.

[111] H. Chung, T. Dai, S. K. Sharma, Y. Y. Huang, J. D. Carroll, and M. R. Hamblin, "The nuts and bolts of low-level laser (Light) therapy," *Ann Biomed Eng*, vol. 40, no. 2, pp. 516–533, Feb. 2012, doi: 10.1007/s10439-011-0454-7.

[112] V. Heiskanen and M. R. Hamblin, "Photobiomodulation: Lasers: vs. light emitting diodes?," *Photochemical and Photobiological Sciences*, vol. 17, no. 8. Royal Society of Chemistry, pp. 1003–1017, 2018. doi: 10.1039/c8pp00176f.

[113] T. I. Karu, "Photobiological Fundamentals of Low-Power Laser Therapy," 1987.

[114] L. F. De Freitas and M. R. Hamblin, "Proposed Mechanisms of Photobiomodulation or Low-Level Light Therapy," *IEEE Journal of Selected Topics in Quantum Electronics*, vol. 22, no. 3, pp. 348–364, May 2016, doi: 10.1109/JSTQE.2016.2561201.

[115] M. R. Hamblin, "Mechanisms and applications of the anti-inflammatory effects of photobiomodulation," *AIMS Biophysics*, vol. 4, no. 3. American Institute of Mathematical Sciences, pp. 337–361, 2017. doi: 10.3934/biophy.2017.3.337.

[116] "Effect of Laser Rays on Wound Healing."

[117] E. Mester, S. Nagylucskay, A. Döklen, and S. Tisza, "Laser stimulation of wound healing.," *Acta Chir Acad Sci Hung*, vol. 17, no. 1, pp. 49–55, 1976.

[118] "Bjordal et al: A systematic review of low level laser therapy with location-specific doses for pain from joint disorders."

[119] A. Christie, G. Jamtvedt, K. T. Dahm, R. H. Moe, E. A. Haavardsholm, and K. B. Hagen, "Effectiveness of Nonpharmacological and Nonsurgical Interventions for Patients With Rheumatoid Arthritis: An Overview of Systematic Reviews," 2007. [Online]. Available: https://academic.oup.com/ptj/article/87/12/1697/2747275

[120] G. Jamtvedt *et al.*, "Physical Therapy Interventions for Patients With Osteoarthritis of the Knee: An Overview of Systematic Reviews," 2008. [Online]. Available: www.ptjournal.org

[121] J. C. Sutherland, "Biological Effects of Polychromatic Light¶," *Photochem Photobiol*, vol. 76, no. 2, pp. 164–170, May 2007, doi: 10.1562/0031-8655(2002)0760164beopl2.0.co2.

[122] M. R. Hamblin, Y. Y. Huang, S. K. Sharma, and J. Carroll, "Biphasic dose response in low level light therapy - an update," *Dose-Response*, vol. 9, no. 4, pp. 602–618, 2011, doi: 10.2203/dose-response.11-009.Hamblin.

[123] A. N. Pereira, C. De Paula Eduardo, E. Matson, and M. M. Marques, "Effect of low-power laser irradiation on cell growth and procollagen synthesis of cultured fibroblasts," *Lasers Surg Med*, vol. 31, no. 4, pp. 263–267, 2002, doi: 10.1002/lsm.10107.

[124] "Biostimulatory windows in low-intensity laser activation: lasers, scanners, and NASA's light-emitting diode array system".

[125] A. P. Castano *et al.*, "Low-level laser therapy for zymosan-induced arthritis in rats: Importance of illumination time," *Lasers Surg Med*, vol. 39, no. 6, pp. 543–550, Jul. 2007, doi: 10.1002/lsm.20516.

[126] V. Haxsen, D. Schikora, U. Sommer, A. Remppis, J. Greten, and C. Kasperk, "Relevance of laser irradiance threshold in the induction of alkaline phosphatase in human osteoblast cultures," *Lasers Med Sci*, vol. 23, no. 4, pp. 381–384, Oct. 2008, doi: 10.1007/s10103-007-0511-5.

[127] R. J. Lanzafame *et al.*, "Reciprocity of exposure time and irradiance on energy density during photoradiation on wound healing in a murine pressure ulcer model," *Lasers Surg Med*, vol. 39, no. 6, pp. 534–542, Jul. 2007, doi: 10.1002/lsm.20519.

[128] P. A. Lapchak, K. F. Salgado, C. H. Chao, and J. A. Zivin, "Transcranial near-infrared light therapy improves motor function following embolic strokes in rabbits: An extended therapeutic window study using continuous and pulse frequency delivery modes," *Neuroscience*, vol. 148, no. 4, pp. 907–914, Sep. 2007, doi: 10.1016/j.neuroscience.2007.07.002.

[129] M. Lunova *et al.*, "Light-induced modulation of the mitochondrial respiratory chain activity: possibilities and limitations," *Cellular and Molecular Life*

Sciences, vol. 77, no. 14, pp. 2815–2838, Jul. 2020, doi: 10.1007/s00018-019-03321-z.

[130] S. Wu, D. Xing, X. Gao, and W. R. Chen, "High fluence low-power laser irradiation induces mitochondrial permeability transition mediated by reactive oxygen species," *J Cell Physiol*, vol. 218, no. 3, pp. 603–611, Mar. 2009, doi: 10.1002/jcp.21636.

[131] I. Golovynska *et al.*, "Red and near-infrared light induces intracellular Ca2+ flux via the activation of glutamate N-methyl-D-aspartate receptors," *J Cell Physiol*, vol. 234, no. 9, pp. 15989–16002, Sep. 2019, doi: 10.1002/jcp.28257.

[132] "Cytochrome c oxidase as the primary photoacceptor upon laser exposure of cultured cells to visible and near IR-range light".

[133] T. I. Karu, L. V. Pyatibrat, S. F. Kolyakov, and N. I. Afanasyeva, "Absorption measurements of a cell monolayer relevant to phototherapy: Reduction of cytochrome c oxidase under near IR radiation," *J Photochem Photobiol B*, vol. 81, no. 2, pp. 98–106, Nov. 2005, doi: 10.1016/j.jphotobiol.2005.07.002.

[134] R. A. Capaldi, F. Malatesta, and V. M. Darley-Usmar, "STRUCTURE OF CYTOCHROME c OXIDASE," 1983.

[135] S. Passarella *et al.*, "Increase of proton electrochemical potential and ATP synthesis in rat liver mitochondria irradiated in vitro by helium-neon laser," *FEBS Lett*, vol. 175, no. 1, pp. 95–99, Sep. 1984, doi: 10.1016/0014-5793(84)80577-3.

[136] V. I. Lozinsky, "Cryostructuring of polymeric systems. 55. retrospective view on the more than 40 years of studies performed in the A.N.Nesmeyanov institute of organoelement compounds with respect of the cryostructuring processes in polymeric systems," *Gels*, vol. 6, no. 3. MDPI AG, pp. 1–59, Sep. 01, 2020. doi: 10.3390/gels6030029.

[137] E. Biela, J. Galas, B. Lee, G. L. Johnson, Z. Darzynkiewicz, and J. W. Dobrucki, "Col-F, a fluorescent probe for ex vivo confocal imaging of collagen and elastin in animal tissues," *Cytometry Part A*, vol. 83 A, no. 6, pp. 533–539, Jun. 2013, doi: 10.1002/cyto.a.22264.

[138] A. Capes-Davis *et al.*, "Match criteria for human cell line authentication: Where do we draw the line?," *Int J Cancer*, vol. 132, no. 11, pp. 2510–2519, Jun. 2013, doi: 10.1002/ijc.27931.

[139] C. Alston-Roberts *et al.*, "Cell line misidentification: The beginning of the end," *Nature Reviews Cancer*, vol. 10, no. 6. Nature Publishing Group, pp. 441–448, Jun. 01, 2010. doi: 10.1038/nrc2852.

[140] M. Uzhytchak *et al.*, "Iron Oxide Nanoparticle-Induced Autophagic Flux Is Regulated by Interplay between p53-mTOR Axis and Bcl-2 Signaling in Hepatic Cells," *Cells*, vol. 9, no. 4, Apr. 2020, doi: 10.3390/cells9041015.

[141] "Non-Thermal Plasma, as a New Physicochemical Source, to Induce Redox Imbalance and Subsequent Cell Death in Liver Cancer Cell Lines".

[142] J. Stancikova *et al.*, "NKD1 marks intestinal and liver tumors linked to aberrant wnt signaling," *Cell Signal*, vol. 27, no. 2, pp. 245–256, Feb. 2015, doi: 10.1016/j.cellsig.2014.11.008.

[143] M. Lunova *et al.*, "Expression of interferons lambda 3 and 4 induces identical response in human liver cell lines depending exclusively on canonical signaling," *Int J Mol Sci*, vol. 22, no. 5, pp. 1–15, Mar. 2021, doi: 10.3390/ijms22052560.

[144] T. D. Schmittgen and K. J. Livak, "Analyzing real-time PCR data by the comparative CT method," *Nat Protoc*, vol. 3, no. 6, pp. 1101–1108, May 2008, doi: 10.1038/nprot.2008.73.

[145] M. Jelinek *et al.*, "Preliminary study of ge-DLC nanocomposite biomaterials prepared by laser codeposition," *Nanomaterials*, vol. 9, no. 3, Mar. 2019, doi: 10.3390/nano9030451.

[146] K. Levada *et al.*, "Progressive lysosomal membrane permeabilization induced by iron oxide nanoparticles drives hepatic cell autophagy and apoptosis," *Nano Converg*, vol. 7, no. 1, Dec. 2020, doi: 10.1186/s40580-020-00228-5.

[147] S. Hayashi and Y. Okada, "Ultrafast superresolution fluorescence imaging with spinning disk confocal microscope optics," *Mol Biol Cell*, vol. 26, no. 9, pp. 1743–1751, May 2015, doi: 10.1091/mbc.E14-08-1287.

[148] A. Lynnyk *et al.*, "Manipulating the mitochondria activity in human hepatic cell line Huh7 by low-power laser irradiation," *Biomed Opt Express*, vol. 9, no. 3, p. 1283, Mar. 2018, doi: 10.1364/boe.9.001283.

[149] R. B. Dell, S. Holleran, and R. Ramakrishnan, "Sample size determination.," *ILAR J*, vol. 43, no. 4, pp. 207–13, 2002, doi: 10.1093/ilar.43.4.207.

[150] J. Jonkman, C. M. Brown, G. D. Wright, K. I. Anderson, and A. J. North, "Guidance for quantitative confocal microscopy," *Nat Protoc*, Mar. 2020, doi: 10.1038/s41596-020-0307-7.

[151] J. Y. Lee and M. Kitaoka, "A beginner's guide to rigor and reproducibility in fluorescence imaging experiments," *Molecular Biology of the Cell*, vol. 29, no. 13. American Society for Cell Biology, pp. 1519–1525, Jul. 01, 2018. doi: 10.1091/mbc.E17-05-0276.

[152] A. Frtús *et al.*, "Mechanical Regulation of Mitochondrial Dynamics and Function in a 3D-Engineered Liver Tumor Microenvironment," *ACS Biomater Sci Eng*, 2022, doi: 10.1021/acsbiomaterials.2c01518.

[153] B. Tian, Q. Luo, Y. Ju, and G. Song, "A soft matrix enhances the cancer stem cell phenotype of HCC cells," *Int J Mol Sci*, vol. 20, no. 11, Jun. 2019, doi: 10.3390/ijms20112831.

[154] J. T. Y. Lee and K. L. Chow, "SEM sample preparation for cells on 3D scaffolds by freeze-drying and HMDS," *Scanning*, vol. 34, no. 1, pp. 12–25, Jan. 2012, doi: 10.1002/sca.20271.

[155] N. Y. Souren *et al.*, "Cell line authentication: a necessity for reproducible biomedical research," *EMBO J*, vol. 41, no. 14, Jul. 2022, doi: 10.15252/embj.2022111307.

[156] "Identity crisis," *Nature*, vol. 457, no. 7232, pp. 935–936, 2009, doi: 10.1038/457935b.

[157] L. Tang, "Investigating heterogeneity in HeLa cells," *Nat Methods*, vol. 16, no. 4, p. 281, Apr. 2019, doi: 10.1038/s41592-019-0375-1.

[158] C. T. Korch and A. Capes-Davis, "The Extensive and Expensive Impacts of HEp-2 [HeLa], Intestine 407 [HeLa], and Other False Cell Lines in Journal Publications," *SLAS Discovery*, vol. 26, no. 10, pp. 1268–1279, Dec. 2021, doi: 10.1177/24725552211051963.

[159] A. Capes-Davis *et al.*, "Check your cultures! A list of cross-contaminated or misidentified cell lines," *International Journal of Cancer*, vol. 127, no. 1. pp. 1–8, Jul. 01, 2010. doi: 10.1002/ijc.25242.

[160] J. L. Almeida, C. R. Hill, and K. D. Cole, "Mouse cell line authentication," *Cytotechnology*, vol. 66, no. 1, pp. 133–147, Jan. 2014, doi: 10.1007/s10616-013-9545-7.

[161] J. L. Almeida, K. D. Cole, and A. L. Plant, "Standards for Cell Line Authentication and Beyond," *PLoS Biol*, vol. 14, no. 6, Jun. 2016, doi: 10.1371/journal.pbio.1002476.

[162] M. A. Feitelson *et al.*, "Sustained proliferation in cancer: Mechanisms and novel therapeutic targets," *Seminars in Cancer Biology*, vol. 35. Academic Press, pp. S25–S54, Dec. 01, 2015. doi: 10.1016/j.semcancer.2015.02.006.

[163] S. Uxa, P. Castillo-Binder, R. Kohler, K. Stangner, G. A. Müller, and K. Engeland, "Ki-67 gene expression," *Cell Death Differ*, vol. 28, no. 12, pp. 3357–3370, Dec. 2021, doi: 10.1038/s41418-021-00823-x.

[164] A. Zhang, X. Wang, C. Fan, and X. Mao, "The Role of Ki67 in Evaluating Neoadjuvant Endocrine Therapy of Hormone Receptor-Positive Breast Cancer,"

Frontiers in Endocrinology, vol. 12. Frontiers Media S.A., Nov. 03, 2021. doi: 10.3389/fendo.2021.687244.

[165] L. T. Li, G. Jiang, Q. Chen, and J. N. Zheng, "Predic Ki67 is a promising molecular target in the diagnosis of cancer (Review)," *Molecular Medicine Reports*, vol. 11, no. 3. Spandidos Publications, pp. 1566–1572, Mar. 01, 2015. doi: 10.3892/mmr.2014.2914.

[166] G. L. Moldovan, B. Pfander, and S. Jentsch, "PCNA, the Maestro of the Replication Fork," *Cell*, vol. 129, no. 4. Elsevier B.V., pp. 665–679, May 18, 2007. doi: 10.1016/j.cell.2007.05.003.

[167] G. D. Bowman, M. O'donnell, and J. Kuriyan, "Structural analysis of a eukaryotic sliding DNA clamp-clamp loader complex," 2004. [Online]. Available: www.nature.com/nature

[168] Y. L. Wang *et al.*, "The Functions of PCNA in Tumor Stemness and Invasion," *Int J Mol Sci*, vol. 23, no. 10, May 2022, doi: 10.3390/ijms23105679.

[169] D. A. Fletcher and R. D. Mullins, "Cell mechanics and the cytoskeleton," *Nature*, vol. 463, no. 7280. pp. 485–492, Jan. 28, 2010. doi: 10.1038/nature08908.

[170] D. E. Ingber, "Mechanical control of tissue growth: Function follows form," 2005. [Online]. Available: www.pnas.orgcgidoi10.1073pnas.0505939102

[171] N. Wang and Z. Suo, "Long-distance propagation of forces in a cell," *Biochem Biophys Res Commun*, vol. 328, no. 4, pp. 1133–1138, Mar. 2005, doi: 10.1016/j.bbrc.2005.01.070.

[172] T. M. Bunnell, B. J. Burbach, Y. Shimizu, and J. M. Ervasti, "β-Actin specifically controls cell growth, migration, and the G-actin pool," *Mol Biol Cell*, vol. 22, no. 21, pp. 4047–4058, Nov. 2011, doi: 10.1091/mbc.E11-06-0582.

[173] J. Seo and J. Kim, "Regulation of Hippo signaling by actin remodeling," *BMB Reports*, vol. 51, no. 3. The Biochemical Society of the Republic of Korea, pp. 151–156, 2018. doi: 10.5483/BMBRep.2018.51.3.012.

[174] Y. Qiao *et al.*, "YAP Regulates Actin Dynamics through ARHGAP29 and Promotes Metastasis," *Cell Rep*, vol. 19, no. 8, pp. 1495–1502, May 2017, doi: 10.1016/j.celrep.2017.04.075.

[175] R. Moreno-Vicente *et al.*, "Caveolin-1 Modulates Mechanotransduction Responses to Substrate Stiffness through Actin-Dependent Control of YAP," *Cell Rep*, vol. 25, no. 6, pp. 1622-1635.e6, Nov. 2018, doi: 10.1016/j.celrep.2018.10.024.

[176] T. Xia, R. Zhao, F. Feng, and L. Yang, "The effect of matrix stiffness on human hepatocyte migration and function-An in vitro research," *Polymers (Basel)*, vol. 12, no. 9, Sep. 2020, doi: 10.3390/POLYM12091903.

[177] S. S. Lin and Y. W. Liu, "Mechanical stretch induces mTOR recruitment and activation at the phosphatidic acid-enriched macropinosome in muscle cell," *Front Cell Dev Biol*, vol. 7, no. May, 2019, doi: 10.3389/fcell.2019.00078.

[178] J. E. Frith *et al.*, "Mechanically-sensitive miRNAs bias human mesenchymal stem cell fate via mTOR signaling," *Nat Commun*, vol. 9, no. 1, Dec. 2018, doi: 10.1038/s41467-017-02486-0.

[179] J. K. H. Hu, W. Du, S. J. Shelton, M. C. Oldham, C. M. DiPersio, and O. D. Klein, "An FAK-YAP-mTOR Signaling Axis Regulates Stem Cell-Based Tissue Renewal in Mice," *Cell Stem Cell*, vol. 21, no. 1, pp. 91-106.e6, Jul. 2017, doi: 10.1016/j.stem.2017.03.023.

[180] N. Liang *et al.*, "Regulation of YAP by mTOR and autophagy reveals a therapeutic target of tuberous sclerosis complex," *Journal of Experimental Medicine*, vol. 211, no. 11, pp. 2249–2263, 2014, doi: 10.1084/jem.20140341.

[181] T. Bui *et al.*, "Functional Redundancy between β1 and β3 Integrin in Activating the IR/Akt/mTORC1 Signaling Axis to Promote ErbB2-Driven Breast Cancer," *Cell Rep*, vol. 29, no. 3, pp. 589-602.e6, Oct. 2019, doi: 10.1016/j.celrep.2019.09.004.

[182] F.-Y. Lee *et al.*, "The mTOR-FAK mechanotransduction signaling axis for focal adhesion maturation and cell proliferation," 2017. [Online]. Available: www.ajtr.org

[183] C. H. Jung, S. H. Ro, J. Cao, N. M. Otto, and D. H. Kim, "MTOR regulation of autophagy," *FEBS Letters*, vol. 584, no. 7. Elsevier, pp. 1287–1295, 2010. doi: 10.1016/j.febslet.2010.01.017.

[184] D. Glick, S. Barth, and K. F. Macleod, "Autophagy: Cellular and molecular mechanisms," *Journal of Pathology*, vol. 221, no. 1. pp. 3–12, May 2010. doi: 10.1002/path.2697.

[185] I. Tanida, T. Ueno, and E. Kominami, "LC3 conjugation system in mammalian autophagy," *International Journal of Biochemistry and Cell Biology*, vol. 36, no. 12. pp. 2503–2518, Dec. 2004. doi: 10.1016/j.biocel.2004.05.009.

[186] N. Liang *et al.*, "Regulation of YAP by mTOR and autophagy reveals a therapeutic target of tuberous sclerosis complex," *Journal of Experimental Medicine*, vol. 211, no. 11, pp. 2249–2263, 2014, doi: 10.1084/jem.20140341.

[187] T. Bui *et al.*, "Functional Redundancy between β1 and β3 Integrin in Activating the IR/Akt/mTORC1 Signaling Axis to Promote ErbB2-Driven Breast Cancer," *Cell Rep*, vol. 29, no. 3, pp. 589-602.e6, Oct. 2019, doi: 10.1016/j.celrep.2019.09.004.

[188] Y. J. Liu, R. L. McIntyre, G. E. Janssens, and R. H. Houtkooper, "Mitochondrial fission and fusion: A dynamic role in aging and potential target for age-related disease," *Mech Ageing Dev*, vol. 186, Mar. 2020, doi: 10.1016/j.mad.2020.111212.

[189] U. Manor *et al.*, "A mitochondria-anchored isoform of the actin-nucleating spire protein regulates mitochondrial division", doi: 10.7554/eLife.08828.001.

[190] A. S. Moore, Y. C. Wong, C. L. Simpson, and E. L. F. Holzbaur, "Dynamic actin cycling through mitochondrial subpopulations locally regulates the fission-fusion balance within mitochondrial networks," *Nat Commun*, vol. 7, Sep. 2016, doi: 10.1038/ncomms12886.

[191] A. S. Moore and E. L. Holzbaur, "Mitochondrial-cytoskeletal interactions: dynamic associations that facilitate network function and remodeling," *Current Opinion in Physiology*, vol. 3. Elsevier Ltd, pp. 94–100, Jun. 01, 2018. doi: 10.1016/j.cophys.2018.03.003.

[192] S. Carsten Johannes Helle *et al.*, "Mechanical force induces mitochondrial fission," 2017, doi: 10.7554/eLife.30292.001.

[193] P. Romani, L. Valcarcel-Jimenez, C. Frezza, and S. Dupont, "Crosstalk between mechanotransduction and metabolism," *Nature Reviews Molecular Cell Biology*, vol. 22, no. 1. Nature Research, pp. 22–38, Jan. 01, 2021. doi: 10.1038/s41580-020-00306-w.

[194] D. B. Zorov, M. Juhaszova, and S. J. Sollott, "Mitochondrial Reactive Oxygen Species (ROS) and ROS-Induced ROS Release," *Physiol Rev*, vol. 94, pp. 909–950, 2014, doi: 10.1152/physrev.00026.2013.-Byproducts.

[195] H. Chen, A. Chomyn, and D. C. Chan, "Disruption of fusion results in mitochondrial heterogeneity and dysfunction," *Journal of Biological Chemistry*, vol. 280, no. 28, pp. 26185–26192, Jul. 2005, doi: 10.1074/jbc.M503062200.

[196] S. Frank, "Dysregulation of mitochondrial fusion and fission: An emerging concept in neurodegeneration," *Acta Neuropathologica*, vol. 111, no. 2. pp. 93–100, Feb. 2006. doi: 10.1007/s00401-005-0002-3.

[197] M. Panel, B. Ghaleh, and Di. Morin, "Ca2+ionophores are not suitable for inducing mPTP opening in murine isolated adult cardiac myocytes," *Sci Rep*, vol. 7, no. 1, Dec. 2017, doi: 10.1038/s41598-017-04618-4.

[198] D. G. Nicholls, "Simultaneous monitoring of ionophore- and inhibitor-mediated plasma and mitochondrial membrane potential changes in cultured neurons," *Journal of Biological Chemistry*, vol. 281, no. 21, pp. 14864–14874, May 2006, doi: 10.1074/jbc.M510916200.

[199] Y. Q. Zhang *et al.*, "Mitochondrial uncoupler carbonyl cyanide m-chlorophenylhydrazone induces vasorelaxation without involving KATPchannel activation in smooth muscle cells of arteries," *Br J Pharmacol*, pp. 3145–3158, 2016, doi: 10.1111/bph.13578.

[200] Y. Song and D. L. Villeneuve, "AOP Report: Uncoupling of Oxidative Phosphorylation Leading to Growth Inhibition via Decreased Cell Proliferation," *Environ Toxicol Chem*, vol. 40, no. 11, pp. 2959–2967, Nov. 2021, doi: 10.1002/etc.5197.

[201] L. Li, K. Prabhakaran, E. M. Mills, J. L. Borowitz, and G. E. Isom, "Enhancement of cyanide-induced mitochondrial dysfunction and cortical cell cecrosis by uncoupling protein-2," *Toxicological Sciences*, vol. 86, no. 1, pp. 116–124, Jul. 2005, doi: 10.1093/toxsci/kfi164.

[202] E. B. Randi, K. Zuhra, L. Pecze, T. Panagaki, and C. Szabo, "Physiological concentrations of cyanide stimulate mitochondrial Complex IV and enhance cellular bioenergetics", doi: 10.1073/pnas.2026245118/-/DCSupplemental.

[203] Y. C. Shen *et al.*, "Activating oxidative phosphorylation by a pyruvate dehydrogenase kinase inhibitor overcomes sorafenib resistance of hepatocellular carcinoma," *Br J Cancer*, vol. 108, no. 1, pp. 72–81, Jan. 2013, doi: 10.1038/bjc.2012.559.

[204] Y. Yang *et al.*, "Mitochondrial UQCC3 Modulates Hypoxia Adaptation by Orchestrating OXPHOS and Glycolysis in Hepatocellular Carcinoma," *Cell Rep*, vol. 33, no. 5, Nov. 2020, doi: 10.1016/j.celrep.2020.108340.

[205] T. Amann *et al.*, "GLUT1 expression is increased in hepatocellular carcinoma and promotes tumorigenesis," *American Journal of Pathology*, vol. 174, no. 4, pp. 1544–1552, 2009, doi: 10.2353/ajpath.2009.080596.

[206] J. S. Park *et al.*, "Mechanical regulation of glycolysis via cytoskeleton architecture," *Nature*, vol. 578, no. 7796, pp. 621–626, Feb. 2020, doi: 10.1038/s41586-020-1998-1.

[207] T. Zuliani *et al.*, "Sensitive and Reliable JC-1 and TOTO-3 Double Staining to Assess Mitochondrial Transmembrane Potential and Plasma Membrane Integrity: Interest for Cell Death Investigations," *Cytometry Part A*, vol. 54, no. 2, pp. 100–108, 2003, doi: 10.1002/cyto.a.10059.

[208] C. Jensen and Y. Teng, "Is It Time to Start Transitioning From 2D to 3D Cell Culture?," *Frontiers in Molecular Biosciences*, vol. 7. Frontiers Media S.A., Mar. 06, 2020. doi: 10.3389/fmolb.2020.00033.

[209] A. S. Serras, J. S. Rodrigues, M. Cipriano, A. V. Rodrigues, N. G. Oliveira, and J. P. Miranda, "A Critical Perspective on 3D Liver Models for Drug Metabolism

and Toxicology Studies," *Frontiers in Cell and Developmental Biology*, vol. 9. Frontiers Media S.A., Feb. 22, 2021. doi: 10.3389/fcell.2021.626805.

[210] H. K. Kang *et al.*, "Establishing a 3D In Vitro Hepatic Model Mimicking Physiologically Relevant to In Vivo State," *Cells*, vol. 10, no. 5, p. 1268, May 2021, doi: 10.3390/cells10051268.

[211] P. C. Georges *et al.*, "Increased stiffness of the rat liver precedes matrix deposition: implications for fibrosis," *Am J Physiol Gastrointest Liver Physiol*, vol. 293, pp. 1147–1154, 2007, doi: 10.1152/ajpgi.00032.2007.-Liver.

[212] S. S. Lin and Y. W. Liu, "Mechanical stretch induces mTOR recruitment and activation at the phosphatidic acid-enriched macropinosome in muscle cell," *Front Cell Dev Biol*, vol. 7, no. May, 2019, doi: 10.3389/fcell.2019.00078.

[213] L. Jin *et al.*, "YAP inhibits autophagy and promotes progression of colorectal cancer via upregulating Bcl-2 expression," *Cell Death Dis*, vol. 12, no. 5, May 2021, doi: 10.1038/s41419-021-03722-8.

[214] A. Totaro *et al.*, "Cell phenotypic plasticity requires autophagic flux driven by YAP/TAZ mechanotransduction," *Proc Natl Acad Sci U S A*, vol. 116, no. 36, pp. 17848–17857, Sep. 2019, doi: 10.1073/pnas.1908228116.

[215] J. Jovel *et al.*, "A Survey of Molecular Heterogeneity in Hepatocellular Carcinoma," 2018, doi: 10.1002/hep4.1197/full.

[216] S. Wu, F. Zhou, Y. Wei, W. R. Chen, Q. Chen, and D. Xing, "Cancer phototherapy via selective photoinactivation of respiratory chain oxidase to trigger a fatal superoxide anion burst," *Antioxid Redox Signal*, vol. 20, no. 5, pp. 733–746, Feb. 2014, doi: 10.1089/ars.2013.5229.

[217] M. Tian *et al.*, "The nanomechanical signature of liver cancer tissues and its molecular origin," *Nanoscale*, vol. 7, no. 30, pp. 12998–13010, Aug. 2015, doi: 10.1039/c5nr02192h.

LIST OF FIGURES

membrane, ColF (green) for collagen, and Hoechst 33342 (blue) for cellular nucleus.

95

homodimer (red), while Hoechst 3334 was used for nucleus counterstaining. Finally, photobiomodulation with 649 nm red laser light was performed.

LIST OF TABLES

LIST OF PUBLICATIONS

The list contains 9 publications in scientific journals, where I contributed either as a first-author or as a co-author during the years of my doctoral studies at the Faculty of Mathematics and Physics, Charles University in Prague. Total number of citations (26th November 2023) is 147, H-index is 6 according the Scopus database.

- Uzhytchak, M., Smolková, B., **Frtús, A.**, Stupakov, A., Lunova, M., Scollo, F., Hof, M., Jurkiewicz, P., Sullivan, G. J., Dejneka, A., & Lunov, O. (2023). Sensitivity of endogenous autofluorescence in HeLa cells to the application of external magnetic fields. *Scientific Reports*, 13(1). https://doi.org/10.1038/s41598-023-38015-x IF=4,6

- Uzhytchak, M., Smolková, B., Lunova, M., **Frtús, A.**, Jirsa, M., Dejneka, A., & Lunov, O. (2023). Lysosomal nanotoxicity: Impact of nanomedicines on lysosomal function. *Advanced Drug Delivery Reviews*, 197. https://doi.org/10.1016/j.addr.2023.114828 IF=16,1

- **Frtús, A.**, Smolková, B., Uzhytchak, M., Lunova, M., Jirsa, M., Petrenko, Y., Dejneka, A., & Lunov, O. (2023). Mechanical Regulation of Mitochondrial Dynamics and Function in a 3D-Engineered Liver Tumor Microenvironment. *ACS Biomaterials Science and Engineering*. https://doi.org/10.1021/acsbiomaterials.2c01518 IF=5,8

- **Frtús, A.**, Smolková, B., Uzhytchak, M., Lunova, M., Jirsa, M., Henry, S. J. W., Dejneka, A., Stephanopoulos, N., & Lunov, O. (2022). The interactions between DNA nanostructures and cells: A critical overview from a cell biology perspective. *Acta Biomaterialia*, 146. https://doi.org/10.1016/j.actbio.2022.04.046 IF=9,7

- Smolková, B., MacCulloch, T., Rockwood, T. F., Liu, M., Henry, S. J. W., **Frtús, A.**, Uzhytchak, M., Lunova, M., Hof, M., Jurkiewicz, P., Dejneka, A., Stephanopoulos, N., & Lunov, O. (2021). Protein Corona Inhibits Endosomal Escape of Functionalized DNA Nanostructures in Living Cells. *ACS Applied Materials and Interfaces*, 13(39). https://doi.org/10.1021/acsami.1c14401 IF=9,5

- Smolková, B., **Frtús, A.**, Uzhytchak, M., Lunova, M., Kubinová, Š., Dejneka, A., & Lunov, O. (2020). Critical analysis of non-thermal plasma-driven modulation

of immune cells from clinical perspective. *International Journal of Molecular Sciences*, 21(17). https://doi.org/10.3390/ijms21176226 IF=5,6

- **Frtús, A.**, Smolková, B., Uzhytchak, M., Lunova, M., Jirsa, M., Hof, M., Jurkiewicz, P., Lozinsky, V. I., Wolfová, L., Petrenko, Y., Kubinová, Š., Dejneka, A., & Lunov, O. (2020). Hepatic tumor cell morphology plasticity under physical constraints in 3D cultures driven by YAP–mTOR axis. *Pharmaceuticals*, 13(12). https://doi.org/10.3390/ph13120430 IF=4,6

- **Frtús, A.**, Smolková, B., Uzhytchak, M., Lunova, M., Jirsa, M., Kubinová, Š., Dejneka, A., & Lunov, O. (2020). Analyzing the mechanisms of iron oxide nanoparticles interactions with cells: A road from failure to success in clinical applications. *Journal of Controlled Release*, 328. https://doi.org/10.1016/j.jconrel.2020.08.036 IF=10,8

- Uzhytchak, M., Smolková, B., Lunova, M., Jirsa, M., **Frtús, A.**, Kubinová, Š., Dejneka, A., & Lunov, O. (2020). Iron Oxide Nanoparticle-Induced Autophagic Flux Is Regulated by Interplay between p53-mTOR Axis and Bcl-2 Signaling in Hepatic Cells. *Cells*, 9(4). https://doi.org/10.3390/cells9041015 IF=6

LIST OF APPENDICES

Appendix I

Frtús, A., Smolková, B., Uzhytchak, M., Lunova, M., Jirsa, M., Hof, M., Jurkiewicz, P., Lozinsky, V. I., Wolfová, L., Petrenko, Y., Kubinová, Š., Dejneka, A., & Lunov, O. (2020). Hepatic tumor cell morphology plasticity under physical constraints in 3D cultures driven by YAP–mTOR axis. *Pharmaceuticals*, 13(12). https://doi.org/10.3390/ph13120430

Contribution: Experimental workflow execution, data acquisition, data analysis, preparing and editing the manuscript

Appendix II

Frtús, A., Smolková, B., Uzhytchak, M., Lunova, M., Jirsa, M., Petrenko, Y., Dejneka, A., & Lunov, O. (2023). Mechanical Regulation of Mitochondrial Dynamics and Function in a 3D-Engineered Liver Tumor Microenvironment. *ACS Biomaterials Science and Engineering*. https://doi.org/10.1021/acsbiomaterials.2c01518

Contribution: Experimental workflow execution, data acquisition, data analysis, preparing and editing the manuscript